

POLITECNICO DI TORINO

Master's Degree in Mechatronic Engineering

Master's Degree Thesis

DEVELOPMENT OF A HAND EXOSKELETON ACTUATED WITH SMA



Supervisors

Prof. Marcello Chiaberge
Prof. Antonio Barrientos
PhD. Silvia Terrile

Candidate

Matilde Brossa

October 2020

Contents

CONTENTS	II
FIGURE INDEX	IV
TABLE INDEX.....	VI
GRAPH INDEX	VII
ABSTRACT.....	1
1 INTRODUCTION	3
1.1 Thesis overview.....	3
1.2 Motivation	4
2 STATE OF THE ART.....	6
2.1 Exoskeletons and robotic devices.....	6
2.2 Comparative table	8
2.3 Mechanical structure	13
2.4 Actuator and power transmission	17
2.5 Sensor and control.....	21
2.6 Prototype characteristics.....	25
3 MECHANICAL DESIGN.....	27
3.1 Hand structure	27
3.1.1 <i>Articulation</i>	27
3.1.2 <i>Dimensions</i>	29
3.1.3 <i>Range of motion</i>	31
3.2 The exoskeleton system	31
3.3 Dynamic simulations.....	33
3.3.1 <i>Hand model</i>	34
3.3.2 <i>Simulations set-up</i>	35
3.3.3 <i>Index finger</i>	36
3.3.4 <i>Middle finger</i>	40
3.3.5 <i>Simulations considerations</i>	41
3.4 Mechanical drawing.....	42
3.4.1 <i>First support S1</i>	43
3.4.2 <i>Second support S2</i>	44
3.4.3 <i>Third support S3</i>	45
3.4.4 <i>Cable set-up</i>	45
3.5 Prototypes realization.....	46
3.5.1 <i>The first prototype</i>	46
3.5.2 <i>The second prototype</i>	48

4 ACTUATOR AND ELECTRONIC IMPLEMENTATION	50
4.1 The Shape Memory Alloys.....	50
4.1.1 <i>History and applications</i>	50
4.1.2 <i>SMA characteristics</i>	51
4.1.3 <i>Different SMA types</i>	52
4.2 Electronic circuit.....	54
4.2.1 <i>The microcontroller</i>	54
4.2.2 <i>Design of the MOSFET circuit</i>	55
4.2.3 <i>Realization of the MOSFET circuit</i>	58
4.3 SMA characterization.....	59
4.3.1 <i>Measurement of the SMA spring resistance</i>	60
4.3.2 <i>Measurement of the SMA spring contraction</i>	63
4.4 Integration of the actuator unit on the prototype.....	66
5 SENSOR AND CONTROL	70
5.1 Superficial electromyography.....	70
5.1.1 <i>sEMG signal</i>	70
5.1.2 <i>sEMG sensor</i>	73
5.2 Control logic code.....	74
5.2.1 <i>Self-motion control</i>	75
5.2.2 <i>The Arduino code</i>	76
5.3 Integration of the sensor and control system on the prototype.....	78
6 CONCLUSIONS	80
6.1 Future work.....	81
ACRONYMS	85
APPENDIX 1 CAD DRAWING	87
APPENDIX 2 ARDUINO CONTROL CODE	97
BIBLIOGRAPHY	99

Figure index

Figure 1 Main elements that compose an exoskeleton [14]	7
Figure 2 Main mechanical structure for matching the finger range of motion (ROM) [7]	13
Figure 3 Direct matching of the joint centres. Left Y. Hasegawa [24] Right HandEXOS A. Chiri [23]	14
Figure 4 Linkage for remote centre of rotation mechanism RCMs Left M. Fontana [16] Right K.Y. Tong [26]	15
Figure 5 Redundant linkage structure: REHAND A. Lince [30]	16
Figure 6 The 4-bar linkage structure. Left A. Wege and G. Hommel [34] Right T. Tang et al. [17].....	16
Figure 7 AFX T. Worsnopp et al.'s exoskeleton [29]	19
Figure 8 ExoGlove (H. K. Yap, J. H. Lim et al.) [19]	20
Figure 9 L.A. Martinez et al.'s control system [36]	22
Figure 10 HANDEXOS control strategy (A. Chiri) [23]	22
Figure 11 Self-motion control set-up [32]	24
Figure 12 Hand structure and articulation joints [40]	28
Figure 13 Finger articulation modelled based on the admissible DOFs [30].....	28
Figure 14 Finger joints and admissible motions [17]	29
Figure 15 Fingers measures references in S. R. Habib and N. N. Kamal analysis [41]....	30
Figure 16 Exoskeleton structure and corresponding names. S1, S2, S3 structural element fixed to the hand. R1, R2, r1, r2 external links of the two 4-bar linkage structures. P1, P2, p1, p2 virtual links of the two 4-bar linkage structures [Source: Author].....	32
Figure 17 Cables set-up on a 4-bar linkage structure exoskeleton that allows flexion (red cable) and extension (blue cable) [6].....	33
Figure 18 Dynamical simulation set-up for index length B.....	37
Figure 19 Inventor model of the structural element S1 [Source: author]	43
Figure 20 Cable path considered for the evaluation of the cable lengths	44
Figure 21 Inventor model of structural element S2 [Source: author]	44
Figure 22 Inventor model of structural element S3 [Source: author]	45
Figure 23 Extension cable and SMA springs set-up on the support S1. From the left two SMA springs (black), the hook (white), the pulley (black) and the extensor cable (blue).....	46
Figure 24 Mechanical model of the exoskeleton designed on the Autodesk INVENTOR	46
Figure 25 Exoskeleton structure of the first prototype	47
Figure 26 Exoskeleton structure of the second prototype.....	49
Figure 27 SMA crystalline structure related with temperature and strain [44].....	51
Figure 28 SMA temperature-stress-strain behaviour [44].....	52

Figure 29 SMA spring relation with heat [46]	53
Figure 30 Circuit schematic. V_{in} = power supply voltage, V_{drv} =PWM driving signal, M1=MOSFET IFR530, SMA R= equivalent resistor of the SMA spring.....	55
Figure 31 Output characteristic of the MOSFET IRF530 at $T_c=25\text{ }^\circ\text{C}$	56
Figure 32 MOSFET circuit set-up	58
Figure 33 Experimental set-up to measure the SMA spring contraction with respect to the PWM and the force applied to it.	64
Figure 34 Experimental set-up of the two SMA springs in electric series and mechanical parallel to simulate the actuation unit of the hand exoskeleton	67
Figure 35 Actuator unit and transmission system mounted on the mechanical structure of the hand exoskeleton	68
Figure 36 Integration set-up of the mechanical structure of the exoskeleton and its actuator unit and electronic circuit	69
Figure 37 Skeletal muscles on the forearm: on the left the dorsal representation of the forearm muscles, on the right the palmar one [47]	71
Figure 38 Block scheme of the filter and conditioning chain in an EMG [48].....	72
Figure 39 sEMG implementation on a volunteer	73
Figure 40 Complete set-up model of the connections between the actuator unit (SMA springs), the sensor unit (the red box), the MOSFET circuit (the green box) and the control system (Arduino light-blue box).....	78
Figure 41 Complete set-up of the exoskeleton with the actuator unit, the sensor unit, the electronic circuit and the control system on a healthy volunteer.	79

Table index

Table 1 Comparative table.....	12
Table 2 Pros and Cons of the actuator system mostly used for exoskeleton systems ..	18
Table 3 Prototype characteristics and the motivations of the design choices.....	26
Table 4 Mean values of finger phalanges lengths (M: male, F: Female) [41].....	30
Table 5 Fingers ROMs [14]	31
Table 6. Fingers lengths of the hand prototype used in the simulations.....	34
Table 7 Resulting torques on each finger joint due to stroke rigidity	36
Table 8 Resistive torques for each index joint due to stroke	36
Table 9 Initial linkage lengths for index simulations	37
Table 10 Measures of external and virtual bars of the index exoskeleton structure	39
Table 11 Resistive torque for each middle finger joint due to stroke.....	40
Table 12 Measures of the external and virtual bars of the middle finger exoskeleton structure	40
Table 13 Average angular velocity of the joints [°/sec] with the applied forces of 5 N and 7 N, considering the exoskeleton structure with the selected linkage lengths	41
Table 14 First prototype external links measures	47
Table 15 Second prototype external links measures.....	48
Table 16 IRF530 MOSFET data.....	55

Graph index

Graph 1 Graphical trends of the first simulation on the MCP index joint	38
Graph 2 SMA Resistance with respect to the driving PWM on the SMA springs A (red) and on spring B (blue)	62
Graph 3 Contraction of the SMA spring A with respect to the PWM and the force applied.....	65
Graph 4 Contraction of the SMA spring B with respect to the PWM and the force applied.....	65
Graph 5 Superficial EMG from the extensor fascicle muscle on a healthy volunteer. Two muscular activation are withdrawn: at 13-17 seconds and 20-24 seconds.	74

Abstract

Shape Memory Alloys (SMAs) are innovative materials whose potential as actuators is being investigated in different fields because of their smart properties. Indeed, this material can recover a predefined shape if subjected to an appropriate thermomechanical process. The purpose of this thesis is to develop a novel hand exoskeleton actuated by SMA springs for the rehabilitation of patients affected by post-stroke hemiparesis. In the first part of the work the actual state of the art is analysed in order to identify the most suitable solutions for implementing the SMA actuation on an exoskeleton device. Afterwards, the exoskeleton is completely designed from the point of view of the mechanical structure, the electronic circuit, and the control system. From the mechanical point of view, a tendon-driven 4-bar linkage structure is implemented. Different dynamic simulations on INVENTOR confirm the structure dimensions and allow an estimation of the needed forces to overcome the stroke rigidity. The design results in an exoskeleton that actuates the two joints of the index finger and of the middle finger. On the basis of the simulations, two prototypes are realized. The characteristics of the SMA springs used for the actuation are experimentally analysed and the SMA actuator unit is implemented on one of the two prototypes to realize a fully operating exoskeleton. A MOSFET circuit is designed on LT-spice to let a PWM current flow through the SMA springs and heat them thanks to the Joule effect. A control system algorithm based on a threshold control is implemented on an Arduino board for achieving the stroke rehabilitation. The superficial electromyography (sEMG) signal is withdrawn from the healthy forearm of the patient to let the patient control the rehabilitation movement thanks to the self-motion control.

1 Introduction

This work aims at designing and realizing a physical prototype of a hand exoskeleton actuated by Shape Memory Alloy (SMA) for stroke rehabilitation controlled by superficial electromyography (EMG) sensors.

This thesis is done under the supervision of the Centre for Automation and Robotics (CAR) CSIC-UPM at the Polytechnical University of Madrid (UPM), which is a joint centre for shared ownership between the UPM and CSIC (Consejo Superior de Investigaciones Cientificas); the project has been developed as an Erasmus Traineeship project of 5 months.

1.1 Thesis overview

The thesis main topics are presented according to the following structure.

- Chapter 1: this chapter is the present introduction and presents the aim, the structure, and the motivation of the thesis.
- Chapter 2: this chapter presents the actual State of the Art on the hand exoskeletons. Different devices have been compared according to their mechanical structure, actuation and power transmission methods, and sensor and control systems.
- Chapter 3: this chapter presents the mechanical design of the hand exoskeleton prototype built for this project in terms of hand structure, force analysis, mechanical realization, and dynamic simulations. Two mechanical prototypes are presented.
- Chapter 4: this chapter presents the SMA actuator and the electronic used for its activation. The SMA springs used as actuators, are analysed under the mechanical and electrical point of view to characterize their behaviour. The electronic circuit is simulated, integrated on the mechanical structure of the exoskeleton, and the behaviour is verified.
- Chapter 5: this chapter presents the sensor and the control logic. Sensor unit, filtering and conditioning of the EMG are explained. The self-motion control is

implemented as the method with which the patient controls the rehabilitation. A control algorithm based on a threshold is implemented on a microcontroller Arduino which manages all the signals.

- Chapter 6: the conclusions are presented in this chapter. It contains some considerations on the present work and some remarks on the future works to improve the prototype.

1.2 Motivation

A *stroke* is a neurological deficit attributed to an acute focal injury of the central nervous system (CNS) by a vascular cause [1]. Ischemia or haemorrhage in the brain may be counted among the main reasons for cerebral vascular accidents which ultimately result in strokes.

According to the research carried out by Roy, Sahadev and Inamadarm [2], nowadays stroke is the major cause of long-term hand disability for adults in the world. Approximately 1.1 million inhabitants of Europe suffer a stroke every year. Moreover, since the incidence rate increases by a factor of 100 between the age of forty and the age of eighty, and because of the progressive aging of the population, the number of cases and the need for treatment are expected to further increase [1].

Over 75 percent of the patients survive, but many of the stroke survivors do have residual disabilities, mostly on the upper limb and hand, many of which require permanent care [3]. Depending on which region of the brain is damaged, different disorders can arise. The loss of upper limb motor control is a disorder that involves 75% of post-stroke patients and is characterized by an unimpaired arm and the other one weaker impaired (hemiparesis) [2]. Nevertheless, post-stroke patients also suffer from weakness of specific muscles, abnormal muscle tone as muscle spasticity and rigidity, and lack of mobility. Spasticity is a continuous contraction of the muscles that causes low hand motion control on the stroke patients and, in the majority of cases, it obstructs basic movements such as the opening of the hand [4].

Hand injuries caused by accidents are common. Hand damages lead to economic consequences both direct costs for operation and rehabilitation and indirect costs due

to the inactivity of the patient [5]. The social aspect is also compromised; indeed, the individual life quality gets worse and thus injured persons tend to be excluded from the productive and fulfilling life within the society.

Currently, *rehabilitation* for motor recovery is performed by physical therapists who hold and repeatedly move the fingers affected by muscular rigidity from the contracted full-flexed position to the maximum range of joint angles [6]. To improve recovery is important to start rehabilitation as soon as possible after the stroke. The rehabilitation must be high-intensity with task-specific repetitive exercises. Highly repetitive therapeutic training can also help rehabilitation in terms of motor function. This kind of exercise is a great time investment for the therapist and raises the rehabilitation costs for the patients [7].

Another fundamental aspect to improve stroke rehabilitation is the patient's motivation. To face this problem therapists set goals which are established through specific measurable and time-dependent recovery objectives [8].

Moreover, this kind of rehabilitation leads to limited results, and patients may still require treatment for a long time before being able to autonomously carry out the activities of daily living (ADL).

To face these problems, an advantageous solution is offered by the adoption of *robotic devices*. Robotic devices utilized in the rehabilitation field are considered a promising method for the relearning and the restoration of the motor functionalities. They can provide high-intensity, repetitive and task-specific treatments [9]. Furthermore, exoskeletons for rehabilitation meet the double goal of increasing the intensity and at the same time reducing the cost of the therapy [2]. Furthermore, these devices can also monitor the patient's progress objectively and reliably, thanks to the control systems implementations and the data collection systems [10]. Thanks to the collected data it is possible to fix patient goals, helping the patient motivation, and to monitor the rehabilitation progress, useful for the therapists.

2 State of the art

2.1 Exoskeletons and robotic devices

The firsts wearable robotic devices appears in the 1960s when the research efforts concentrated on the realization of force augmentation and rehabilitation systems [11]. A well-known branch of wearable robotic devices, directly attached to the human body, are the so called exoskeletons [12]. They are wearable external apparatuses created to support and power the user's motion doing a variety of tasks. The exoskeleton is employed in different applications because of the wide diversity of tasks it can perform. In the *industrial and military sectors*, the aim is to enhance human ability. Exoskeletons improve an individual physical capability of resistance and force and are used in tasks such as pick-and-place heavy objects, carry heavy loads, reduce the burden in physically demanding tasks. A practical example is about people whose work concerns repetitively exertion of grasping forces which are exposed to develop musculoskeletal disorders with a higher probability. Therefore, to decrease this risk it is important to reduce the physical manual burden on these workers, and so the exoskeleton is used to assist the worker movement and amplify their forces [7]. Moreover, exoskeleton applications involve works whose aim is to move heavy materials in environments where it is difficult to enter with vehicles and where forklifts are not present. In this case, the device worn by the user is directly controlled by human motion [2]. Thanks to reciprocal coordination the exoskeleton allows the user to perform very precise tasks and to deal with materials of great weight in an unorganized and narrow environment. Exoskeletons are also used to detect human movements by the usage of sensors and replicate them on humanoid robots that operate remotely in hazardous or dangerous environments [11]. This application involving haptic interaction is typically realized with a virtual reality interface. In the industrial applications, the interaction with the human and the environment is a crucial aspect.

Nowadays, the research is more developed and focused on exoskeleton applications in the *medical sector*. Differently from the previous applications, in which the devices are usually worn by healthy subjects, in this case the exoskeleton aims at assisting an

impaired person to perform basic ADL and at rehabilitating the impaired subjects by accelerating their recovery. Assistive exoskeletons are used for supporting mobility for people with injuries which affect their nervous system or the musculoskeletal apparatus and assisting elder people in the ADL [13]. Usually, the system is designed to be compact, lightweight, and portable. Another important requirement is to keep possible interaction with the surrounding environment. On the other hand, in the case of rehabilitation, the system must provide active and repetitive forces to the human articulations helping the wearers to improve their muscular mobility.

Because of the multiple functions that the hand performs the *robotic devices for hand* motions attracted the attention of several research groups in different application fields since the '80s [12].

The hand exoskeleton systems are the combination of mechanical structures, actuator and transmission methods, sensors, and control (Figure 1).

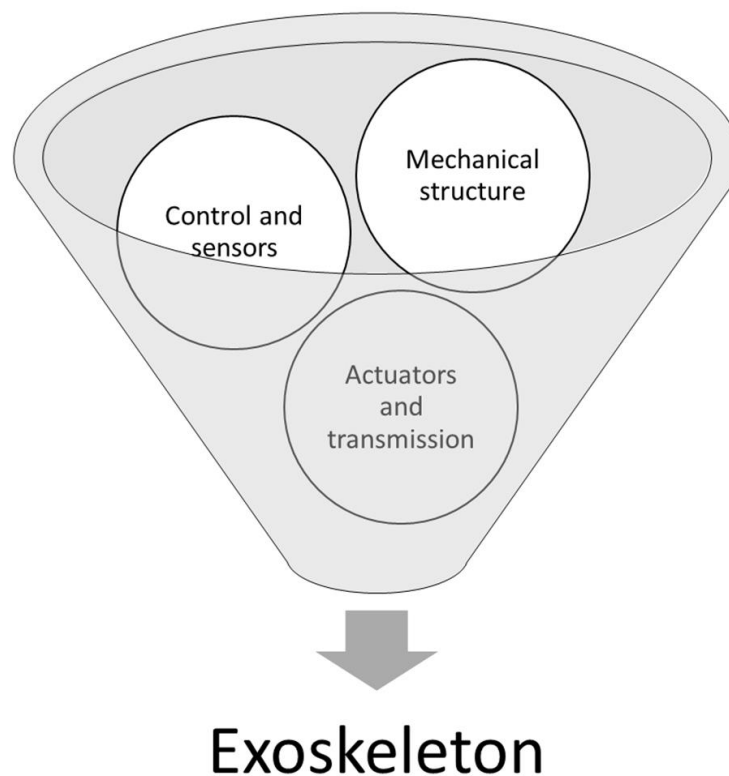


Figure 1 Main elements that compose an exoskeleton [14]

These three elements are mainly used to classify different types of exoskeletons. Moreover, also the number of degrees of freedom (DOFs), the range of motion, and the number of fingers to be actuated can be considered as classification criteria. Based on the specific application the exoskeleton, the designer faces a wide range of choices, and each decision leads to both advantages and disadvantages. The designer must carefully balance its characteristics in terms of lightweight, portability, tactile sensing capability and force generation [12]. With respect to the goal of the rehabilitation, exoskeletons can be passive or active. A passive exoskeleton aims at supporting the rehabilitation providing the full motion to the patient. An active one is intended to generate a resistive force against which the wearer has to move [7].

2.2 Comparative table

Some hand devices have been analysed and compared to study the main characteristics of the present result of the research. The prototypes under study are the most innovative devices in the medical field from 2005 up to now, so as considering the lasts 15 years of research.

The main aspects of each analysed prototype are located in suitable sections of the following Table 1. The name of the researchers and the name of the prototype, when present, are reported in column *Prototype*, and the publication year of the research is reported in the following column *Date*. In column *Type*, three different devices can be found: exoskeletons, gloves, and robotic hands. As explained above, exoskeletons are devices used to assist the user's motion; gloves are wearable devices that differ from the exoskeleton because of the flexibility of the material by which they are made. For this reason, they are classified under soft-robotics devices. Finally, robotic hands are robotic devices whose characteristics are the humanoid configuration of the hand articulations, of its Degree of Freedom (DOF) and of its Range of Motion (ROM). The column *Aim* reports the medical objective of the device. Most of the prototypes fall into the rehabilitation, stroke rehabilitation, and assistive purpose.

Actuation & Transmission and *Other info* refer to more detailed characteristics of the prototypes, such as force generation, the transmission of the movements, and more

specific features related to the realization of the prototypes. These aspects are fundamental for the design of a hand exoskeleton device and are examined in depth in the following chapter State of the art.

PROTOTYPE	Date	Type	Actuation & Transmission	Aim	Other info
HandSOME Elizabeth B. Brokaw et al. [3]	2011	Exoskeleton	Motors and springs	Stroke Rehabilitation	- Actuates index-middle-ring and little fingers together and the thumb independently
Hiroshi Yamaura, Kojiro Matsushita et al. [6]	2009	Exoskeleton	Motor bars linkage Tendon-driven	Stroke Rehabilitation	- 3 pulleys, 2 links and 2 wires - Actuates single finger flexion and extension - Bending sensor to control the device on a “data glove”
MANO L. Randazzo, I. Iturrate et al. [13]	2017	Exoskeleton	Linear servomotor Tendon-driven	Rehabilitation	- Chest pack with control unit: Closed loop control of position. - Active control of flexion and extension of all fingers - Powered by LiPo battery. - Forces at fingertips btw 0-20N.
ReHand A. Lince [14]	2016	Exoskeleton	Motor 4-bars linkage Tendon-driven	Stroke Rehabilitation	- Underactuated system of pulley to transmit forces. - 8 active DOF. - Control system based on sEMG
Kim, Yeongjin et al. [15]	2014	Exoskeleton Robot Hand	SMA tendons and passive springs	Stroke Rehabilitation	- Computer vision system to control joints angles. - Cooling system
HE M. Fontana et al. [16]	2009	Exoskeleton	RCM Cable transmission Motors	Accurate force displaying	- Portable hand exoskeleton few Newton forces - High accuracy of forces exerted on index and thumb - RCM mechanism
T. Tang, D. Zhang et al. [17]	2013	Exoskeleton	SMA spring 4-bar linkage Gears	Rehabilitation	- 3D printed 4 bar-linkage - Heating via current (2A) - Cooling via natural convection
Exo-glove H. In, B. B. Kang et al. [18]	2015	Glove	Motor Tendon-driven	Assist	- Force produced: 20 N pinch and 40 N for grasping - Actuates thumb, index, and middle finger
Exoglove H. K. Yap, J. H. Lim et al. [19]	2015	Glove	Soft pneumatic actuators	Rehabilitation and assist	- High customization - PneuNets actuator and Fiber-Reinforced actuator - Low grasping and pinching forces
J. Yang, J. Shi and H. Xie [20]	2015	Exoskeleton	SMA spring Tendon-driven	Rehabilitation	- Actuates 5 fingers - Low responding speed and low force as output. - Jointless exoskeleton

PROTOTYPE	Date	Type	Actuation & Transmission	Aim	Other info
A. M. B. Hamid et al [21]	2015	Glove	SMA springs Tendon-driven	Rehabilitation	- Actuates flexion of the index - 2A of current to get a max of 1.6N
HANDEXOS A. Chiri et al. [22] [23]	2009 - 2011	Exoskeleton	DC motor Cable transmission	Stroke Rehabilitation	- Direct match of joint centre. - Lightweight(114,9g) low encumbrance, palm free and fingertips free. - Natural ROM activation of all DOFs. - 3 force sensors, and 2 hall sensors, control system PID. - Underactuated system.
Y. Hasegawa et al. [24] [25]	2008 - 2011	Exoskeleton	DC-motors Tendon-driven	Assistive hand	- Force estimated by an electrode - Index actuated by 3 motors, thumb no motors - 3 active joints for index-ring-little fingers 2 active joints for thumb. - PD-control system actuated by EMG signal - DC motors
K. Y. Tong et al. [26]	2010	Exoskeleton	Linear actuators	Stroke Rehabilitation	- VCR, underactuated portable system. - Max force 23N. - Adjustable fingers length. - Controlled by EMG
AFX C. L. Jones et al. [27] [28]	2010 - 2012	Exoskeleton	DC-motor Tendon-driven	Stroke Rehabilitation	- Lightweight: 138g. - 3 PID control (real-time control), optical encoder gives a joint angle feedback. - Rotational axis aligned with the human ones. - Control in torque, position, and real time control implementation.
AFX T. T. Worsnopp et al. [29]	2007	Exoskeleton	DC-motor Tendon-driven	Stroke Rehabilitation	- Independent control of each joint. - 4 section connected in series. - Control in position and force based on sensors. - Rotational axis aligned with the human ones.
A. Lince, N. Celadon, A. Battezzato [30]	2017	Exoskeleton	Motor 4-bars linkage Tendon-driven	Stroke Rehabilitation	- Underactuated system, each finger has 4 revolute joints chain - Simpler, lightweight (390g) - Control based on EMG

PROTOTYPE	Date	Type	Actuation & Transmission	Aim	Other info
A. Wege and A. Zimmermann [31]	2007	Exoskeleton	Motor Bars linkage	Stroke Rehabilitation	<ul style="list-style-type: none"> - Actuates five fingers - Force sensors integrated - EMG sensors
H. Kawasaki et al. [32]	2007	Exoskeleton (Robot)	Motor Bars-linkage structure	Rehabilitation	<ul style="list-style-type: none"> - Each finger joint actuated by a servomotor - Control system based on sensors - Self-motion control
J. Arata et al. [33]	2013	Exoskeleton	Pneumatic actuation	Stroke Rehabilitation	<ul style="list-style-type: none"> - Three-layered sliding spring mechanism - Compact lightweight - Actuates five fingers.

Table 1 Comparative table

2.3 Mechanical structure

A hand exoskeleton is a kind of robotic device also called active orthosis. It is directly connected to the human hand and the exoskeleton mechanical structure together with the hand anatomic structure composes a single dynamical system where forces and torques are coupled [12]. The hand exoskeleton is mainly developed for rehabilitation and assistive purpose and it has to match requirements in terms of wearability, avoid pain elicitation to the user, and the mechanical structure of the exoskeleton has to be designed to guarantee the hand dexterity. In order to meet this objective, the artificial system should match the physiological articular DOFs to guarantee the mobility of the system [7]. Moreover, based on the research carried out by P. Heo et al., to ensure user safety in case of rigid linkages exoskeletons, their centre of rotations have to be coincident with the axes of the articulations joints.

The exoskeleton mechanism of a single finger is considered as a constructive unit. It is possible to focus on the index to analyse the different existing implementations since it is the only finger present in every (or almost) hand exoskeleton structure, and typically the other fingers implementations follow the same structure as the index [12]. Exoskeletons can be classified according to their mechanical structure. The most important and common solutions are represented in Figure 2.

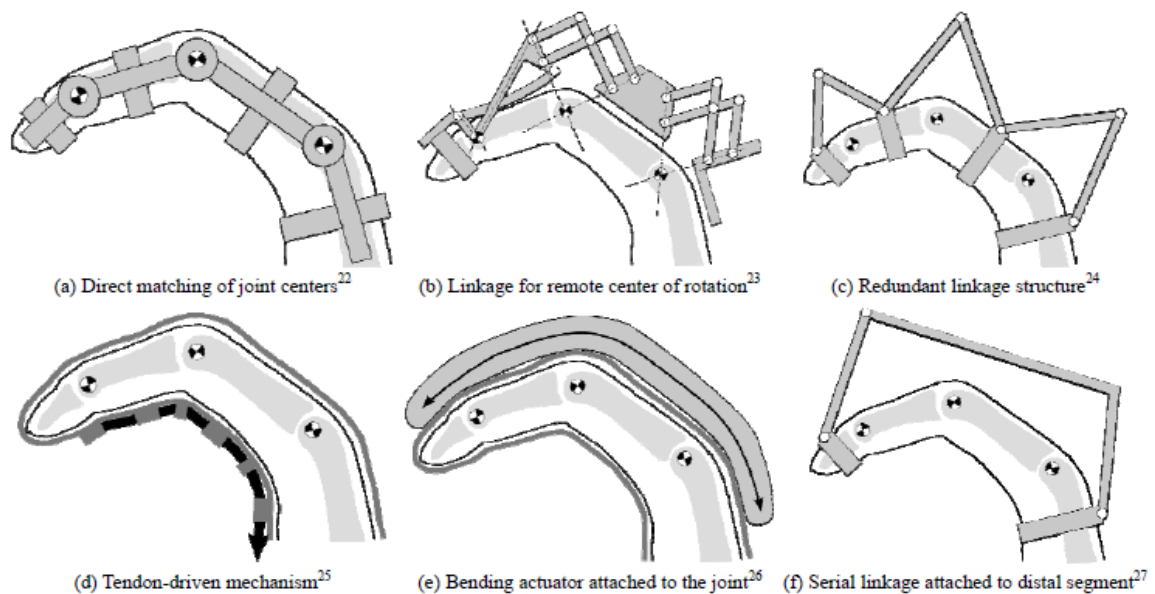


Figure 2 Main mechanical structure for matching the finger range of motion (ROM) [7]

The most intuitive structure to be considered is the *direct matching of the joint centres* (a) of Figure 2. It is the case of the hand exoskeleton developed by Y. Hasegawa [24], showed in Figure 3 on the left. This specific exoskeleton aims at increasing the user fingertip forces. Therefore, using direct matching of the joint centre structure, the palm and fingertips are free, and it allows contact with the environment object. A disadvantage of this mechanical implementation is that the structure is patient-specific since the joint distances depend on the subject phalanx lengths, so it is less versatile and it leads to an increase in total rehabilitation costs [7]. A similar *direct matching of the joint centres* structure is the one realized by A. Chiri called HANDEXOS (right image in Figure 3). In this implementation, the different sizes of the wearer phalanges are taken into account. Indeed, the HANDEXOS can adapt to different patient hand, because the relative distances between the joints can be set thanks to a slider-crank-like mechanism [23]. This solution lets the palm and fingertips free to interact with the environment, but it can be inconvenient for building a multi-fingered structure since it requires physical space between the fingers to locate the joints mechanisms (P. Heo et al.).

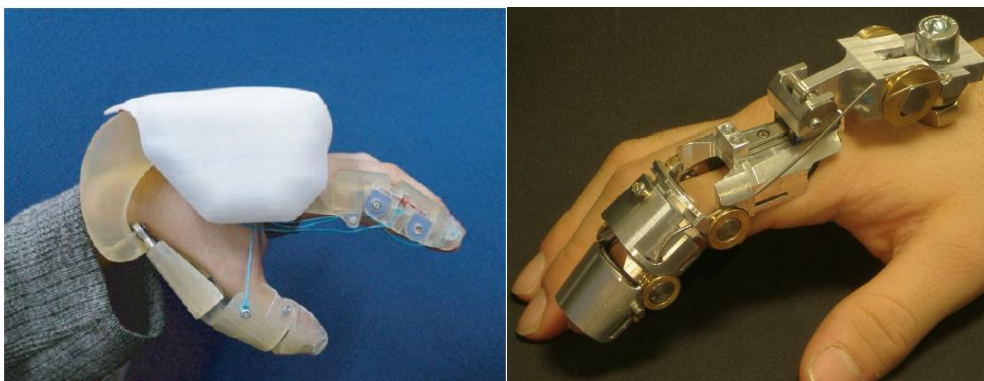


Figure 3 Direct matching of the joint centres. Left Y. Hasegawa [24] Right HandEXOS A. Chiri [23]

In the case of *linkage for remote centre of rotation mechanism* RCMs (b) of Figure 2 (or remote centre of motion RCM), the rigid external linkages only encumber the dorsal side of the hand, so that each finger is free of moving, thus ensuring the full range of motion (ROM) and avoiding interferences with human articulation. Moreover, it allows the wearer to grasp objects with direct contact between hand and environment. This structure is based on the concept of articulation joints matching with the remote centre of rotation (RCR), so the relative rotation axis of the links coincides with the relative

rotation axes of the corresponding phalanges. There exists a different mechanism able to implement this concept. The hand exoskeleton of M. Fontana is an example of this mechanical structure (left image in Figure 4 [16]). It is implemented using the remote centre of the motion system and is composed of two parallelograms connected among them to form a 6 links mechanism. Keeping an extremity fixed, the other can rotate around the remote centre of rotation. This structure is repeated twice to actuate the metacarpophalangeal (MCP) and proximal interphalangeal (PIP) joints. The distal interphalangeal (DIP) joint is actuated using a different implementation, consisting of a RCM as well, but which exploits a crossed parallelogram design [16]. Another kind of RCMs set-up is the one implemented in the hand exoskeleton designed by K.Y. Tong (right image in Figure 4). The remote centre of motion feature is based on the relative rotation of two connected arcs matching the finger joints [26].

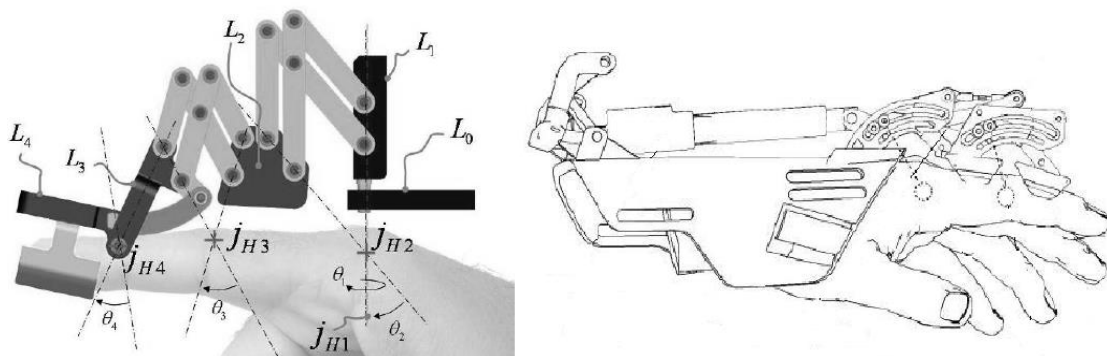


Figure 4 Linkage for remote centre of rotation mechanism RCMs Left M. Fontana [16]
Right K.Y. Tong [26]

This kind of actuation transmission is also used in the case of *redundant linkage structure* Figure 2 (c), also called a 4-bar linkage structure. With this structure, different patients can use the same mechanical design system since it is an adjustable solution independent of the phalanges lengths. Another advantage is that the exoskeleton structure only lies on the dorsal side of the hand, as the previous mechanical set-up of the RCM. The 4-bar linkage mechanism is characterized by two external physical bars, which compose the exoskeleton, and two virtual bars which are the finger bones adjacent to the joint to be actuated [14]. The exoskeleton designed by A. Lince is part of this category (shown in Figure 5). The system is composed of a 4-bar linkage structure

with tendon-driven transmission exoskeleton which provides an active force for the MCP and PIP of four fingers.

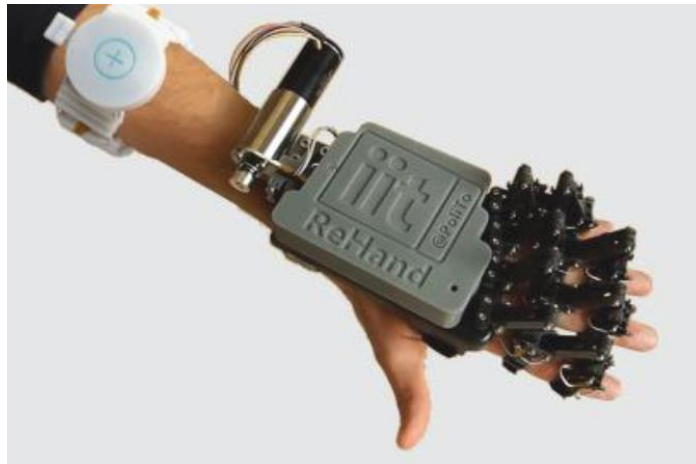


Figure 5 Redundant linkage structure: REHAND A. Lince [30]

The same structure is utilized in the A. Wege and G. Hommel hand exoskeleton, see Figure 6 on the left. More precisely, it consists of a single finger exoskeleton for the middle finger, and it admits a more accurate motion control.

The 4-bar linkage structure is also implemented in a different way in the T. Tang et al. (Figure 6 on the right). This exoskeleton consists of a structure composed of two 4-bar linkage structure per finger actuated independently. Differently from the previous exoskeletons, this utilizes a gear transmission method and a SMA actuation system. These authors prioritize the lightness and portability of the device instead of the single DOF actuation [17].

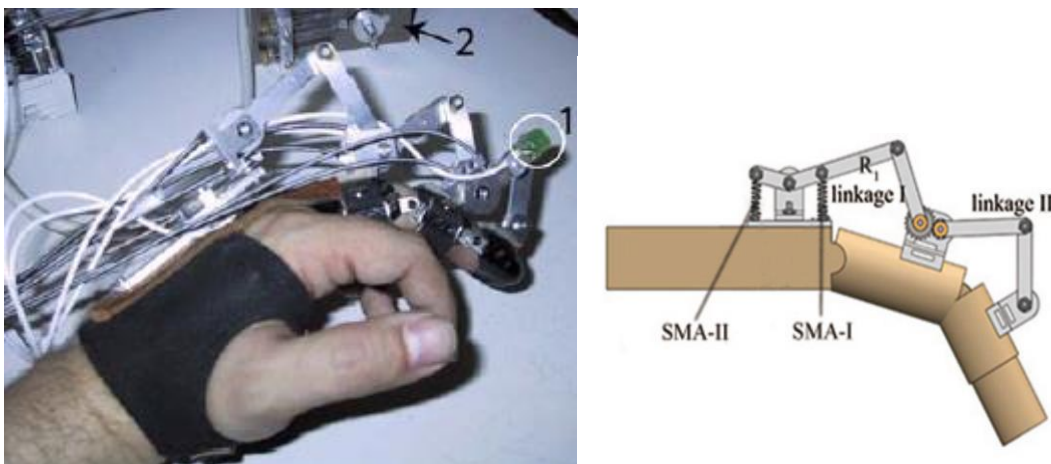


Figure 6 The 4-bar linkage structure. Left A. Wege and G. Hommel [34] Right T. Tang et al. [17]

Finally, the centre of rotation concept can be reviewed. This is the case of a *jointless tendon-driven mechanism* (d), *bending actuator attached to the joint* (e), and the *serial linkage attached to the distal segment* (f) in Figure 2.

These solutions, and in particular the jointless tendon-driven and the bending actuators, are lighter and more compact from the structural point of view because they do not require any rigid structure as it is the wearer's hand which provides the skeletal structure for the motion of the actuated device [7]. For this reason, they are typically implemented on flexible gloves. The complexity of the control system and of the physical structure is reduced since the DOFs to be controlled are less than the articulation joints DOFs. On the other hand, these simplified structures could possibly generate an incorrect motion sequence on the finger articulation. It means that in case of the finger extension, the joint more distant from the wrist is extending in priority with respect to the nearer joint: DIP bends the first, then PIP, and finally MCP. This is a non-physiological sequence, which is to be carefully evaluated. Nowadays it is not known whether an incorrect sequence influences the rehabilitation result, but it can surely lead to joint stress and pain [20].

2.4 Actuator and power transmission

Another important aspect to characterize the exoskeleton is the way it is powered. Based on the specific application, hand exoskeletons can be implemented using different actuators and transmission methods. Nowadays, the principal actuators employed for this purpose are electric motors, pneumatic and hydraulic actuators, artificial muscles, and piezoelectric actuators. A brief overview is presented in the table below (Table 2).

Hand exoskeleton systems	PROS	CONS
Pneumatic and hydraulic	Lightweight and small	Wight and incumbrance
	Velocity performances	Noise
	Reduced weight on locus	Not precise controlled
Electric motors	Power to mass ratio	
	Easy to control	Wight and incumbrance
	Widely available	Low power density
	Low cost	Heat dissipation
Artificial muscles: SMA	High power	
	Lightweight and small	Works at high temperature
	High power weight ratio	Difficult to control
Piezoelectric		High cost
		Noise
		Need amplification unit

Table 2 Pros and Cons of the actuator system mostly used for exoskeleton systems

The devices can have the DOFs independently actuated or be underactuated. The underactuated devices are systems where the number of actuators is smaller than the number of actuated kinematic DOFs of the mechanisms. The wearer's hand and the mechanical structure provide the kinematic constraints for the motion of the exoskeleton device without limiting the hand dexterity [7]. In the underactuated systems, the motion is controlled less precisely, but the device results to be lighter and more compact. An example of a widely underactuated exoskeleton is the one conceived by A. Lince [14]. Indeed, it requires a single DC motor to actuate the flexion and extension of MCP and PIP joints of the four fingers. In order to do that a complex movable pulleys and cables system transmits the motion from the motor units to the 4-bar linkage structure [30].

The motion is mainly transmitted through cables, linkages, and gears systems, or in some specific applications, the actuator is directly connected to the exoskeleton. The linkages mechanism has the advantage of being a robust structure that can provide high power transmission to the phalanges, and its cons are incumbrance and weight. The

cable transmission is simple and can be combined in different configurations as gloves, linkages structures, or in the direct match with the centre of rotation. This transmission is called tendon-driven transmission and is a widely used method because of the advantage of remotely actuate the system, usually on the backside of the hand or on the forearm to reduce the inertia of the movable parts [23]. The tendon-driven actuation can be done either on each articulation joint separately [24], or exploiting the underactuated solution, using a single cable to actuate the whole finger structure [23]. The *electric motors* are the most common way to actuate the hand exoskeleton. The electric motor characteristic is to provide high power actuation, to be available in a large variety of models and sizes, and to be easy to control; on the other hand, their disadvantage is that they could be too heavy and bulky [20]. Electric motors used in this kind of application are mainly the DC motors, ultrasonic motors, and linear motors. In the case of rehabilitation, usually, more than one motor is needed for each finger. For the prototype HANDEXOS in Figure 3, two motors are needed, one for the extension and one for the flexion of the MCP, PIP, and DIP joints. The power generated by the motor is transmitted by cables to the exoskeleton structure. The device made by A. Wege and G. Hommel guarantees the independent actuation of MCP, PIP, and DIP joints both for extension and flexion and it allows the abduction and adduction of the MCP joint (Figure 6). In order to do that, it requires a more complex actuation unit, which consists of 4 independent motors one for each finger DOF and a gear transmission system.

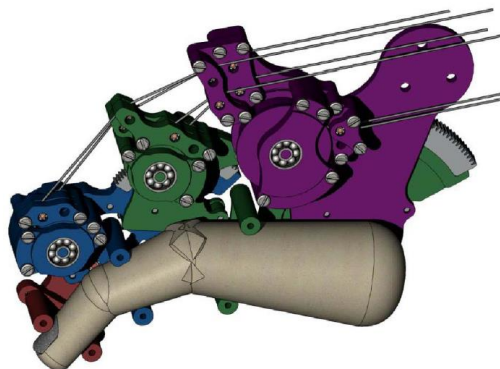


Figure 7 AFX T. Worsnopp et al.'s exoskeleton [29]

The exoskeleton designed by T. Worsnopp et al., reported in the Figure 7, actuates independently 3 DOFs per finger, and requires two motors for each joint, one for the

flexion and one for the extension for a total of 6 motors per finger. Since it means a lot in terms of weight and space, the actuation units are displaced, and the motion is transmitted by cables.

The *pneumatic and hydraulic actuators* are also widely used. Its main advantage is the power transmission implementation which allows a lightweight and small size design as it does not need a rigid structure as support, and it is directly integrated on the hand. On the other hand, pneumatic and hydraulic actuators require a voluminous and noisy unit to actuate and control the system, which is typically displaced in a non-movable place [7]. This actuator-transmission coupled system operates imitating the action of the tendon system of the hand flexor and extensor muscles. Based on the way it is implemented it works as an underactuated exoskeleton, and the single DOFs of the fingers are not precisely controlled, and often this category of power systems are assembled on exoskeletons in which the centre of rotation concept is overlooked. Thanks to its flexibility, in the rehabilitation and assistive hand exoskeleton field, the pneumatic actuation is implemented on active gloves, and they represent the most common actuation method in the soft robotic implementations [35]. This is the case of ExoGlove (see Figure 8) a glove made by customizable pneumatic actuators [19]. It can provide accurate control of each finger separately in an underactuated manner, acting simultaneously on the MCP, PIP, and DIP joints.

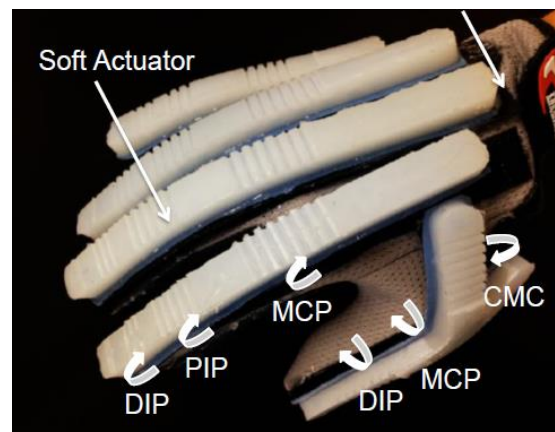


Figure 8 ExoGlove (H. K. Yap, J. H. Lim et al.) [19]

Another remarkable type of actuator is the *shape memory alloy (SMA)* which is part of the *artificial muscles'* category. In the case of the exoskeleton actuator, it is usually

implemented as a straight wire or as a spring. An example of exoskeleton actuated by SMA is the prototype of T. Tang et al. in Figure 6 in which the SMA springs are directly connected to the rigid links, and a gear system transmits the motion to the articulation joints. To actuate the prototype a current flows through the SMA spring, which changes its properties moving the linkage structure and so the MCP and PIP joints. The SMA actuator is also used in the case of tendon-driven systems. This is the case of the exoskeleton designed by J. Yang, J. Shi and H. Xie, a jointless tendon-driven system that could be implemented as an active glove. This system is actuated via a combination of series of SMA springs, and is able to transmit the correct physiological moving sequence to the fingers [20].

2.5 Sensor and control

Sensors and control are fundamental aspects to correctly actuate the exoskeleton. Sensors are used to measure the mechanical or biomedical signals, and report the values to the control system which elaborates and implements the exoskeleton actuation. In these implementations, they are mainly used for three purposes. First, they can be used to sense the human intention to actuate the exoskeleton. Secondary sensors are used to generate feedback signals to guarantee a correct force generation and proper motion of the devices considering the mechanical parameters of the parts. Finally, the sensors are intended to monitor and do some study on the exoskeleton and human interaction. Based on the exoskeleton aim, different strategies can be implemented. To control an exoskeleton aiming to assist patients it is necessary to detect the user intention of motion and to transmit the signal to the control unit. The controller amplifies the user muscular force actuating the exoskeleton so that it allows the user to perform the desired action. The most direct method is to place sensors on the exoskeleton and measure the force the user exerts at the interface of the mechanical structure. This kind of implementation measures force signals to evaluate the patient's intentions directly from the hand to be assisted. This is the case of the assistive exoskeleton implemented by L.A. Martinez et al. in Figure 9, where force sensing resistors (FSR) are used directly on the fingertips of the patient to sense their intention. FSRs are resistive sensors that

measure the pressure applied to it and modified their resistance proportionally. Other sensors are fixed on the mechanical structure to measure the exoskeleton joints angles and are used by the controller as a feedback signal to correctly control the motor position. These data are compared in the controller which sends the signal of actuation after a defined threshold on the signal generated by the FSR sensor [36].

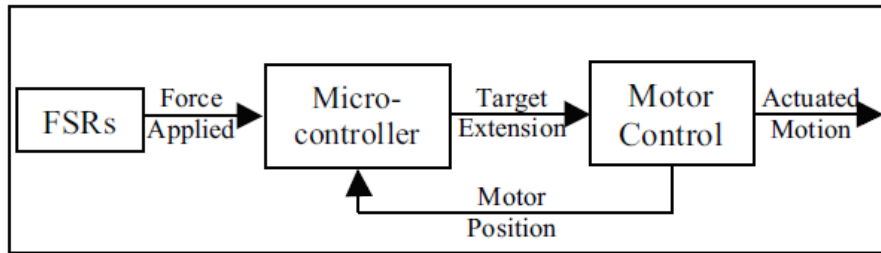


Figure 9 L.A. Martinez et al.'s control system [36]

In the case of *rehabilitation*, the control strategy implementation usually is organized as a hierarchical two-layer control, and for this reason, different types of sensors are used in the same exoskeleton to get different signals to control the device.

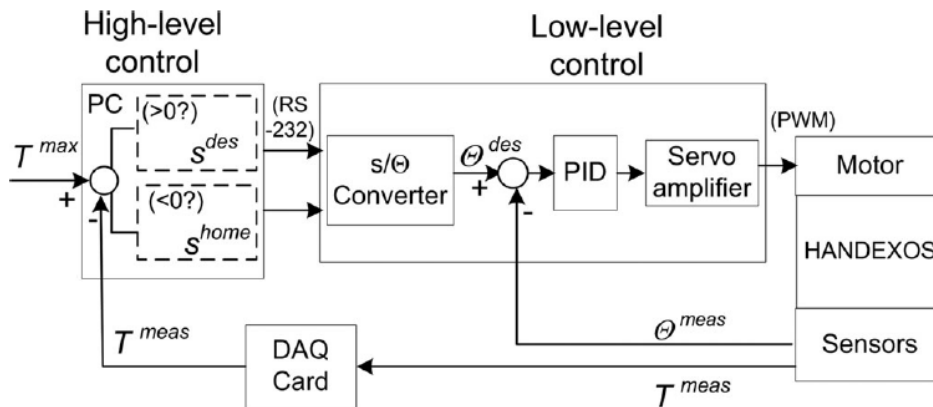


Figure 10 HANDEXOS control strategy (A. Chiri) [23]

In the HANDEXOS prototype sensors are implemented both in the exoskeleton and in the actuator, see Figure 10. Three force piezoelectric sensors are fixed in the internal shells of the exoskeleton to sense the interaction force of the fingers. The control is organized in a hierarchical way, the low-level control is responsible for the position and

is implemented as a classical PID closed-loop control which senses the motor position by the usage of magnetic encoder and drives the motor to the correct position thanks to a PWM current. The high-level control runs on a PC and is used to set the rehabilitative tasks to be performed [23].

Biomedical signals as surface electromyography (sEMG) are often used to drive the control system at the low-level control. Surface EMG is a non-invasive technique to sense the electrical potential of the skeletal muscle's activity [7]. The sEMG sensors are exploited in case of rehabilitation to drive the exercises. An EMG driven control system is implemented to drive the prototype designed by K.Y. Tong [26]. Since the signal is patient-specific and depends on the electrode application, the EMG signal is previously measured on the patient in rest and activation phases in order to calibrate the control action which is implemented based on a threshold. Afterward, the rehabilitation can begin: the surface sensors measure the muscular activity of the injured hand, and based on the signal they get, the controller generates the answer. Different answers can be generated depending on where the EMG is located. Hasegawa uses a similar implementation [24]. The control system is based on a bioelectric potential switching control algorithm based on a threshold. The signal is measured on the surface and based on its amplitude two algorithms can be implemented. If the bioelectric potential exceeds a threshold the grasping force control is implemented, and the wearer's pinching force is amplified so that the patient is assisted in its action. If the signal is lower than the threshold the finger-following control is activated, and the patient is free of movement since the wire of the tendon-driven system is slaked.

Another strategy used to drive rehabilitation is the self-motion control shown in the figure below (Figure 11). Since typically the paralysis does not affect both hands, the patient's healthy side produces the reference motion for the impaired limb. The muscular activity is sensed usually thanks to an equipped glove and the signals are used to drive the movement of the hand to be rehabilitated. In this way, the impaired hand reflects and replicates in a symmetric way the driving hand motion [37] [32]. This strategy is used for the prototype conceived by H. Kawasaki et al. The joints angles of the healthy hand are measured thanks to a data glove. Afterward, the reference joints

angles are elaborated by the control CPU and a PD control sets the joint angles of the impaired hand.

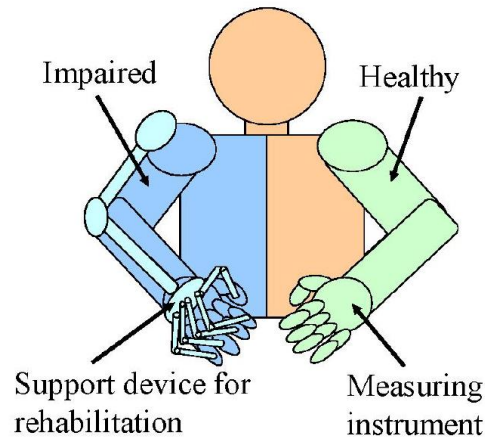


Figure 11 Self-motion control set-up [32]

The biomedical signals are also sensed in order to evaluate the follow-up of the therapy progresses. This is the case of the exoskeleton realized by L. Randazzo et al., which is integrated with an electroencephalogram signal (EEG) used to evaluate the elaboration of the motion in the patient brain during the rehabilitation [13]. In a similar way, the device of A. Wege and G. Hommel exploit the EMG to get data and study the physiotherapy progress of patients [34].

Each exoskeleton is specific in terms of mechanical and actuator unit, and for this reason it needs a specific type of sensing and control systems. In the case of the SMA, which is a nonlinear and hysteretic material, different approaches have been studied to control this material and the most common is still the PID based control. In order to easily set-up the control scheme the SMA element must be actuated using a pulse width modulation inputs, so that it can reduce the total energy consumption and it can be easily controlled [38]. A position-control for the length of the SMA element is realized based on the feedback signal of the electric resistance of the material. This method has been discussed in K. Ikuta, M. Tsukamoto, S. Hirose article. Indeed, the resistance value refers to a ratio of transformation between the two phases of the SMA. So, by monitoring the resistance value of the SMA during the activation it is possible to get the

position of the SMA without making direct measurement of the alloy temperature [39]. This method is not used since the SMA must be positioned in a precise way, and due to hysteresis and aging factors the system must be calibrated before each application. Alternatively, the control of the SMA is done by using PD or PID controllers based on the joint position of the exoskeleton link or based on the exerted force of the user.

2.6 Prototype characteristics

As a result of the analysis of the actual state of the art, the hand exoskeleton prototype characteristics are defined. This hand exoskeleton aims at restoring the dexterity of the hand in patients affected by residual hemiparesis rigidity in post-stroke patients thorough a repetitive rehabilitation movement. The rehabilitation movement consists of an assisted extension and a free flexion of the fingers.

The prototype takes into consideration the rehabilitation for the index and middle fingers as they are the most used fingers together with the thumb. The structure is designed as a 4-bar linkage structure actuated by SMA springs and the motion is transmitted by nylon cable running on pulleys to allow the use of a displaced actuator unit. Superficial electromyography (EMG) fixed on the healthy forearm of the patient controls the rehabilitation actuation thanks to the self-motion control. A threshold algorithm on the EMG signal implemented on an Arduino board drives the actuation of the rehabilitation movement.

The hand exoskeleton characteristics and the motivations of the design choices of the prototype are briefly presented in the table below.

	Prototype characteristics	Motivations
Aim	Stroke rehabilitation	<ul style="list-style-type: none"> • Major cause of long-term hand disability for adults • Useful for all patients with hemiparesis (not only due to stroke)
Finger to be rehabilitate	Index and middle finger	<ul style="list-style-type: none"> • Two of three most used finger to accomplish tasks • Same geometrical structure for both fingers
Mechanical design	4-bar linkage structure	<ul style="list-style-type: none"> • Robust structure • High power transmission • Palm and fingertips are left free • Compatible with different lengths fingers
Transmission method	Pulleys and Nylon cable	<ul style="list-style-type: none"> • Possibility of implementing both flexion and extension • Displaced actuator unit • Underactuated solution
Actuator	SMA springs	<ul style="list-style-type: none"> • Light and low encumbrance • High power weight ratio • Easy to actuate
Control system	Self-motion control based on sEMG	<ul style="list-style-type: none"> • Patients themselves control their rehabilitation • Help to recover of disabled functions

Table 3 Prototype characteristics and the motivations of the design choices

The motivation of each design choice, and the specific characteristics of the design and the realization of the hand exoskeleton prototype are deeply presented in the following chapters based on the three main aspects: Mechanical Design, Actuator and electronic implementation, and Sensor and control.

3 Mechanical Design

The exoskeleton structure is a two 4-bar linkage structure and is tendon-driven by cables. The tendon-driven transmission is considered to work with displaced actuators, so the SMA unit is located on the dorsal side of the hand. The exoskeleton is underactuated, the two considered joints of each finger are coupled, and a single SMA unit moves the whole structure. The 4-bar mechanism has the advantage to be compatible with fingers of different lengths. Due to the reduced complexity of the SMA springs actuator the device is compact and light.

The exoskeleton *working principle* is the following. The exoskeleton has the same architecture structure for each finger and the SMA springs unit actuator is connected to the cable to simultaneously actuate the two fingers together. The actuation action leads the hand to the extended position, according to the rehabilitation goals. When the extended position is reached and the actuator is no longer active, the wearer can flex the fingers and return to the original position with the hand closed. This movement must be autonomously done by the wearer.

3.1 Hand structure

The fundamental element analysed for this rehabilitation exoskeleton is the hand. The hand is a quite complex and fundamental body organ since it is used for the main tasks which interfaces humans with the environment, as grasping objects, and sensing.

3.1.1 Articulation

The human hand is composed of 19 bones, 14 joints, distal to the carpal, and it has more than 20 degrees of freedom DOFs [7].

Index, middle, ring, and little fingers are composed of four phalanges namely distal, intermediate, proximal, and metacarpal, respectively.

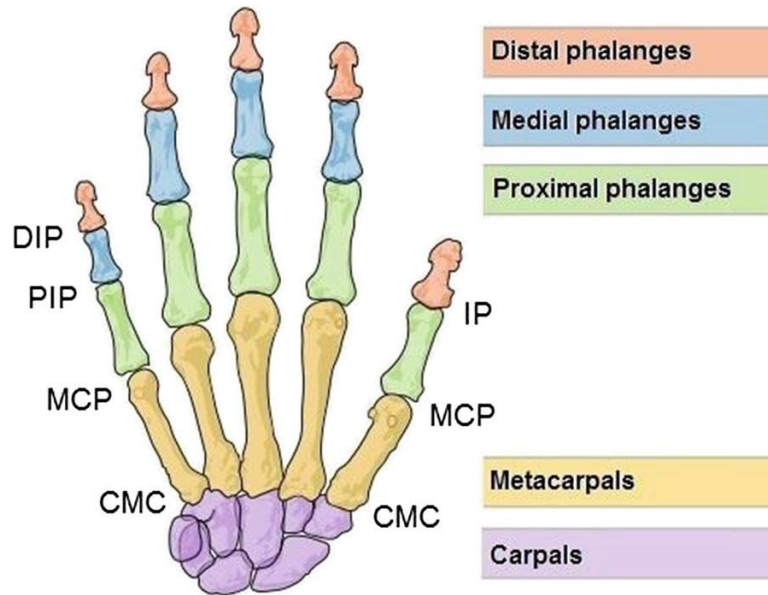


Figure 12 Hand structure and articulation joints [40]

Each of these fingers is composed of four corresponding joints, shown in Figure 12, from the tip to the wrist: distal interphalangeal (DIP), proximal interphalangeal (PIP), metacarpophalangeal (MCP), and humate-metacarpal (HM) near the wrist. The thumb, instead, is composed of three phalanges distal, proximal, and metacarpal phalanges and characterized by three articulations, interphalangeal (IP) metacarpophalangeal (MCP) and carpometacarpal (CMC) on the palm [14].

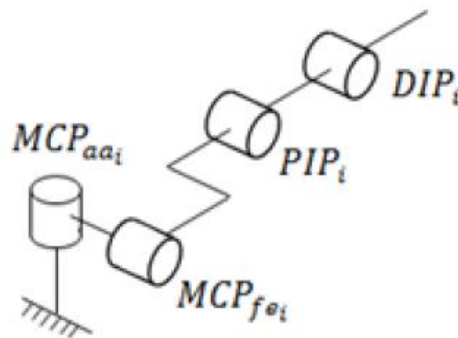


Figure 13 Finger articulation modelled based on the admissible DOFs [30]

As shown in Figure 13, the MCP joints of the four fingers are classified as ellipsoidal joints and can be modelled by two DOFs joint each, allowing both flexion-extension and adduction-abduction motions (Figure 14). The same motions of flexion-extension and

adduction-abduction are guaranteed for the CMC articulation of the thumb that is classified as a sellar joint. The other articulations corresponding to the IP joints are bicondylar joints with greater congruency between the bony surface [7]. However, for simplicity, they are generally modelled with a single DOF to allow flexion-extension motion.

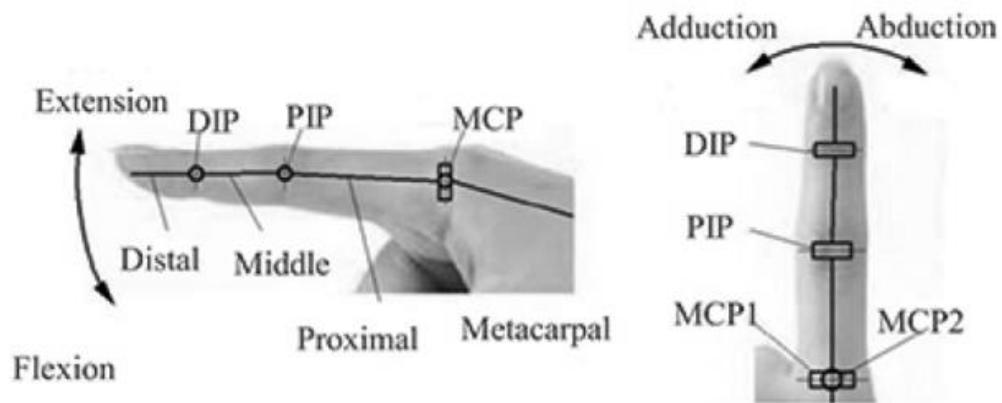


Figure 14 Finger joints and admissible motions [17]

3.1.2 Dimensions

Each finger can be considered as a set of links connected by joints. To understand its behaviour, it is important to focus on the dimensions of the hand and of the phalanges that compose it. Different studies measure the length of the phalanges, considering different reference systems. As Figure 15 shows, in S. R. Habib and N. N. Kamal analysis, the phalanges measures are taken from the point where fingers bifurcate from the hand palm to the following joint, and these lengths are measured on both hands of 159 normal healthy adult volunteers [41].

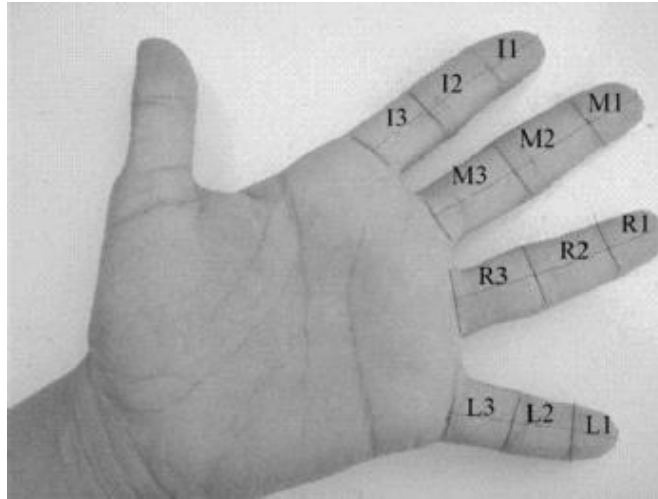


Figure 15 Fingers measures references in S. R. Habib and N. N. Kamal analysis [41]

The results are reported in Table 4 as the mean value of the measurements of long phalanges lengths classified by subject's gender (M: male, F: Female) and sub-classified in right and left hand.

Finger length (mm)		Index			Middle			Ring			Little		
		Distal	Middle	Prox.									
M	Right	23,2	23,7	26,5	26,0	27,7	28,0	22,9	25,6	27,6	19,6	19,2	25,1
	Left	23,2	23,9	26,1	26,0	28,2	27,5	23,0	25,9	27,8	19,5	19,8	14,9
F	Right	22,3	22,4	24,5	24,4	25,5	25,6	21,2	23,4	25,2	17,9	17,4	22,6
	Left	22,0	22,4	23,5	22,4	24,3	25,3	21,3	23,6	24,9	17,7	17,7	22,6

Table 4 Mean values of finger phalanges lengths (M: male, F: Female) [41]

Other studies consider different standards for the measures of the phalanges lengths. In the case of the research of J. Yang, J. Shi and H. Xie, the total lengths of the phalanges are measured as the distance from the finger articulation, and so from the MCP to the PIP and from the PIP to the DIP and from the DIP to the end of the phalanx. In the case of the index finger, the measures are the following [20]:

- Proximal phalanx 45 mm
- Middle phalanx 25 mm
- Distal phalanx 20 mm

3.1.3 Range of motion

Another important aspect that must be taken into consideration is the articulation static constraints which define the hand functional range of motion (ROM). ROMs are defined as the angular range to perform 90% of the hand activities. The following Table 5 shows the angular value referred to each hand joint [14].

Finger	Joint	Flex (°)	Ext (°)	Abd/Add (°)
Thumb	TMC	50-90	15	45-60
	MCP	75-80	0	5
	IP	75-80	5-10	5
Index	CMC	5	0	0
	MCP	90	30-40	60
	PIP	110	0	0
	DIP	80-90	5	0
Middle	CMC	5	0	0
	MCP	90	30-40	45
	PIP	110	0	0
	DIP	80-90	5	0
Ring	CMC	10	0	0
	MCP	90	30-40	45
	PIP	120	0	0
	DIP	80-90	5	0
Little	CMC	15	0	0
	MCP	90	30-40	50
	PIP	135	0	0
	DIP	90	5	0

Table 5 Fingers ROMs [14]

Articulation ROM can be considered as a limitation of the free movements of each joint independently from the positions of the other couplings.

3.2 The exoskeleton system

In this system the first 4-bar linkage structure drives the metacarpophalangeal joint MCP, while the second 4-bar linkage is used to move the proximal interphalangeal joint PIP. To reduce the complexity, the actuation of the distal interphalangeal DIP joint is not considered. The mechanism is called 4-bar because of the presence of two external

linkages R1 and R2 and two virtual linkages that connect the metacarpophalangeal MCP joint with the rotational point on the fixed structures. The first virtual linkage of the first 4-bar mechanism, called P1 in the figure below, goes from the rotational point of the support S1, on the dorsal side of the hand, to the MCP joint. The second virtual linkage P2 connects the MCP joint with the support S2 fixed on the first phalanx (see Figure 16). The same mechanism characterizes the second 4-bar linkage structure and it works for the proximal interphalangeal PIP joint in the same way as the previous structure worked for MCP joint. The names of this second mechanism linkages are the same as the firsts, but with lower case letters.

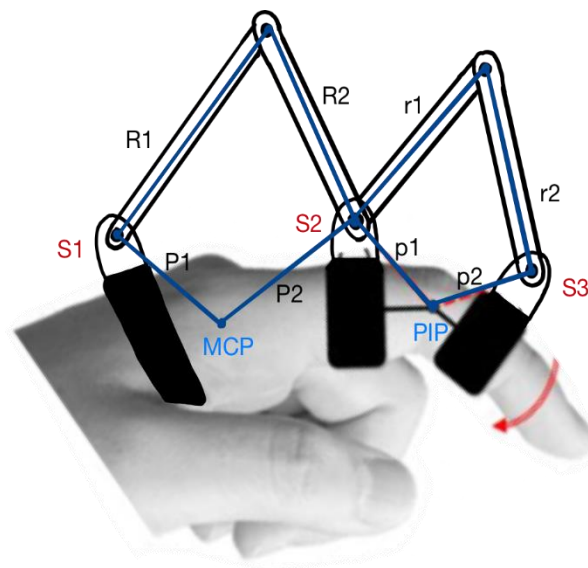


Figure 16 Exoskeleton structure and corresponding names. S1, S2, S3 structural element fixed to the hand. R1, R2, r1, r2 external links of the two 4-bar linkage structures. P1, P2, p1, p2 virtual links of the two 4-bar linkage structures [Source: Author]

The cable-driven exoskeleton needs 5 couples of pulleys per each finger. The pulleys are located two, one on each side of the support structures S1, S2, and S3, two on the coupling between R1 and R2, and two on the coupling between r1 and r2. Based on the way the cable passes on the pulleys the two movements, one of extension and the other of flexion, can be implemented by applying a pulling force on one end of the cable, while the other end of the cable is fixed on the S3 extremity as shown in the figure below (Figure 17) [22].

Both set-up implementations are available, one on each side of the structure, and each one needs an independent cable. The cable for the finger extension is fundamental: it is

connected to the actuator springs and transmits the rehabilitative motion to the whole finger. The cable in the flexion set-up is optional: if needed the cable extremity is connected to passive springs which help the patient to return to the original flexed position in the case he or she cannot perform the movement autonomously. Passive springs could also be inserted at the flexion cable extremities in order to help the SMA recover faster the initial position (see chapter 4.1.2 for the SMA working principle).

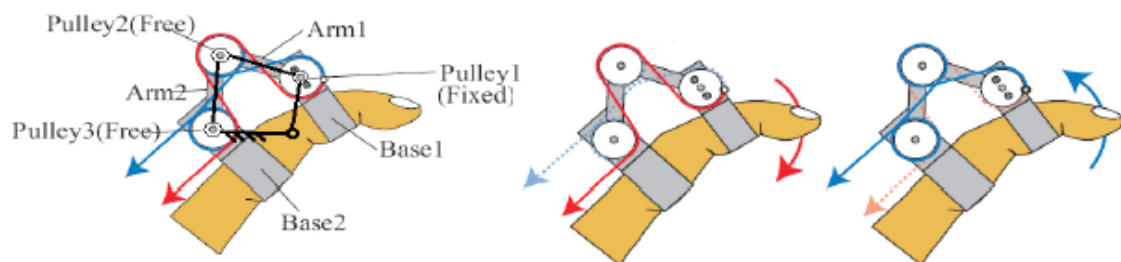


Figure 17 Cables set-up on a 4-bar linkage structure exoskeleton that allows flexion (red cable) and extension (blue cable) [6]

The exoskeleton structure to be built involves two fingers: index and middle finger. In order to evaluate the rehabilitation movement to be imposed by the exoskeleton, it is important to know that the stroke causes a continuous contraction of the hand muscles. Indeed, it is important to remember that the stroke acts as a resistance to the finger extension as if forces of the following values $F_{prox} = 10\text{ N}$, $F_{middle} = 6\text{ N}$, $F_{dist} = 3\text{ N}$ are applied to the centre of mass of each phalanx respectively [22]. For this reason, in this hand exoskeleton for rehabilitation, the main aim is to help and assist the patient with the finger extension starting from the flexed position.

3.3 Dynamic simulations

Dynamical simulations are carried out for evaluating two main aspects:

- to verify if the exoskeleton actuator force is sufficient to overcome the stroke muscular rigidity, with different lengths of the linkage bars;
- to minimize the actuation force by selecting the optimal lengths of the exoskeleton links.

Consequently, it is possible to size the SMA springs actuation unit.

The dynamical simulations are done using Autodesk INVENTOR and the simulations are done for the index and then for the middle finger separately. A hand model is introduced to correctly simulate the interaction between the exoskeleton and the hand itself. In the simulation the stroke rigidity on the MCP and PIP joints is considered as opposing torques applied on the finger joints. The exoskeleton forces are inserted in the model as external forces applied on the exoskeleton structure.

The simulations use a simplified model. The results are only used to evaluate the direction of the motion to understand if the force is sufficient. The magnitude of the angular velocity is considered to identify the best linkage lengths. Therefore, the evolution in time of the joints angles is not significant.

3.3.1 Hand model

To simulate the forces and torques acting between the exoskeleton and the hand, a model of a hand has been done. The hand used for the simulations, is composed of the index, the middle finger, involving three phalanges each, and the “hand-base” which corresponds to the metacarpus of the hand. The phalanges length considered is the one previously presented as the length between the finger joints. The diameter of the index phalanges is measured on four different patients and, the value is kept constant for both fingers, as this value is not particularly significant in the simulation.

The values used in the simulations are reported in the following Table 6. Lengths A corresponds to the lengths measured by S. R. Habib and N. N. Kamal, lengths B refer to the lengths of the research of J. Yang, J. Shi and H. Xie.

	INDEX			MIDDLE		
	Proximal	Middle	Distal	Proximal	Middle	Distal
Diameter [mm]	18	14	14	18	14	14
Length A [mm]	24,5	22,4	22,2	25,6	25,5	23,4
Length B [mm]	45,0	22,4	22,2	51,0	25,5	23,4

Table 6. Fingers lengths of the hand prototype used in the simulations

The phalanges are constrained by the usage of rotational joints since PIP and DIP joints only allow flexion and extension as shown in Figure 14. The hand-base and the first phalanx of the fingers are connected by spherical joints because the MCP also admits abduction and adduction, and the spherical joint is necessary to correctly carry out the simulations.

3.3.2 Simulations set-up

Concerning the exoskeleton, to reduce the complexity only the relevant parts have been considered for the simulations and the structural element S1 is simplified. The whole system composed by the hand and by the exoskeleton models is then assembled.

In practice, for the dynamic simulation, the assembly previously made is opened on the Dynamic Simulation environment on Inventor. In this way, the constraints imposed in the assembly environment are automatically converted into standard joints.

Due to the hyper-constrained model of the two 4-bar linkages, even if the mechanism is able to move correctly, it includes too many loads to be calculated on the joints according to the method used by Inventor. To avoid this problem the MCP joint between the hand-base component and the first phalanx on the index is set as a spherical joint even if only the rotational DOF is actuated. In this way, the mechanism will correspond to the real phalanx movement, and works correctly without any deformation in the parts.

At this point, the forces are imposed. The resistive force acting on the articulation joints due to stroke muscular rigidity is applied as an internal joint moment, with the direction opposing the extension of the finger.

The torques acting at each joint can be computed knowing the phalanges lengths and the force values due to stroke which causes a muscular rigidity of the finger [22]. The computed values are reported in Table 7, and they are computed considering the lengths B of the previous table, since these are the values which refer to the distance between the finger joints. As forces, the same values are used for the calculation of the index as well as of the middle finger torques.

	INDEX			MIDDLE		
	Proximal	Middle	Distal	Proximal	Middle	Distal
Phalanges lengths [mm]	45	22,4	22,2	51	25,5	23,4
Forces at centre of mass [N]	10	6	3	10	6	3
Resulting torques [Nm]	0,225	0,067	0,033	0,255	0,077	0,035

Table 7 Resulting torques on each finger joint due to stroke rigidity

The forces imposed by the exoskeleton transmission cable on the exoskeleton are included in the simulations as external forces of the same value applied directly on the structure supports. The forces directions are chosen according to the direction of the cable that runs over the pulleys.

The simulations are done separately for each finger.

Since the hand exoskeleton structure is actuated by means of a cable, to simplify the model only three forces are applied on the support structures S2 and S3. The force the cable exerts on the structure S1 is not considered because the hand-base is fixed and used as reference for the computation of the joint angles. The model considers that the forces are applied as if the cable passes on pulleys of 10 mm diameter. For this reason, the direction of these forces is coherent with the disposition of the extension cable (reported in Figure 17), and changes according to the position and size of the linkages and phalanges.

3.3.3 Index finger

Figure 18 below represents the set-up considered in the *index simulations* in the INVENTOR environment.

Joint	Maximum Torque
MCP	0,225 Nm
PIP	0,067 Nm
DIP	0,033 Nm

Table 8 Resistive torques for each index joint due to stroke

The black arrows represent the forces applied as external forces by the exoskeleton on the hand, the three values are kept equal to each other in every simulation. On the joints are applied the internal torques corresponding to the value declared in Table 8.

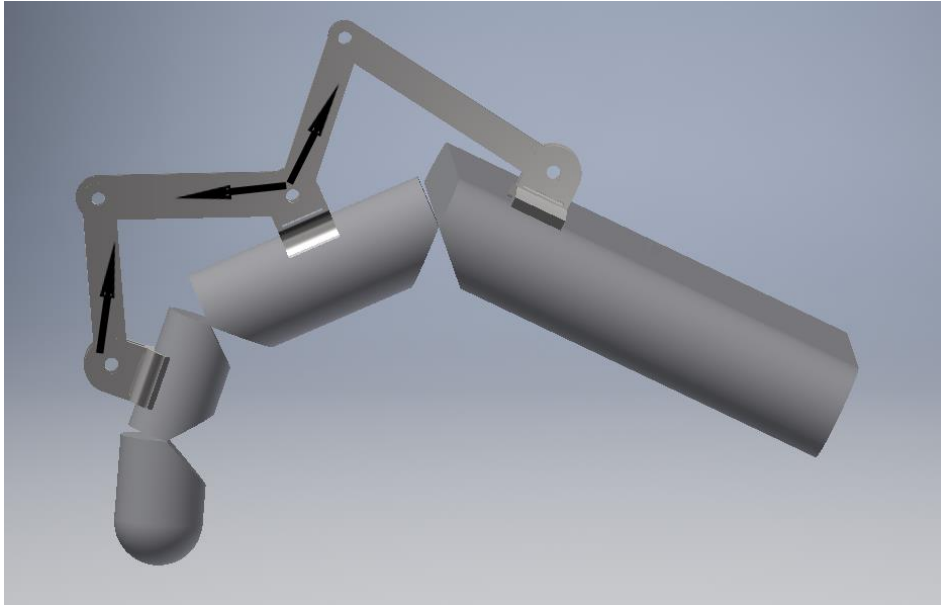


Figure 18 Dynamical simulation set-up for index length B

The *lengths B* are used as phalanges lengths in the model since lengths B are measured as the distance between the finger joints, and this reference frame is more appropriate for this evaluation with respect to lengths A, which consider the distance from the fingers bifurcation (in case of the first phalanx).

The initial linkage lengths are taken from T. Tang et al.'s model of the 4-bar structure used in his exoskeleton [17]. Therefore, initial linkage measures are reported in Table 9.

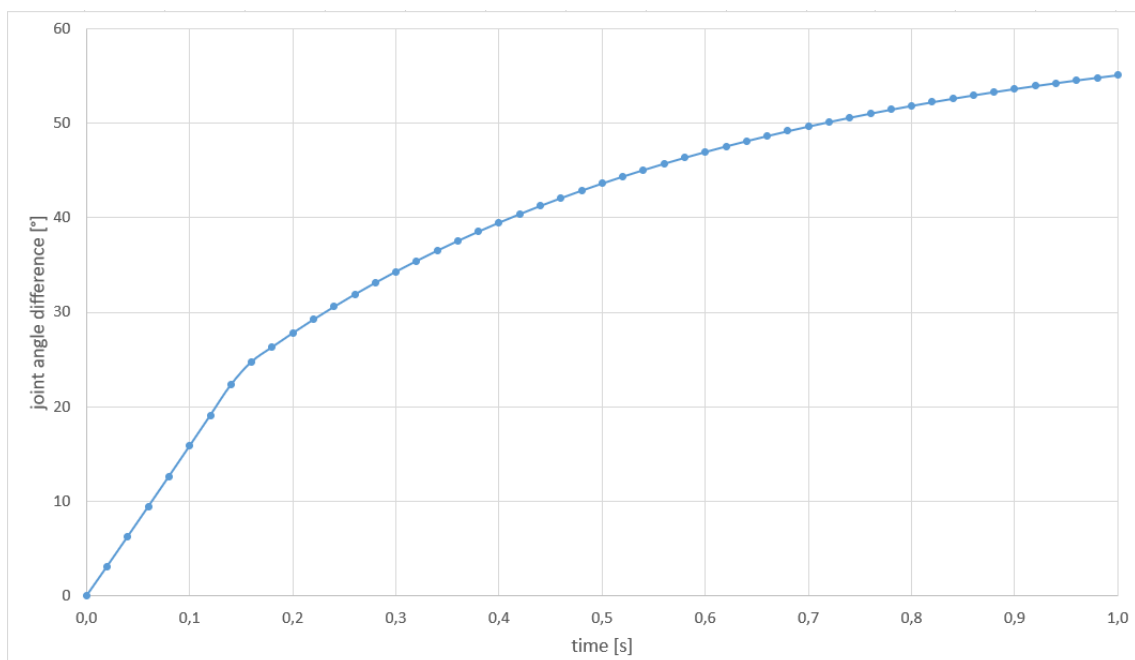
4-bar linkage 1	lengths [mm]	4-bar linkage 2	lengths [mm]
R1	40,0	r1	30,0
R2	25,0	r2	25,0

Table 9 Initial linkage lengths for index simulations

Different dispositions are simulated. By changing the linkage dimensions, the index articulation follows different motion trends.

The initial joint angles are the same for each simulation and is set to a prefixed value corresponding to the flexed position of the finger. The results of each simulation are collected as graphical outputs where the angular positions of the MCP and PIP joints are evaluated in time. The graphs are elaborated to have a final representation of the difference between the prefixed (starting) angle and the final joint angle in degrees ($^{\circ}$). The difference between the initial angle and the final angle reached by the finger joints are evaluated in a simulation time of 1 second.

The simulations are carried out starting from high applied forces of 30 N. These simulations have a graphical output which is divided in two different regions, as the one reported below.



Graph 1 Graphical trends of the first simulation on the MCP index joint

The first region has a nearly linear behaviour and increases the angular value with a constant slope.

To analyse the trends the attention is focused on the first region. The linear data are collected and from that values the parameters of a linear interpolation are computed. The interest of this computation is the parameter correspondent to the slope of the interpolation vector. This parameter corresponds to the average angular velocity of the considered joint, the values obtained from the simulations with the final linkages lengths

are reported in Table 13 for both fingers. As first check, the slope parameter must be positive. If this condition is met, it means that the joints angles are increasing and therefore the exoskeleton forces are sufficient to overcome the stroke rigidity, and as a consequence, the hand is executing the right movement of extension. The force applied by the exoskeleton is then reduced in the following simulations to find the minimum sufficient force able to correctly move the hand. While reducing the applied forces the linear region in the graph widens and the region with lower slope reduces. As a result of this analysis it was possible to verify that, with the linkages lengths of the T. Tang et al.'s model, forces of about 5-7 N are sufficient to move the exoskeleton as requested and to bring the fingers to a fully extended position.

Once the forces are set, the attention focuses on the linkage's lengths. The study is done as before, and the slopes of the linear regions are compared. At first, it is noticed that proportionally longer linkage structures need lower forces to reach the same results. Afterward the linkage relations are evaluated changing the lengths of the single linkages one by one, thus modifying the lengths ratios. As a conclusion the linkage lengths are selected, and the measures of the two 4-bar linkage structure are reported in the following table.

4-bar linkage 1	lengths [mm]	4-bar linkage 2	lengths [mm]
R1	45,0	r1	35,0
R2	30,0	r2	30,0
P1	21,9	p1	19,1
P2	21,3	p2	24,7

Table 10 Measures of external and virtual bars of the index exoskeleton structure

With these final linkage lengths, a last simulation is done to verify the needed actuation force. As a result, the value of 5 N turns out to be sufficient to correctly move the whole structure.

3.3.4 Middle finger

Afterward, the *middle finger* is considered. The forces simulating the cable actions are positioned in the same way as in the index simulations, and the set-up as the previous one in Figure 18 but with the middle finger lengths. In this case, the resistive torques due to the stroke acting on the finger joints are reported in the table below.

Joint	Maximum Torque
MCP	0,255 Nm
PIP	0,077 Nm
DIP	0,035 Nm

Table 11 Resistive torque for each middle finger joint due to stroke

Also in this case, for the same reason explained above, the phalanges length used in the simulation refers to lengths B of Table 6. To design the external linkage lengths of the middle finger the idea is to relate proportionally the results obtained from the previous index simulations with the actual phalanges lengths, in order to have an initial measures reference. The same forces identified for the index finger are taken as initial force value for the dynamic simulation of the middle finger, as the range 5-7 N seems to be a reasonable guess.

Several simulations are done to verify the behaviour of the middle finger exoskeleton. The procedure utilized in case of the middle finger analysis is the same as the one previously made for the index. After some analyses, the final values in the case of the middle finger linkages lengths are defined and the two 4-bar linkage values are reported in the following Table 12. The results in terms of lengths relations between linkages obtained in this case correspond with the ones previously obtained for the index.

4-bar linkage 1	lengths [mm]	4-bar linkage 2	lengths [mm]
R1	50,0	r1	40,0
R2	35,0	r2	35,0
P1	22,7	p1	19,2
P2	21,9	p2	25,8

Table 12 Measures of the external and virtual bars of the middle finger exoskeleton structure

It results that in terms of forces the 5 N obtained for the index are confirmed for the middle finger.

	Index		Middle finger	
	MCP	PIP	MCP	PIP
5 N	23,2	14,7	28,2	8,4
7 N	28,2	17,9	31,5	11,9

Table 13 Average angular velocity of the joints [°/sec] with the applied forces of 5 N and 7 N, considering the exoskeleton structure with the selected linkage lengths

Also in this case, the average angular velocity of the MCP and PIP joints of the middle finger final structure subject to the resulting forces are reported in the previous Table 13.

3.3.5 Simulations considerations

In addition to the two main goals described above, the simulation model has been used to perform some additional verifications valid in the case of both fingers.

- First, it is analysed the influence of the distance between the support structures S1, S2 and S3 and the hand joints on the slope parameter. It is verified that even if the structure is displaced of some millimetres the results are still coherent. This is an important result, since fixing the mechanical structure on the patient hand cannot be highly precise and it depends on the set-up phase and by the fixing method of the Velcro straps.
- An additional analysis is carried out, and an important consideration is made. Even if the lengths of the phalanges changes of some millimetres the simulation slope follows the same trend. This is a positive outcome as it shows that the exoskeleton can be worn by patients with different hand sizes, but it still satisfies the fundamental aim of hand extension require by the stroke rehabilitation.

In addition to the specific results obtained for the index finger and for the middle finger separately, described in the two paragraphs above, it is possible to draw some remarks by comparing the two sets of results together:

- i. The two 4-bar structure designed for the index finger and for the middle finger result to be proportional to length of the respective finger, but in both cases the

minimum sufficient force to correctly actuate the structure can be considered as 5 N. This means that the two fingers can be actuated by means of a single actuator unit and in particular by a single transmission cable.

- ii. It is possible to notice that once the structures are defined, the index finger and middle finger average velocities are similar in case of MPC joints and PIP joints. This means that when actuated, the two fingers will move together.
- iii. The average velocities of the MCP joints are higher than the average velocities of the PIP joints. According to these simulations, when the exoskeleton is actuated the first phalanges will reach the extended position before the second phalanges. This result matches the correct physiological movement of the finger extension.

As a conclusion, and in particular from point *i* above, it follows that the exoskeleton actuator unit can be the same for actuating the two fingers at the same time. Therefore, the force of the actuator shall be 5N per each finger, for a total of 10 N.

3.4 Mechanical drawing

In the present subchapter, the work of mechanical drawing of the exoskeleton components is described. The drawing activity refers to the final prototype, realized of aluminium and 3D printed PEGT parts. A preliminary prototype, made of standardized modular bars, has also been realized in the first phases of the project in order to have a physical model for preliminary considerations on the structure and its mechanical characteristics. The components of this first prototype have also been drawn, and 3D printed but describing their drawing is not deemed necessary.

The exoskeleton mechanical structure is drawn using Autodesk INVENTOR® Professional. The detailed drawings of the elements presented below are grouped in the Appendix 1 CAD drawing.

Three support elements and the linkages are drawn.

3.4.1 First support S1

The *first support*, called *S1* and shown in Figure 19, is the element fixed on the dorsal side of the hand-base and is used as reference for the movements of the other parts.



Figure 19 Inventor model of the structural element S1 [Source: author]

Starting from the right-hand side of Figure 19, there are two couples of rounded supports with a central hole. The hole is the centre of rotation of the first external links of the 4-bar mechanism, both for the index and for middle finger.

The distance between the two supports of the same couple must be sufficient to host the first link R1. The distance between the first couple and the second couple of supports must be sufficient to contain the two internal pulleys.

On the left hand of support S1, lies a plate with 5 holes with diameter $\varnothing = 2$ mm. These holes are the ones where the SMA springs unit and the optional passive springs must be fixed.

Since the support S1 hosts the SMA unit it must be sufficiently long to allow the complete extension of the SMA springs. Some studies are carried out to size the support. First, the lengths difference of the transmission cable during the actuation is analysed. The cable set-up analysed is the one corresponding to the extension movement (blue cable in Figure 17). The cable path is computed in the two extreme configurations of extended and flexed finger both for the index and the middle finger, Figure 20 shows the consider cable set-up.

The trigonometric calculations are done starting from the values of the exoskeleton linkages, previously reported, and a diameter of the pulleys corresponding to $\varnothing = 12$ mm. The other measures, as the heights of the structures S1, S2 and S3 are taken from the following models. The difference in lengths of the cable in the extension configuration during the extension of the fingers is about $\Delta x = 20$ mm for both fingers.

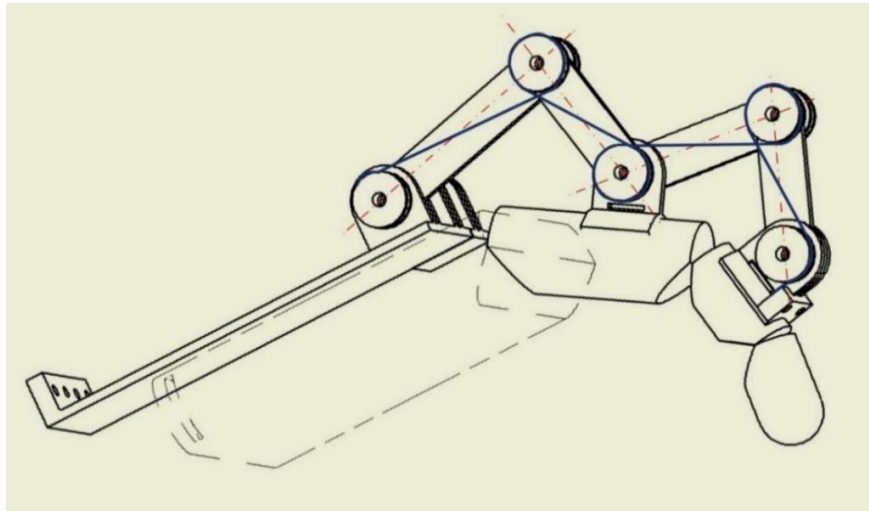


Figure 20 Cable path considered for the evaluation of the cable lengths

Afterward, the mechanical and geometrical characteristics of the selected actuators are considered, as the SMA spring lengths in the compressed configuration and the space required by the fixing elements. As conclusion the total length of support S1 results in $l = 94 \text{ mm}$.

3.4.2 Second support S2

The *supports S2* are two supports fixed on the first phalanx of the respective index and middle finger and are shown in the figure below (Figure 21). A hole is present on the top of the structure, thus the first and second 4-bar linkage mechanism have a coincident axis on it. A rectangular slot is present in the lower side, to let a Velcro strap through to fix the structural element to the patient finger. The lower part is made with a cylindrical shape to fit the fingers.



Figure 21 Inventor model of structural element S2 [Source: author]

3.4.3 Third support S3

The *supports S3* are two supports fixed on the second phalanges of both fingers. As shown in Figure 22, these structural elements are similar the S2 supports. The only difference is that these structures are the ones where the cables terminations are fixed to. For this reason, an additional flange is added on the external side of both S3 support structures. On the flange two holes are located to fix the cable ends.



Figure 22 Inventor model of structural element S3 [Source: author]

3.4.4 Cable set-up

In order to actuate two fingers with a single actuator unit, the extension cable (the blue cable in Figure 17) must be the same cable for index and middle finger. The cable passes from the extremity of support S3, fixed at the end of the index, through the SMA actuator unit, to the other extremity of the S3 exoskeleton on the middle finger. The actuator unit is equipped with a hook connected to a pulley which allows to redistribute the cable forces when actuated.

Since the cable responsible of the extension is the same for both fingers, it is convenient to let it run in the internal side of the exoskeleton that is in the space facing the two fingers as shown in Figure 23. Therefore, the two independent cables for the passive springs will be placed on the external side of the exoskeleton (if included).

The four link bars R1, R2, r1 and r2 are connected by bolts and nuts to each other, to the pulleys and to the support structuresFigure 23.

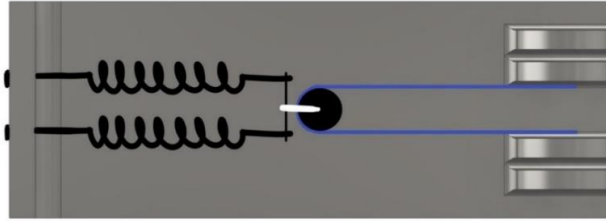


Figure 23 Extension cable and SMA springs set-up on the support S1. From the left two SMA springs (black), the hook (white), the pulley (black) and the extensor cable (blue).

3.5 Prototypes realization

Based on the previous studies and simulations, two mechanical prototypes are mounted starting from the model designed on the Autodesk INVENTOR® and represented in Figure 24.

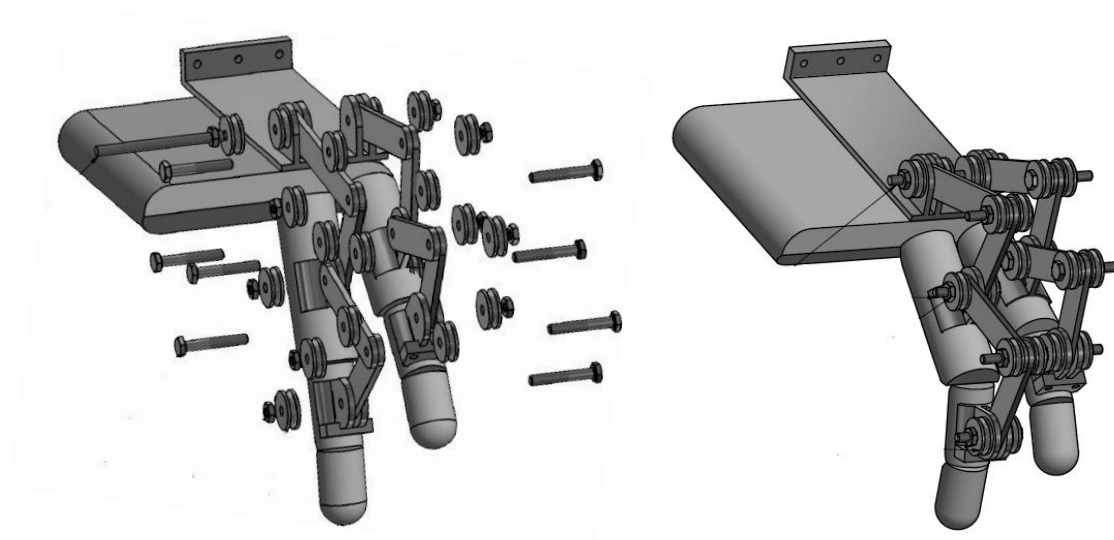


Figure 24 Mechanical model of the exoskeleton designed on the Autodesk INVENTOR

3.5.1 The first prototype

The *first prototype* is entirely composed of plastic elements, the bolts and nuts being the only metal elements in this prototype.

The structural supports S1, S2 and S3 are 3D printed using the CAD drawings. The material used for the structures is the Polyethylene Terephthalate, also called PEGT. This material has a high flexural modulus of 2100 MPa and resistance to heat distortion up to a temperature of 70 °C.

The links are built starting from standardized pre-drilled bars, for this reason the linkages lengths do not exactly correspond to the ones previously defined from the dynamical simulations. The linkage distance between the connecting holes used for this structure are reported in Table 14.

	4-bar linkage 1	Lengths [mm]	4-bar linkage 2	Lengths [mm]
INDEX	R1	45	r1	30
	R2	45	r2	30
MIDDLE FINGER	R1	45	r1	30
	R2	45	r2	30

Table 14 First prototype external links measures

The main difference between these parts and those presented in the previous sub-chapter is the central hole on the three support structures. Indeed, the pulleys utilized are standard parts with internal diameter of $\varnothing = 4$ mm. For these reasons the whole structure uses M4 bolts.

The exoskeleton structure of the first prototype is shown in Figure 25.

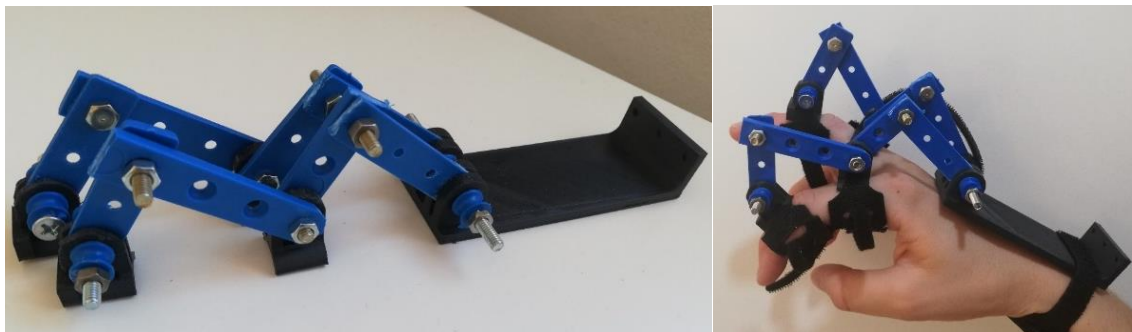


Figure 25 Exoskeleton structure of the first prototype

Bolts and nuts fix the linkages and the pulley to each other and to the structural elements S2 and S3. To connect the finger structure to the support S1 a threaded axis M4 is used. Velcro straps are inserted in the slots obtained in supports S2 and S3 to allow a customized fixing of the structure to the patient phalanges. Support S1 is tied to the hand base by means of two Velcro straps: one on the wrist and one on the hand palm (not shown in the figure).

The correctness of the range of motion of the fingers is verified. Indeed, the patient wearing this exoskeleton can move the two fingers and eight degrees of freedom are guaranteed for each finger: flexion-extension of the MCP, adduction-abduction of the MCP, the flexion-extension of the PIP and finally the flexion-extension of the DIP. This prototype is mounted to visualize the physical exoskeleton and the verify the range of motion of the structure.

Afterward, a more sophisticated prototype is realized.

3.5.2 The second prototype

This *second exoskeleton prototype* is built according to the finalized drawings and is intended to be actuated in real conditions (on-patient) to test the overall functionality of the device.

- As in the first prototype, the support elements S1, S2, S3 are 3D printed of the same material used for the previous prototype. The central hole is $\varnothing = 2$ mm, to use M2 bolts and nuts.
- The pulleys are standard elements made of brass with $\varnothing = 2$ mm bore.
- The exoskeleton links are made starting from a flat aluminium bar of 15 x 1.5 mm cross section. The eights elements are cut using as hole-to-hole distance of the measures obtained from the dynamical simulations. The hole-to-hole distances of each link are reported in Table 15.

	4-bar linkage 1	Lengths [mm]	4-bar linkage 2	Lengths [mm]
INDEX	R1	45	r1	30
	R2	35	r2	30
MIDDLE FINGER	R1	50	r1	35
	R2	40	r2	35

Table 15 Second prototype external links measures

The second prototype structure is represented in Figure 26 below. The pulleys are mounted in the internal junctions of the linkage structure, to facilitate the cable path. The pulleys and the linkages are fixed together with bolts which are tightened with nuts. The bolts heads are positioned in the internal face of the links in order to minimize the

risk of interference of the bolts extra lengths with the motion of the exoskeleton structure.

As in the previous case, the prototype is completed with Velcro straps to fix the exoskeleton to the patient's hand.

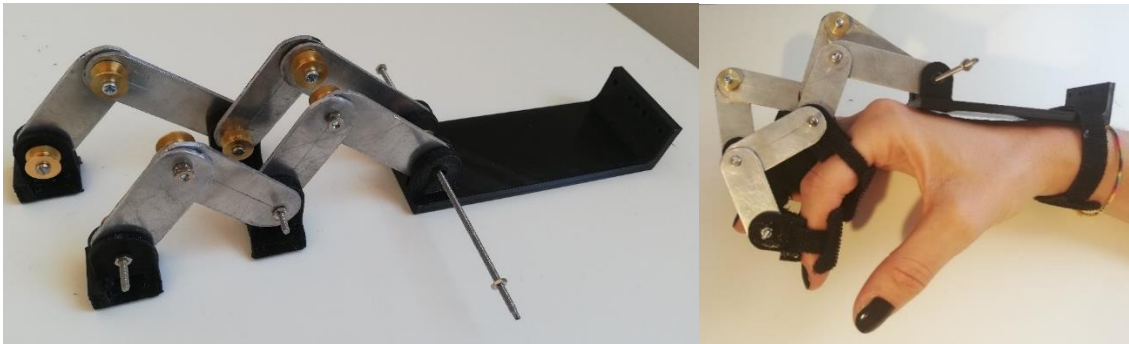


Figure 26 Exoskeleton structure of the second prototype

Also, this second prototype guarantees the fingers DOFs without interference of the parts. A $\varnothing = 1.5$ mm nylon cable is added around the pulleys as previously explained to allow the transmission of the forces in the extension set-up. The nylon is chosen as material for the cable since it is flexible to wrap around the pulleys and it can slide with no significant friction.

The two prototypes are complete under the mechanical point of view.

4 Actuator and electronic implementation

The actuator and its electronic system are presented in this chapter. The mechanical force of the exoskeleton is provided by an actuator unit whose main components are SMA springs. As a result of the dynamical simulation, the needed pulling force is about 10 N and it is transmitted by a cable which actuates both fingers together.

The electronic system is composed of the microcontroller Arduino, the superficial EMG sensor, and a MOSFET circuit that integrates the SMA springs as resistive load.

4.1 The Shape Memory Alloys

As mentioned before, the exoskeleton moves thanks to Shape Memory Alloy (SMA) springs. SMAs are materials that transform thermal energy into mechanical energy. Their characteristic is that when a SMA is exposed to a temperature above a defined threshold for a certain interval of time, it can recover a previously defined shape. These are rather innovative materials whose utilization is increasing in several industrial domains, including the robotic and biomedical field, thanks to their characteristic such as lightness, simple actuation methods and reduced cost.

4.1.1 History and applications

The first documentation on the shape memory alloys dates to the end of the 1930s, but it's only around the late 1960s that the first industrial applications and patents appear, particularly in the military and aeronautical sectors. In the 1970s SMA started to be applied in biomedical applications. Indeed, it was the biomedical industry to first study and utilize the shape memory alloy made by Nickel-Titanium, also called NiTiNOL, for dental applications in 1975. However, the interest of these alloys have increased their application only in recent years, because of the improvement of the alloys characteristics [42]. Some interesting applications are in the aeronautical industry like the modification of the aircraft lifting surfaces to match different flight condition [42]. Other application can be found in the robotic field as the one presented by D. Reynaerts

et al. in the medical application of a worm-like mobile robot used for gastro-intestinal diagnostic and intervention [43]. More applications can be found in other sectors as the military, civil and automotive.

4.1.2 SMA characteristics

The SMA behaviour is based on the *shape memory effect* (SME), which consists in a change of the material properties when the material changes from an initial crystalline structure to a different one. The austenite is the crystalline structure of the SMA at high temperatures, and it corresponds to a body centred cubic crystal form. The austenite is also called parental phase since it is the condition at which the material recovers when heated. On the other hand, the martensite, or product phase, is stable at low temperatures, and is characterized by a face centred cubic structure [44]. When the alloy is in the product phase, (cold condition) the martensite could transition from a twinned state to a detwinned one if a pulling force is applied. The induced stress results in a residual plastic deformation ϵ_r . The SMA reversible cycle is represented in Figure 27.

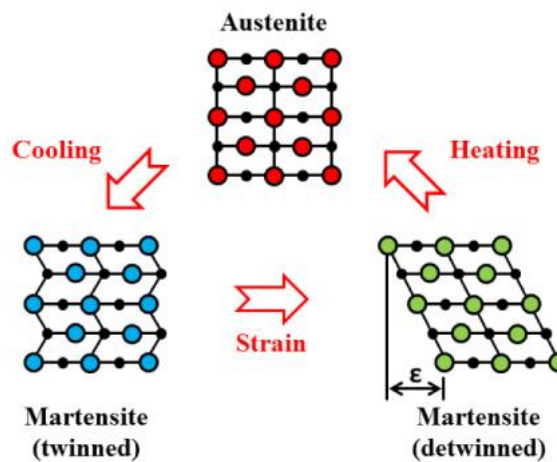


Figure 27 SMA crystalline structure related with temperature and strain [44]

The temperature variation also results in a change of the stress-strains relation, which is strictly related to the material characteristics.

The transition from the plastic deformed phase (detwinned product phase) to the undeformed parental phase is induced by heat and such transition can generate high forces.

Another property of the SMA is called Super-elastic effect and can be observed at high temperatures when the crystal stable structure is the austenite. In this case if a stress is applied the material changes in martensite phase and the material shows a strain. However, this product phase is unstable at high temperature and as soon as the stress is released it immediately recovers the austenite crystalline structure and so the parental shape with no strain, Figure 28.

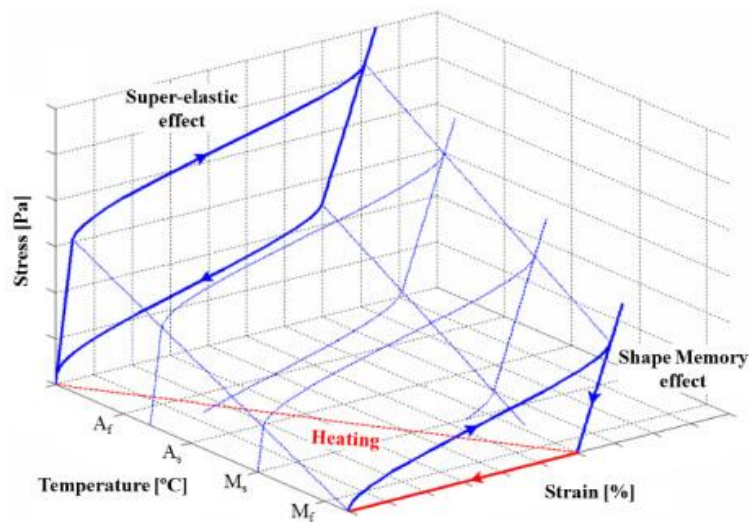


Figure 28 SMA temperature-stress-strain behaviour [44]

The phase transition also implies variations of the material electrical properties like, in particular, the electrical resistivity.

4.1.3 Different SMA types

The Shape Memory Effect (SME) is a property common to a variety of alloys such as Cu-Zn, Cu-Zn-Se, Fe-Mn-Se, Au-Cd. Mechanical and electrical properties change based on the material composition and on the percentage of each component in the alloy.

The alloy most used in robotic applications and most studied today is the nickel-titanium alloy known as NiTiNOL. It is generally composed of 49-57% nickel and the remaining part of titanium, plus other components in residual amount. This alloy is considered one of the smartest materials because of its brilliant capability to recover its parental shape,

and its great mechanical and electrical properties. For these characteristics, NiTiNOL is chosen as the SMA actuator used in the exoskeleton in the present project. Nevertheless, some factors limit its commercial application. Indeed, the total contraction is limited. The material can contract at most 8% of the total length of the wire in the state transition, and, in this condition, it can only endure few cycles before the alloy properties fail. Another consistent limit of the material is that once the SMA is heated, it needs a time interval to completely cool down and recover to the initial crystalline structure before it can be subjected to another heating cycle [45]. The NiTiNOL transformation range in order to modify its crystalline structure is between 50°C to 110°C, indeed the material phase transformation from martensite phase (low temperature) to austenite phase (high temperature) is a process that manifests itself is a range of temperatures [44].

The SMA properties highly depend on their production processes. The NiTiNOL alloy is typically produced by an annealing process at a temperature of the order of 500°C. In this process it is possible to set the alloy geometrical shape. Indeed, the material is produced and can be used in different forms. It is generally available as wire, pipe, springs, and ribbons, depending on application needs. The most used in biomedical applications are springs, with predefined *parent shape* of a compressed spring. When it is required, after a cold deformation, the spring is heated, and it returns to the initial parent shape, by reducing its length and generating high forces. The SMA spring thermomechanical cycle is represented in Figure 29.

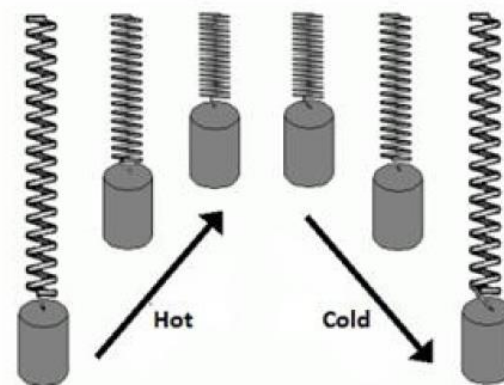


Figure 29 SMA spring relation with heat [46]

4.2 Electronic circuit

A common method to actuate the SMA is letting an electric current flow through the component thus heating the material by Joule effect. In order to easily modulate the amount of energy transmitted to the material a current with pulse width modulation (PWM) is typically used. This consists in a square-wave input with a constant amplitude in which it is possible to modulate the percentage of on-time and off-time in the total period. Indeed, changing this ratio, also called duty-cycle (dc), it is possible to control the total power transmitted to the material, and so to control the heating process. This modulation is easily performed by using a simple MOSFET circuit, which connect the microcontroller PWM output to the circuit.

In the present subchapter, the microcontroller and the MOSFET circuit are described.

4.2.1 The microcontroller

The microcontroller chosen is an Arduino UNO board. It is based on the ATmega328 microcontroller. The operating voltage is of 5 V and the recommended supply voltage is between 7 and 12 V.

This device is chosen since it is a versatile device, easy to implement, and it has pins dedicated to the pulse width modulation generation. In particular the PWM signal used as output is generated thanks to the function `analogWrite()`, and the output signal has the following characteristics:

- Type of signal 8 bits (scale of 0-255)
- Frequency 490 Hz
- ON-time voltage 5 V
- OFF-time voltage 0 V

To program the board an Integrated Development Environment (IDE) is available: the Arduino IDE. In the following chapter the algorithm implementation for the rehabilitation is presented.

4.2.2 Design of the MOSFET circuit

The circuit to control the current flow on the SMA is designed on LT-spice and the schematic is shown in Figure 30.

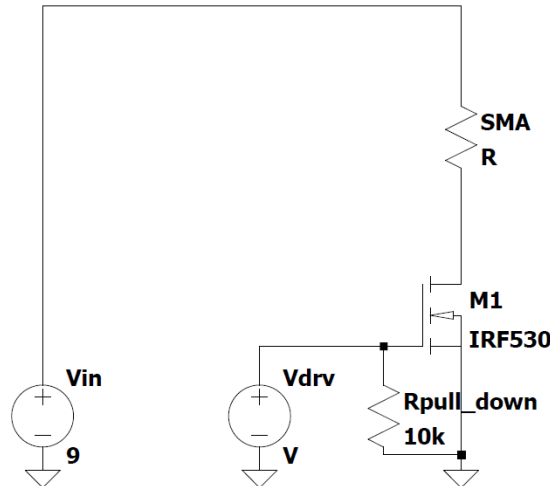


Figure 30 Circuit schematic. V_{in} = power supply voltage, V_{drv} =PWM driving signal, $M1$ =MOSFET IFR530, $SMA R$ = equivalent resistor of the SMA spring.

The first element being considered is the switch. For this scope, a MOSFET is used. This element is chosen since it can directly connect the microcontroller digital output to the electrical circuit. When a voltage is applied between the MOSFET source and the gate pins, the MOSFET closes the circuit and lets the current flow.

The control signal which exits from the microcontroller is a PWM signal. The MOSFET switch opens and closes the circuit according to the PWM frequency and duty-cycle imposed by the microcontroller. The chosen MOSFET is an enhancement n-channel, model IRF530 produced by VISHAY. The data declared by the producer are reported in the table below, and the output characteristic shown in Figure 31.

V_{DSS}	<i>Drain-to-Source breakdown voltage</i>	100 V
$R_{DS(on)}$	<i>Static Drain-to-Source On-resistance</i>	0.16 Ω
$Q_g (Max.)$	<i>Total gate charge</i>	26 nC
Q_{gs}	<i>Gate-to-Source charge</i>	5.5 nC
Q_{gd}	<i>Gate-to-Drain charge</i>	11 nC
$P_D @ 25^\circ C$	<i>Power dissipation</i>	88 W

Table 16 IRF530 MOSFET data

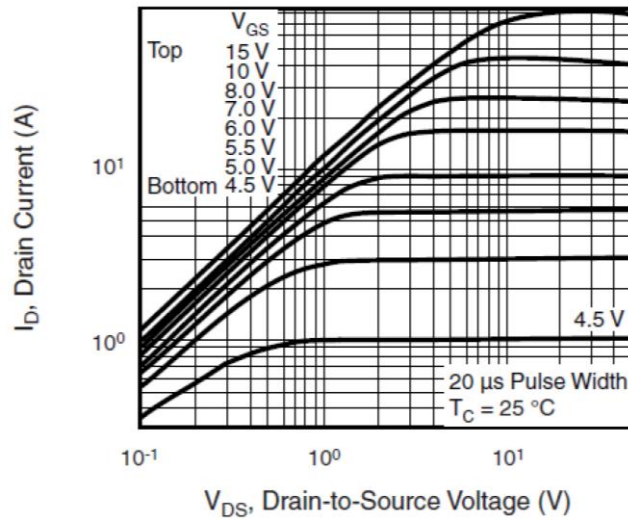


Figure 31 Output characteristic of the MOSFET IRF530 at $T_c=25\text{ }^\circ\text{C}$

The IRF530 has an elevated commutation speed compatible with high frequency and so with the Arduino output signal which has a frequency of 490 Hz. Moreover, the IRF530 activation voltage is compatible with the Arduino output voltage, which has an amplitude of 5 V. Besides, the voltage of the PWM driving signal guarantees a drain current of about $I_D = 3\text{ A}$, as shown in the characteristic curve in Figure 31.

As it is shown in Figure 30, the IRF530 source port is connected to ground, the drain port is connected in series with the SMA springs and with the voltage power supply. Finally, the gate port is connected in parallel to the driving signal of the PWM and a pull-down resistor. The driving signal exits from the Arduino microcontroller whose internal resistance of the pins is of 10 M Ω . Consequently, since it is a high impedance, a pull-down resistor of 10 k Ω is needed to avoid the microcontroller pin fluctuation. This is a phenomenon that occurs when the logic switch of the MOSFET is open and the driving pin of the microcontroller is not connected to grounds. This condition generates noise that can be sensed as a wrong value on the microcontroller pin.

As explained before, the SMA is a material whose electrical resistance varies according to its temperature, so it takes different values during operation. To guarantee a quite constant current flow through the SMA springs, the MOSFET is operated in order to work in the saturation region where it behaves as a current generator. In this condition even

if the resistance load on the drain branches varies, the current flowing through can be considered quite constant. This condition is true as far as the SMA electric resistance is in the order of magnitude of Ohms.

With reference to the circuit in Figure 30, a model is done in order to simulate it and to verify the values of the electric quantities to guarantee its correct behaviour. The model has been realized with LT-spice, and three main aspects are evaluated in simulations:

- the current flowing on the drain branch
- the power loss on the MOSFET
- the pull-down resistance

For these simulations, the SMA spring is represented as a resistor with the constant value of $R_{SMA} = 1.4 \Omega$ as the average of the resistor value of the SMA during the heating process (experimentally obtain).

The driving signal V_{DRV} used in the simulation has the following parameters:

OFF-time amplitude:	0 V
ON-time amplitude:	5 V
Period:	0.002 sec
Rise time:	10 ns
Fall time:	10 ns

The simulation PWM period and amplitudes are set in order to match the Arduino UNO output signal characteristics.

The chosen power supply offers up to 3 A and 9 V. Indeed, a maximum voltage of 9 V is recommended in order to limit the risk of electric shock since the exoskeleton will be fixed on the patient forearm. The duty-cycle is set to 50% to limit the total power transmitted to the SMA resistor.

The following results are obtained as outcome of the simulations:

- The maximum intensity of the current flowing in the SMA resistor in the conditions represented by the model is 2.48 A of amplitude, which corresponds to 1.75 A RMS. Such value is less than the power supply maximum current, thus confirming the suitability of the selected power supply. It is verified

experimentally in the following sub-chapter that this current is compatible with the activation of the SMA.

- The power loss in the MOSFET component are calculated from the following formula:

$$P_{\text{mosfet}} = I_d * V_{\text{ds}}$$

And the resulting value from the simulation is a peak value of $P_{\text{mosfet}} = 13.71 \text{ W}$, such power is under the threshold of maximum power dissipation declared in the component datasheet Table 16.

- At last, it is verified that the pull-down resistor is appropriate. From the vendor it is declared that the resistor can dissipate up to 0.5 W. The simulated peak value of the power is 25 mW. Therefore, there is not risk that the resistor burns.

4.2.3 Realization of the MOSFET circuit

Afterward, the physical circuit is mounted. The MOSFET, the pull-down resistor, and the power supply structures are assembled, and their pins are tin welded. Two terminal blocks are fixed to the board to clamp the cables connected to the SMA spring and to the 9 V power supply. The physical set-up is shown in the figure below.

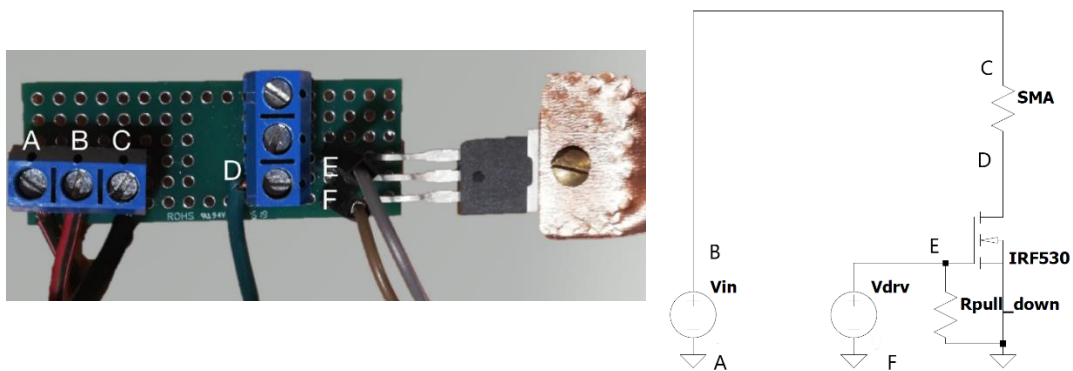


Figure 32 MOSFET circuit set-up

From the left to the right the following connection are made:

- A → Power supply ground (GRD)
- B → Power supply voltage (V_{IN})
- C → Connection to the SMA spring
- D → Connection to the SMA spring
- E → Arduino PWM signal (V_{DRV})
- F → Arduino ground (GRD)

The pull-down resistor is connected from the connecting pin E to the connecting pin F. Even though the power dissipated in the MOSFET is compatible with the chosen MOSFET, a copper heat dissipator is fixed on the MOSFET extremity to avoid the risk of the component overheating.

4.3 SMA characterization

After the design and realization of the electronic circuit, the physical system is completed with the selection of the SMA actuator spring.

The spring selected for the actuation of the hand exoskeleton is a commercial component produced by the company FUXUS of Koeln, Germany. The declared spring characteristics are as follows:

- ID 3300058
- Transition temperature 65 ± 5 °C
- Total contracted length 25 mm (including eyelets)
- Spring diameter 6 mm
- Number of turns 21
- Wire diameter 0.75 mm

Unfortunately, the above technical data declared by the vendor are limited and not sufficient to correctly model the behaviour of the spring and to properly control the whole exoskeleton system. In addition it must be considered that SMAs are innovative materials still produced in relatively small quantities, and that their nonlinear pseudo-elastic thermomechanical response may change depending on several microstructural and macrostructural phenomena [38], with a high sensitivity to the alloy composition and properties of each production slot.

For these reasons, it was decided to carry out a series of tests to characterize the behaviour and main properties of the selected spring. Starting from the consideration that each SMA component is potentially unique in terms of percentage of nickel and titanium, and so in properties and behaviour, the characterization has been carried out on two NiTiNOL springs of the same type.

Two main aspects are studied. The first series of tests focuses on the electric properties, as the variation of the spring resistivity versus the duty-cycle of the driving signal and so versus the current flow is measured. The second series of tests aims at measuring the spring mechanical characteristics and, in particular, the contraction of the spring as a function of the force applied on its extremity and of the duty-cycle of the driving signal.

4.3.1 Measurement of the SMA spring resistance

The aim of the *first set of measurements* is to examine the influence of the current duty-cycle on the spring electric resistance.

The best way to characterize the resistance should be as a function of temperature. However, due to the difficulty to perform a direct measurement of $R = f(T)$ due to the geometry of the spring, it was decided to characterize the resistance as a function of the current flow. The characterization is therefore performed for different values of current duty-cycle, in the temperature steady state condition following the heating transient.

Two sets of measurements are made for each spring. One with the contracted spring, and one with the spring extended to a pre-fixed value of 90 mm, corresponding to a spring total length sufficient to actuate the exoskeleton. This because, as explained in chapter 4.1.2, the strain of the spring influences the crystal phase of the alloy and therefore its macroscopical properties.

For a defined duty-cycle value the circuit is activated. The voltage across the spring and the current intensity are measured at the same time by means of two separate multimeters. From these two measurements the resistance of the SMA spring is computed.

To guarantee a complete cooling of the spring and the recovery of the initial temperature condition, a time interval of 2 minutes is waited between each measurement. In each case, the spring is let free (without applied loads) while cooling down and it is arranged in the experimental set-up once the alloy is fully cooled at room temperature. This process is fundamental not to lose the alloy shape recovery properties.

The room temperature is about 24 °C. The current flowing in the SMA spring is driven by the PWM signal with a frequency of 490 Hz. The 9 Volts power supply and the implemented circuit (described in Figure 30) result in a square wave current of 2.48 A of amplitude, according to the result of the simulation previously made.

Is important to notice that in these measurements the power supply voltage is still constant, and the current amplitude is considered to remain constant too, without taking into consideration the variations of the SMA resistance, because of the current imposed by the MOSFET in case of a fixed value of voltage at the gate-source pin (see the output characteristic of the MOSFET reported in Figure 31).

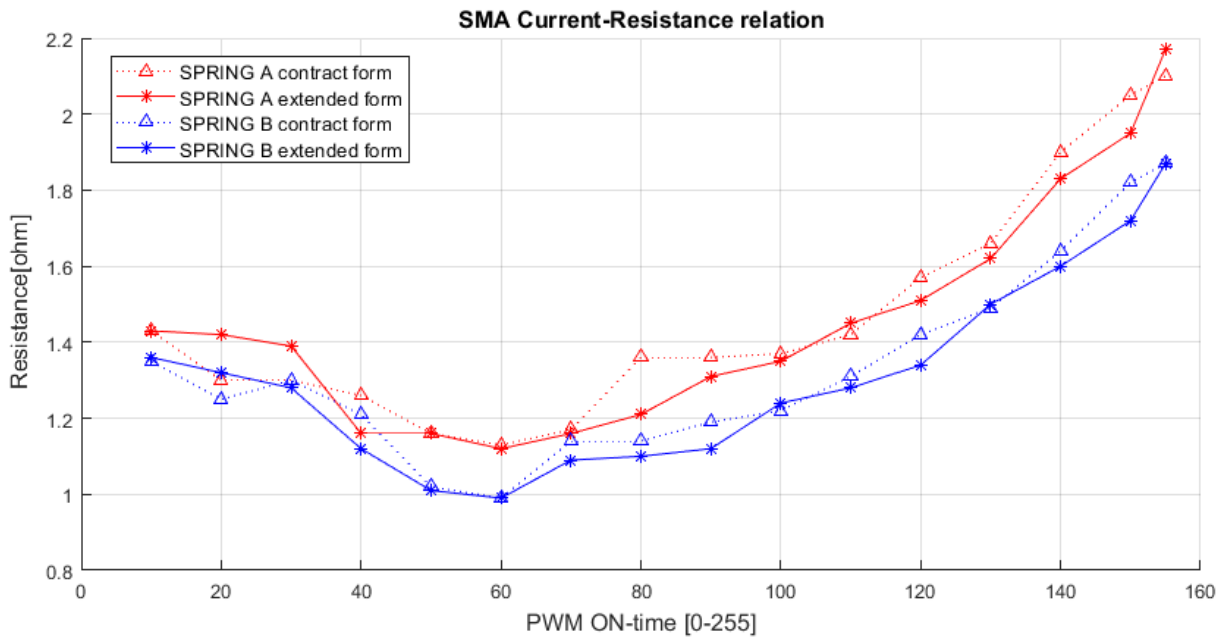
The duty-cycle of the current flowing in the spring is modified for each measurement. Since the PWM signal controlling the current is an 8-bit signal, its range goes from 0 to 255. For simplicity, throughout the following experimental characterization, this scale from 0 to 255 will be utilized to refer to ON-time of the PWM the duty-cycle.

After some qualitative tests to identify the spring proper working range, an ON-time of 155 is selected as the highest value to be used in the experimental characterizations. Since this value is able to correctly satisfy the requirement, it is decided not to exceed it in order to avoid the risk of overheating the components. The measurements are taken for ON-time values that go from 0 to 155 with a constant interval of 10.

Since the SMA properties change according to its temperature, the resistance can be computed from the voltage and the current flowing on it. For these computations, the average values of current and voltage at steady state are taken into consideration. The average values of current and voltage across the SMA springs are measured and the value of the spring resistance for each PWM value is computed. The first set of measurements is performed with the spring starting from a contracted shape (parental shape) and it is let free of movement during the experiment. In the second set of measurements, the spring starts from an extended length of 90 mm, and it is kept constrained to the starting position during the whole heating process.

Both sets of measurements are repeated for the two springs identified as A and B.

The results obtained for each spring in the two sets of measurements are reported in Graph 2.



Graph 2 SMA Resistance with respect to the driving PWM on the SMA springs A (red) and on spring B (blue)

The following remarks can be drawn:

- As expected, the resistance of the springs depends on the current flowing on it. The two springs behave following the same trend; spring A has a higher resistance with respect to spring B, independently of the current and of the set-up.
- At a higher value of ON-time both springs show a lower resistance in the extended position.
- It is possible to notice a minimum of the SMA spring resistance at the ON-time value of 60. According to MacGregor the lower peak on the resistance reached by the SMA corresponds to the SMA temperature where all the material is in the austenite form. After that temperature, the resistance increases again proportionally to the increase of the SMA temperature [45]. Indeed, it seems that the driving signal of 60 PWM at the steady state condition is enough to reach the temperature that completely transform the material from the martensite to the austenite phase.

Another interesting evidence was observed during the execution of the tests: during the temperature transient, before the spring reaches its thermal steady-state, the reading

of the multimeter display showed large fluctuations. This fact can be probably explained by the phase transitions of the SMA crystalline structure, from martensitic to austenitic, which happens in a non-continuous and non-homogeneous way. This effect is not evident in the reported data, as the measurements are taken at thermal steady-state.

4.3.2 Measurement of the SMA spring contraction

In the *second set of measurements* the deformation of the SMA springs during a heating cycle is measured, as a function of the force and of the duty-cycle of the PWM.

The two springs A and B are studied separately. One extremity of the spring is fixed to a vertical structure, and at the other extremity, a weight is hung by means of a nylon cable. Both extremities of the springs are connected to the circuit through electric cables to allow the current flow through it.

The upper extremity of the spring is fixed to the set-up fixture support by means of a bolt, together with the lug of the electric cable.

The lower moving spring extremity is connected to the alimentation cable by means of an alligator clip. A light and flexible electric cable is chosen, in order to minimize the influence, it can cause to the movement of the spring during the measurements.

The spring initial length is set to 90 mm because this is the sufficient length to actuate the exoskeleton. During the experiments, the SMA is actuated with different values of PWM, and with different weights hung on the extremity and the contraction value is measured. The ruler used for the measurement of the spring contraction is fixed on the structure and its scale has a resolution of 0.5 mm. The measurements are repeated for five different weights corresponding to forces applied on the spring from 1 N to 5 N (comprehensive of the fixing elements). The set-up is shown in Figure 33.

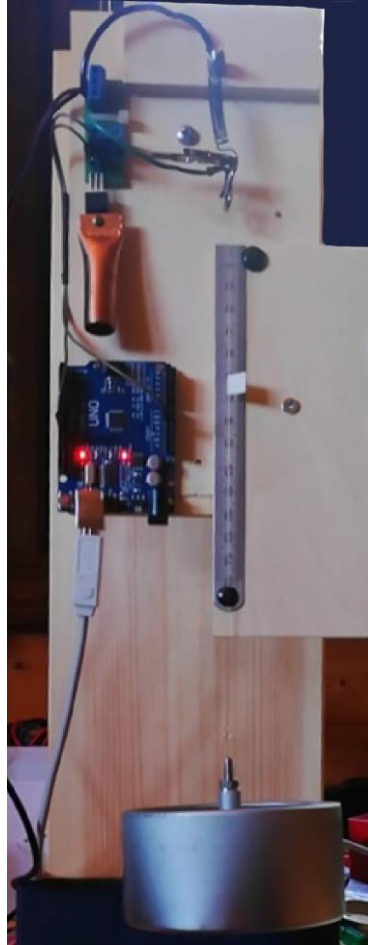
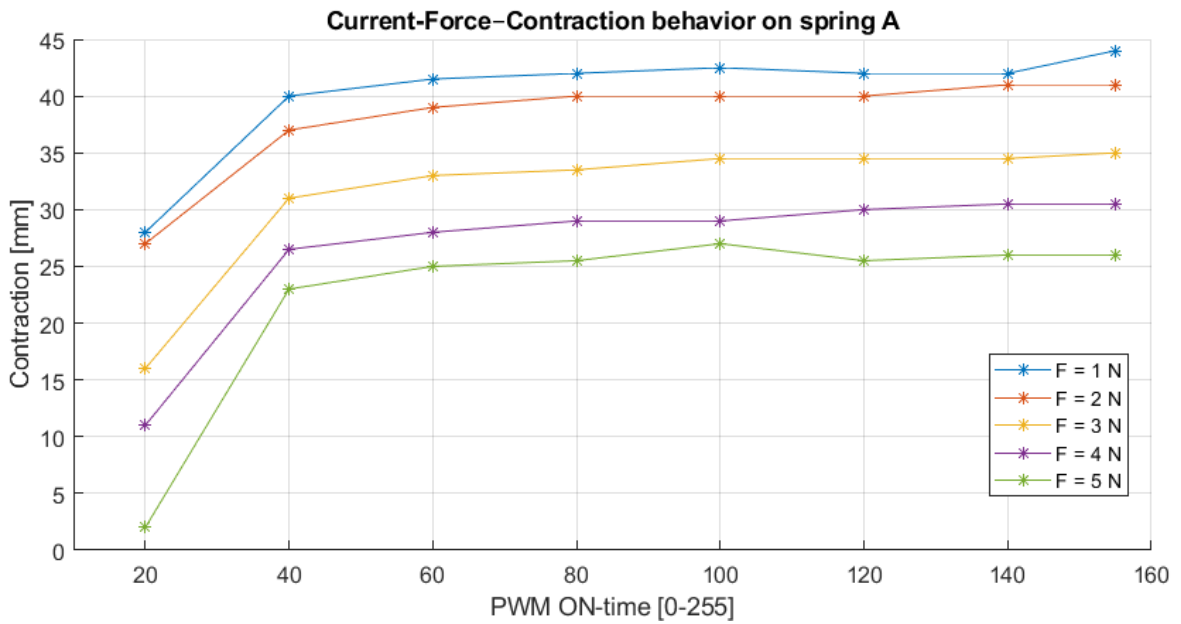


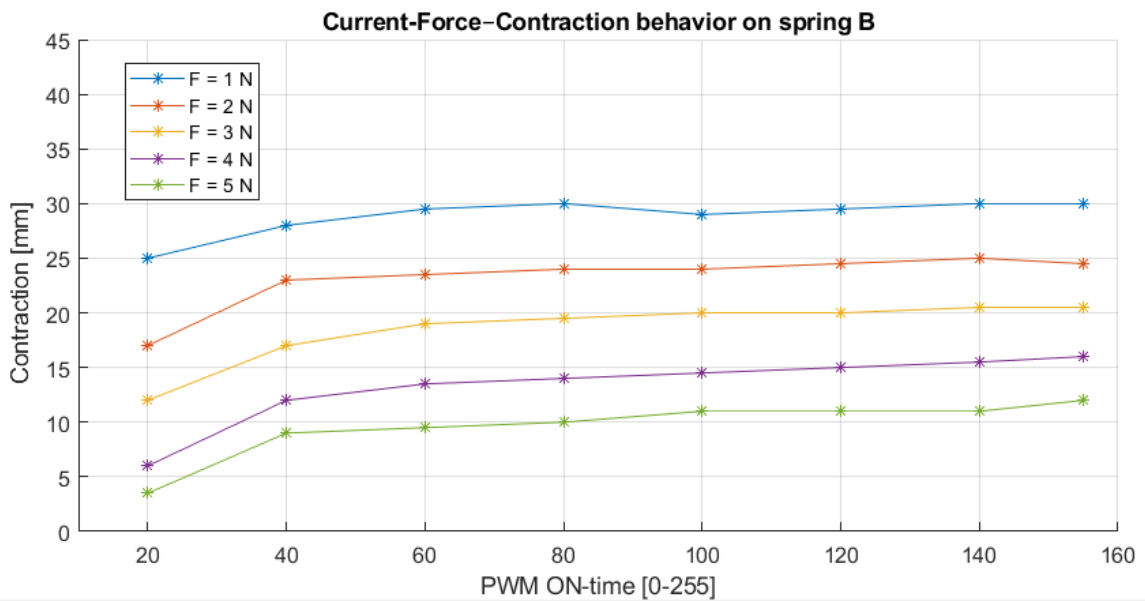
Figure 33 Experimental set-up to measure the SMA spring contraction with respect to the PWM and the force applied to it.

The duty-cycle value of the current flowing on the SMA spring is modified for each measurement. Considering 155 on 255 the highest admissible ON-time value for the PWM as explained before, the measurements are taken from 0 to 155 with a constant interval of 20. A time interval of 2 minutes separates each measurement to let the SMA spring cool down to the same initial ambient temperature of 24 °C. The cool down process is made with the spring free of movement: the weight is detached from the spring, to let the alloy return to its original martensite phase.

The values measured during the experiment are reported in the following graphs representing for each applied force the contraction at each value of PWM. Graph 3 shows the data regarding spring A and Graph 4 shows the ones related to spring B.



Graph 3 Contraction of the SMA spring A with respect to the PWM and the force applied



Graph 4 Contraction of the SMA spring B with respect to the PWM and the force applied

The two SMA springs have the same behaviour. Higher is the force applied, lower is the contraction of the springs.

In any case, the springs generate enough force to lift the weight under any different combination of applied forces and current duty-cycles, but below a certain PWM duty-cycle, the contraction of the springs significantly reduces. This behaviour is due to the fact that low duty-cycle is not enough to generate elevated heat on the alloy and

consequently not enough to reach the activation temperature of the whole material. Therefore, the spring is not able to recover the parental shape and to generate the complete contraction. These results confirm the observation done in the electronic analysis regarding the complete alloy transformation in the austenite phase at a value of PWM ON-time of 60. Indeed, around an ON-time of 60 both springs are able to recover almost completely their original shape, and so to return to the austenite form, with only a limited variation of the deformation for values of duty-cycle above 60 (a maximum difference of about 2.5 mm).

Moreover, when the spring is subject to a current flow with a low duty-cycle, it employs a higher amount of time to reach a steady-state condition. This is not evident in the graphs, but it is observed during the execution of the tests.

Finally, the measurements show a higher force generation for spring A with regards to spring B.

4.4 Integration of the actuator unit on the prototype

The current-force-contraction tests have shown that each spring can generate approximately 5 N with a deformation of around 25 mm. Since to operate the exoskeleton 10 N with a spring deformation about 20 mm are required (see chapter 3.4, and chapter 3.3.5) both SMA springs are needed.

A solution for the actuator unit is designed: the two SMA springs are placed in parallel under the mechanical point of view so that they can generate a force up to 10 N and a contraction about 20 mm. From the electrical point of view, the two springs are arranged in series so that the same current flows in both springs. Due to the output characteristic of the MOSFET (Figure 31) at constant driving voltage V_{GS} in the saturation region, it is possible to consider as heating current I_D flowing through the two SMA springs, the same current value previously considered in the simulations and tests with only one spring. Indeed, considering the resistance of a single spring as in the previous LT-spice model $R_{SMA} = 1.4 \Omega$ the current difference flowing on the drain branch from a model with a single spring ($R_{SMA} = 1.4 \Omega$) with respect to the model with two springs in series

($2 * R_{SMA} = 2.8 \Omega$) is about 3%, so the current flow on the SMA springs can be considered the same as the one considered before and the previous analysis are still considered valid.

Thanks to this design the alimentation cables are connected at the same side of the structure where the springs extremities are fixed, letting the other two extremities free of movement. The free-of-movement spring extremities are connected to a threaded brass shaft, which guarantees the current flow. The springs are fixed by nuts at the two extremities of the shaft, so that the two springs have enough space to extend and contract without interfering each other during the process.

To simulate the correct movement of the actuator unit the SMA springs are mounted on a wooden board and the exoskeleton behaviour has been simulated as shown in Figure 34. A pulley is connected to the shaft to distribute the actuator force between the two actuated fingers.

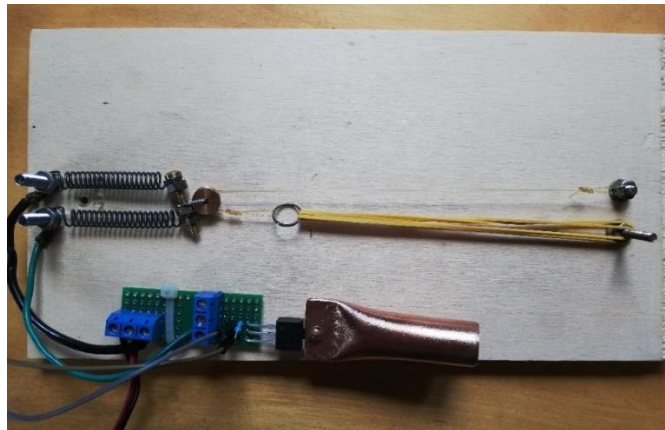


Figure 34 Experimental set-up of the two SMA springs in electric series and mechanical parallel to simulate the actuation unit of the hand exoskeleton

The set-up confirms the correct flow of the current through the SMA springs and the contraction of the actuation unit at the movable extremity. However, as previously remarked, the two SMA springs do not contract simultaneously, as the spring A moves faster.

Finally, the actuator unit is mounted on the mechanical structure of the hand exoskeleton, Figure 35. The electrical cables of the circuit are connected to the

extremities of the SMA springs by means of the same bolts which hold the springs to the support S1.

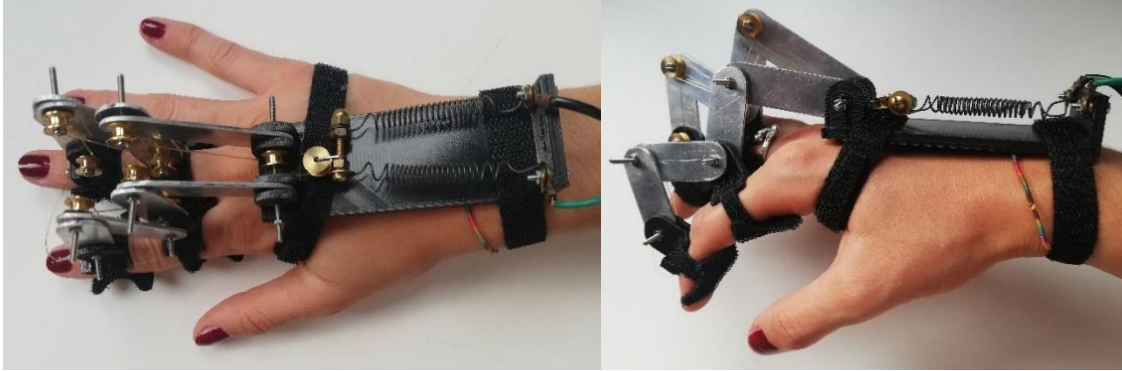


Figure 35 Actuator unit and transmission system mounted on the mechanical structure of the hand exoskeleton

On the other side of the actuator unit, the nylon cable goes to the exoskeleton of each finger running onto a pulley, coaxial with the rotation axis of the first linkage (R1). This axis sets the limit for the spring elongation. Since the cable is under strain, the two springs are suspended on the structure S1. Avoiding the contact between the springs and the structure is an important objective because the SMA can reach high temperatures, which can damage the 3D printed structure. Therefore, care must be taken in the connection between the fixed extremities and the electrical cables. In the prototype shown in Figure 35 a washer and an additional nut are inserted in order to avoid a direct contact between the heated part and the plastic support. For a next step prototype, a tightening solution which provide at the same time a good electrical as well as thermal insulation shall be implemented.

The exoskeleton is worn on a right hand and is actuated to verify its correct behaviour (the set-up is reported in Figure 36). To drive the actuation a PWM with an ON-time of 155 is applied. During the operation, the SMA springs heat up and the exoskeleton extend the index and middle fingers.

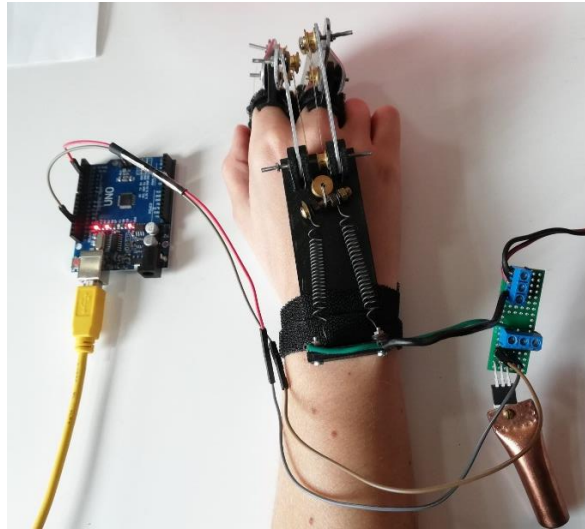


Figure 36 Integration set-up of the mechanical structure of the exoskeleton and its actuator unit and electronic circuit

This last test represents only a qualitative test, but it provides an overall confirmation of the completeness and correctness of the work performed so far. The exoskeleton correctly fits the hand, in a sufficiently tight and stable way, also during the application of the actuator force.

5 Sensor and control

To sense the patient's intention and to drive the actuation of the hand exoskeleton, the self-motion control and a *superficial electromyographic sensor* (sEMG) are used.

The activity of the extensor muscles is sensed as an electric signal which is detected by the superficial EMG, and when the movement is sensed the control algorithm implemented on the Arduino board evaluates the signal received and drives the actuation. The control algorithm is based on a threshold control which activates the extension of the patient's fingers of the injured hand when the patient activates the mirrored extensor muscles on the healthy forearm.

5.1 Superficial electromyography

The superficial electromyography (sEMG) is a non-invasive detection method used to sense the myoelectric activity, which is the bioelectrical potential which drives the muscular activity during contraction.

5.1.1 sEMG signal

By reading the muscular biopotential it is possible to monitor the contraction of the muscle fibres, which makes this signal useful in order to control the hand exoskeleton. Based on the specific muscle to be monitored, the EMG sensors can be positioned in different parts of the body and different muscular signals can be withdrawn, and from the analysis of the sEMG signal it is possible to estimate the forces exerted by the specific muscles. In the case of a hand exoskeleton, the muscles to be monitored are the ones located in the forearm, which control the fingers movement. In particular, the muscular fascicles responsible of the finger flexure are located in the internal (palmar) side of the forearm, and the muscular fascicles responsible of the finger extension are located in the external (dorsal) side (see Figure 37). Since the exoskeleton studied in this project is focused on the rehabilitation of the finger extension, only the muscle fascicles located on the dorsal side of the forearm are to be sensed.

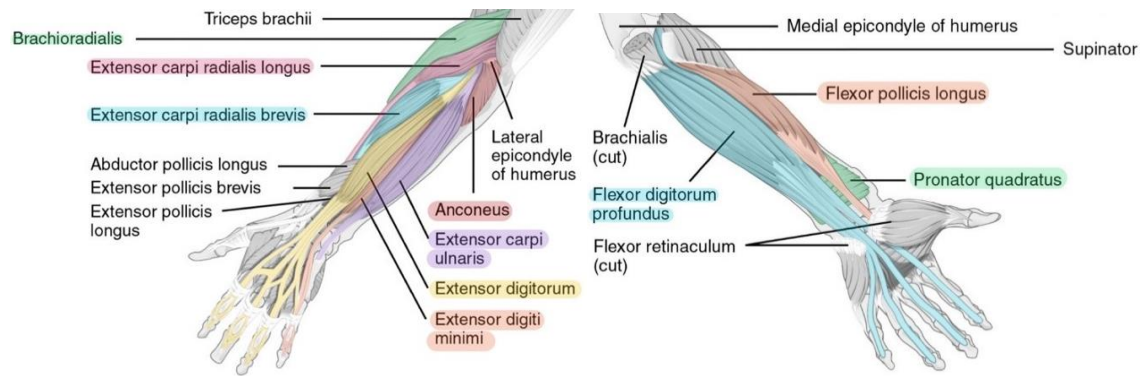


Figure 37 Skeletal muscles on the forearm: on the left the dorsal representation of the forearm muscles, on the right the palmar one [47]

However, it must be kept in mind that most stroke patients have unilateral impaired muscular activity. This means that the finger extensor muscles of the injured arm might not be suitable for withdrawing the EMG signal. In this case, the EMG signal can be sensed from the healthy arm: the exoskeleton replicates the movement of the healthy hand on the injured hand, thus working in a mirror way. This control method is the so-called self-motion control.

The sensing electrodes for electromyography can be arranged in different configurations, such as in single differential or dual differential mode, can be placed at different interelectrode distances, may vary in terms of material used, and so on.

The electromyograph selected for this work utilizes three sensors in order to measure two electric potential differences. In particular, two electrodes are to be positioned on the extensor muscle fascicle to sense the muscular biopotential, and the third electrode is positioned as reference for the sEMG signal in a neutral, bony position where no specific muscular biopotentials are present, such as the elbow or the wrist.

The reference electrode is necessary because the superficial EMG collects the muscular signal on the skin above the muscular fascicles under exam, so the background muscular activity is also sensed. The reference electrode is used to eliminate the common muscular electrical noise from the signal collected by the sensing electrodes.

Indeed, in addition to information related to the biopotential of the muscle, the sEMG signal contains a lot of different information. Therefore, the EMG signal withdrawn by the electrodes needs to be processed and analysed. This is done by means of an electronic board, which is responsible for filtering and conditioning the signal, removing

the noise, and amplifying the output according to the requirements. A typical block schematic of the EMG board is shown in Figure 38 [48].

After processing, the biopotential signals of the sensed muscle is translated into an output voltage, typically represented graphically as [mV] vs. time [sec].

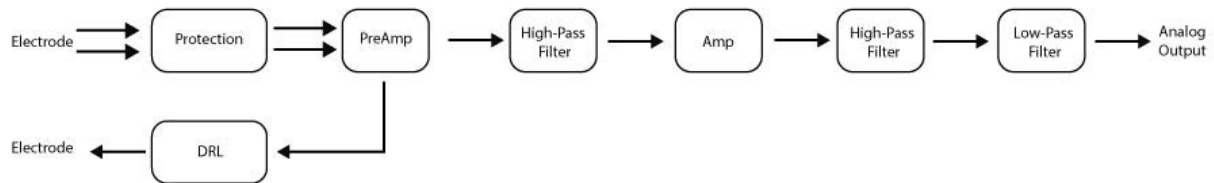


Figure 38 Block scheme of the filter and conditioning chain in an EMG [48]

1. **Protection:** Provides ESD (Electrostatic discharge) protection, Overvoltage protection, and Overcurrent protection. Moreover, it filters the radio waves to prevent them to enter the following block.
2. **Preamplifier:** Is typically implemented as an instrumentation amplifier through three operational amplifiers, it provides a single-end signal output starting from the sensed voltages.
3. **High-Pass Filter:** eliminates the DC component. It is implemented as a simple RC first-order filter.
4. **Amplifier:** provides an output voltage coherent with the input voltage range of the ADC.
5. **High-Pass Filter:** eliminates the DC component of the signal after the amplifier. It is implemented as the previous one.
6. **Low-Pass Filter:** limits the frequency range to 60Hz. It is a third-order active filter with a gain of 15.
7. **DRL circuit (Driven Right Leg):** is an electronic circuit typically combined to the filtering and conditioning of the biological signal. It reduces the Common-mode interference of the sensed signal. Biological signals are usually very small electrical signals, in the order of milli-micro Volts, and can be obscured by the interferences of the electrical lines at 50/60 Hz. The DRL circuit, thanks to the reference electrode, eliminates this interference.

The output signal depends on the filter and conditioning chain and so it depends on the sensor board used, in the case of our application, the output signal is a digital signal which ranges between 0 to 1023.

This superficial EMG requires an external power supply, preferably with a voltage within the range ± 9 V, to minimize the risk of electric shocks.

5.1.2 sEMG sensor

The sEMG sensor device has been selected. The sensor unit is composed by a filter and conditioning chain implemented on a board which works as explained in the previous sub-chapter and generates the output signal read by the Arduino board; three electrodes used to withdraw the sEMG signal from the patient; and two 9 Volts batteries connected to guarantee a ± 9 .

The mode of operation has been tested on a healthy volunteer to visualize the output range of the signal and verify the difference in range between the activation and rest muscle conditions. The three electrodes are positioned on the forearm of the volunteer and connected to the sensor board. The sensor board is connected to the Arduino and to the external power supplies. The set-up is shown in Figure 39.

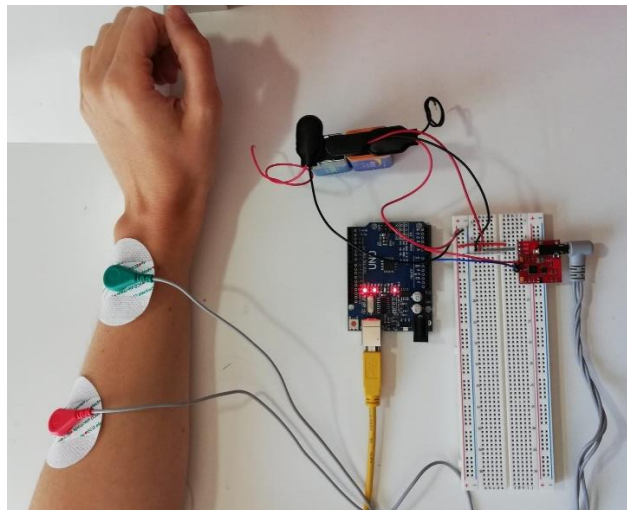
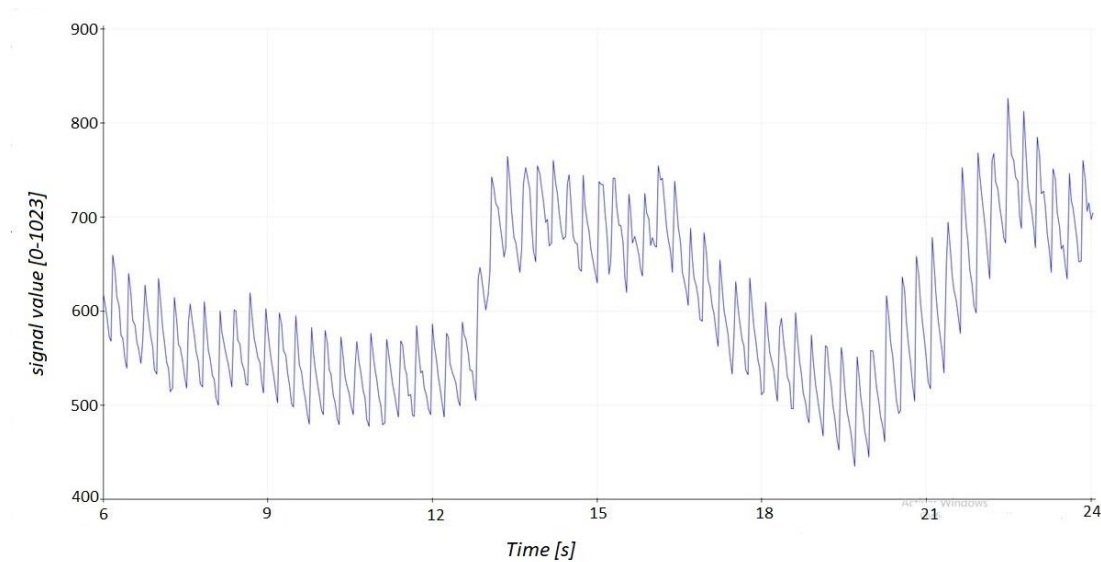


Figure 39 sEMG implementation on a volunteer

The wearer is asked to activate the extensor muscles, the sEMG signal is withdrawn and the output range of the sEMG signal is visualized on the Arduino. As explain before, the

sEMG signal varies according to the electrodes position and the muscular activities. For this reason, different signals have been withdrawn and, in general, it results that the sEMG signal is around 500-600 on a scale between 0 and 1023, when the hand is in rest condition with the fingers in the flexed position; the sEMG signal reaches peaks of 750-800 during the extension of the fingers (one of the sensed signal is reported in Graph 5)



Graph 5 Superficial EMG from the extensor fascicle muscle on a healthy volunteer. Two muscular activation are withdrawn: at 13-17 seconds and 20-24 seconds.

The signal is quite noisy despite the filter and conditioning chain, but it shows different range of values when the muscular fascicle is in rest condition and when it is activated. Therefore, it is possible to use this signal to control the rehabilitative motion.

5.2 Control logic code

The control of the exoskeleton is based on a threshold on the sEMG of the extensor muscles of the finger of the healthy hand. The control logic works as follows to activate the exoskeleton: the sEMG signal is sensed on the healthy forearm extensor muscles, it is sent to the Arduino board that uses the input signal in the control algorithm. The Arduino generates a PWM signal as output which is responsible for enabling the actuator unit. This output changes the activation ON-time of the PWM according to the sEMG read as input. If the muscular activity is sensed the rehabilitation movement is activated

and for a predefined time interval the Arduino stops reading the sEMG input signal. This time interval is considered as time to let the patient perform the extension of the finger and to let him/her get back to the initial position of flexed finger, before performing another cycle of rehabilitation.

The control system is based on a *switching control algorithm* based on a predefined threshold on the sEMG signal. Since the sEMG signal is patient-specific the threshold must be chosen before the rehabilitation. The switching control algorithm consists in the following:

- When the signal exceeds the threshold value, the rehabilitation cycle is activated. At first the PWM current flows on the SMA springs and actuates the hole exoskeleton at the same time: both fingers reach the extended position together. Once the final position is reached, the output current is set to zero and a time interval allows the patient to go back to the original flexed position.
- If the sEMG signal is below the predefined threshold it means that the patient is not activating the finger extensor and the SMA springs behave as normal passive springs.

This kind of control system is suitable for hand rehabilitation since it allows the patient to perform repetitive exercises for the flexion-extension movements.

5.2.1 Self-motion control

The self-motion control, shown in Figure 11, is implemented since most of hand injured patient need to rehabilitate only one hand; so are patients affected by stroke, who usually have half of the body musculature affected by spasticity and abnormal muscular tone (hemiparesis), as explained before. For this reason, is not possible to directly control the exoskeleton by withdrawing the superficial EMG signal on the forearm to be rehabilitated. The self-motion control is considered to be the right solution since it allows the patient to guide its own rehabilitation on the impaired hand thanks to the healthy forearm. Indeed, this implementation uses the signal withdrawn on the symmetric skeletal muscles, on the healthy side of the body, to drive the rehabilitation of the stroke affected part. In this way the patient can be aware and guide its own

rehabilitation, it is expected that the self-motion control facilitate the recovery of the injured functionalities [32].

5.2.2 The Arduino code

The switching control algorithm is running on the *Arduino board*. To program and upload the control code the *Arduino software IDE* is used.

The Arduino board receives the superficial EMG signal, compares it with a predefined threshold, and, according to the switching control algorithm, gives the driving PWM signal as output. Of course, when the sEMG signal is below the predefined threshold, the PWM duty-cycle is set to zero, and the output results to be a null signal.

The sEMG output signal has been analysed in the previous sub-chapter; it is important to remember that the signal read by the Arduino depends on the filtering and conditioning chain. In this case the sEMG unit gives as output a signal which ranges between 0 to 1023.

The control algorithm code is composed of the following functions:

- `setup()`: this function runs only once, when the board is powered as the first operation. It allows the initialization of the functionalities used in the code. Two pins are enabled, one as input and one as PWM output. The serial communication is initialized with 9600 bits per second.

In this section, the *threshold_setup* function (presented below) is called to set the sEMG threshold value to drive the PWM. This initial set-up is fundamental since the sEMG is patient-specific and depends on the electrodes disposition.

- `loop()`: this function is where the main code stays. It runs continuously in a loop. The *EMG_read()* function, responsible for reading the input sEMG value, is called at each cycle. Afterward, a global Boolean variable called *blink* is used as a driven value to produce the PWM. If the *blink* value is equal to 1 a while loop, generating the PWM output, runs until the pre-defined delay expires. The delay is needed to let the SMA actuator heat-up and perform the whole rehabilitation movement without interruption and to let the patient recover the initial position of flexed finger. The `analogWrite()` function is used to generate a PWM output signal. The

output signal is a square wave at 490 Hz which ranges between 0 and 5 Volts, and the Duty-Cycle is set to 150 out of a range of values from 0 to 255 (the choice of the value is explained in chapter 4.3).

- `EMG_read()`: The `EMG_read` function reads the sEMG signal from the input pin `digitalRead()` and compare the values sensed with the pre-set threshold. If the sensed value is less than the threshold, the `blink` global variable is set to 0 and the signal on the output pin corresponding to the PWM is set to zero. When the sensed sEMG value is greater of the pre-set `voltage_threshold` value, the Boolean variable `blink` is set to 1, and a time-dependent variable called `executiondelay` takes the value of the program execution time in that instant.
- `threshold_setup()`: this function runs to set up the patient-specific sEMG threshold. It only needs to be executed once before the normal execution of the control strategy begins. The threshold setting requires the following procedure. The patient is asked to extend the finger, and the sEMG signal of the muscular activation is sensed. A plot window shows the graphical visualization of the sEMG sensed, while on the serial monitor, the operator is requested to manually set the patient-specific threshold, based on the trend shown. In the second part of the function, the correctness of the inserted value is verified. The `voltage_threshold` must be an integer value in the interval of 0-1023. In case of a not valid value, the code shows an error message, and terminates its execution. If the inserted value respects the requirements, the function shows the imposed `voltage_threshold` value on the serial monitor and the main code executes.

To verify the correctness of the control logic, the Tinkercad program is used to simulate its behaviour. Since the main aim is to check the code correctness, the Arduino and the breadboard real circuit are simplified, and few functions are modified to let it works correctly. A button simulates the sEMG input, and a Led simulates the output of the electronic circuit containing the SMA actuator unit.

The code runs as expected. First, the window containing the input graph opens, and it shows the button input values [0-1] taken in the predefined time interval. Afterward, it

is requested to insert a threshold value. In the real application, this value must be chosen according to the sEMG and based on the shown trend. In this simulation, since the simplify input is a logic button (0 or 1) it is set to 1. Moreover, it is possible to observe the correct behaviour of the code with the LED visual output.

Once the simulation confirms the correctness of the algorithm, the code is implemented on the Arduino board. Now, it is possible to make the real connection with the input signal coming from the sEMG board and the output signal of MOSFET circuit.

5.3 Integration of the sensor and control system on the prototype

The whole system is integrated in the complete prototype. The sensor unit is assembled and is connected by jumpers to the Arduino board. The Arduino board is connected to the MOSFET circuit and to the actuator unit, which are already mounted on the exoskeleton. The final set-up is built according to the self-motion control principle. The complete set-up model of the connections is shown in Figure 40.

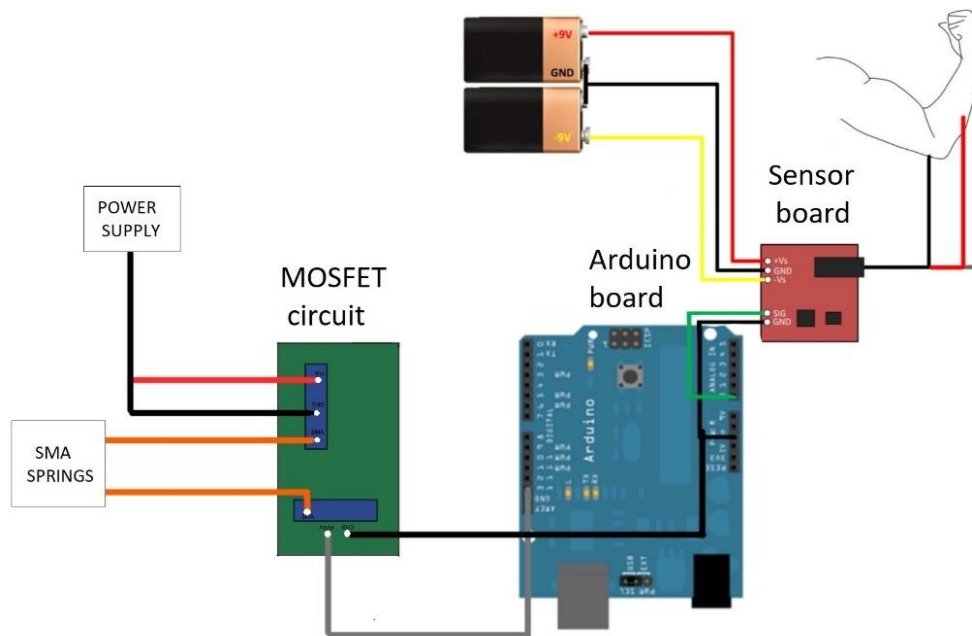


Figure 40 Complete set-up model of the connections between the actuator unit (SMA springs), the sensor unit (the red box), the MOSFET circuit (the green box) and the control system (Arduino light-blue box).

Once the connections are done, the whole system is worn by a healthy volunteer in order to simulate the behaviour of the whole system and to verify the correct rehabilitation movement. The three electrodes have been fixed on the left forearm in order to sense the fingers extensor muscle fascicle, and the exoskeleton is mounted on the right hand. The complete set-up, which includes the exoskeleton mechanical structure, the electronic implementation, the control unit and the sensors is shown in Figure 41 below.

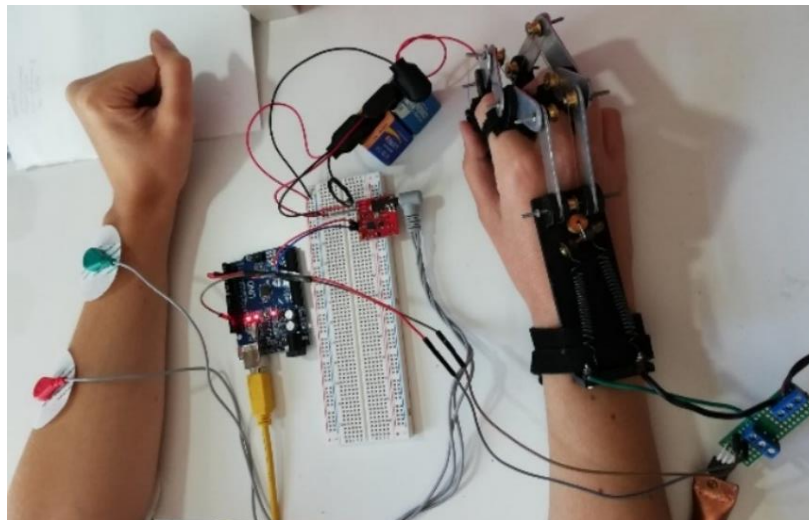


Figure 41 Complete set-up of the exoskeleton with the actuator unit, the sensor unit, the electronic circuit and the control system on a healthy volunteer.

Afterward, the whole electronics is powered, and the threshold control algorithm is verified. As expected, when the wearer activates the extensor muscle on the left hand, the control algorithm recognizes the signal and activates the PWM output signal which lets the current flow through the SMA springs. In this way the exoskeleton is activated, and the rehabilitative movement begins. The device works as expected.

6 Conclusions

In this thesis a physical prototype of a hand exoskeleton actuated by Shape Memory Alloy (SMA) for stroke rehabilitation controlled by superficial electromyography (EMG) sensors has been studied and implemented.

The mechanical structure designed and realized is the 4-bar linkage structure, which matches the hand physiological movement and is able to perform the rehabilitation movement of finger extension of the index and middle fingers. In this solution the entire hand palm and fingertips are left free to interact with the environment. Moreover, the realized exoskeleton is widely adaptable to patients with different sizes of phalanges, thanks to the adaptability of the 4-bar linkage structure, and to patients with different finger diameters, thanks to the Velcro straps solution.

The mechanical structure is designed with Autodesk INVENTOR and different dynamical simulations are done on the model to size the exoskeleton and to estimate the needed force to overcome the stroke rigidity. From the dynamical simulations it results that the two fingers to be actuated need forces of the same order of magnitude to overcome the stroke rigidity and extend the fingers. For this reason, it is possible to use a single actuator unit to move both fingers together. Therefore, an underactuated system is implemented and the two fingers to be rehabilitated move together when a pulling force of 10 N is applied on the cable. This solution optimizes the number of actuators to a single unit and so it reduces the total encumbrance and weight of the exoskeleton device and it reduces the number of actuator controls to a single one. The transmission of the forces generated by the actuator is performed by a nylon cable and is redistributed thanks to a pulley. This solution allows the usage of a displaced actuator unit, avoiding contacts between the heated parts of the actuator and the patients' hand.

The actuator unit is composed by two SMA springs in parallel under the mechanical point of view to obtain the necessary force and the necessary contraction lengths of the springs to correctly move the fingers. The activation of the SMA springs is obtained by means of a current flow through them, so that the SMA heats-up thanks to the Joule effect. A series of experimental measurements are carried out to characterize the electronic and mechanical properties of the selected springs.

A MOSFET circuit is designed on LT-spice and built in order to let the current flow when required. Since the electrical resistance of the SMA springs depends on their temperature and varies during operation, the MOSFET is implemented in order to work in the saturation region so that the current exiting from the drain pin can be considered constant. The springs are connected in series under the electrical point of view, and, in this way, the same current actuates both springs at the same time. The advantage of this solution is that the electric connections to the SMA springs are located on the fixed extremities for both springs, limiting the movable parts of the electric circuit.

To drive the current flow, a control algorithm is implemented on an Arduino board. The control algorithm is based on the sEMG signal withdrawn from the healthy forearm of the patient and it controls the rehabilitation of the patient's injured hand, thus allowing the patient to self-control the exoskeleton. The algorithm is based on a threshold to be imposed on the withdrawn sEMG signal. The signal exceeds the threshold when the extensor muscle is activated, and it activates the rehabilitation movement on the injured hand. The prototype is designed for the rehabilitation of the extension movement of the index and middle fingers, but it could be improved to perform also other applications such as the flexion movement of the fingers.

Besides, the exoskeleton is a low-cost device, and easy to replicate. The prototype has been physically built in its mechanical structure, MOSFET circuit and control implementation. The exoskeleton functioning has been tested: it is easy to wear and seems to operate in a correct way to be successfully employed in the rehabilitation of patients affected by post-stroke hemiparesis.

6.1 Future work

Some considerations can be done on the work performed:

- The first consideration is about the SMA springs. The two springs utilized have characteristics somehow different from one another. Moreover, the two SMA springs were subjected to different series of experiments and, on the long run, the alloy seems to lose part of its recovery property during the heating cycles. To obtain a more performant actuator unit it is possible to substitute the SMA

springs with two new ones, possibly coming from the same batch of production in order to reduce their differences in thermomechanical characteristics. In this way, having similar behaviour of the springs optimizes the heat-up process and actuation.

- Moreover, to improve the prototype design, it is possible to study a SMA spring with more performing characteristics in order to use a single spring to actuate the whole system. With a single SMA spring it is possible to select an appropriate MOSFET in order to obtain a wider linear range of contraction with respect to the PWM ON-time (see Graph 3 and Graph 4) to implement a more precise control algorithm.
- The mechanical design can be optimized by the selection or by the realization of customized components: linkage bars can be slimmer, thus making the whole design lighter and less cumbersome; the nylon cable can be substituted with a material with good flexural properties, but with lower yield deformation under tension.
- As a matter of fact, to provide a complete device for rehabilitation, the mechanical design of the exoskeleton, shall be completed with the addition of the missing fingers. For the ring finger and little finger, the design is the same as for the index and middle finger, just with recalculated lengths of the linkages and forces. For the thumb it will be necessary to design a different structure due to the different conformation of the thumb in terms of degrees of freedom and anatomy of the phalanges.
- Another objective to be considered in future developments is the need of a safety analysis of the device as a biomedical application. As main aspects, the following should be considered: the electrical quantities of voltage and current, the thermal point of view and finally the limits of the range of motions of the finger joints.
- As a fundamental step of the future work, the prototype device must be validated on post-stroke hemiparesis patients under the supervision of physiotherapists to verify the correct behaviour of the whole exoskeleton device.

A last consideration related to the work performed in this thesis project concerns the very particular conditions in which the work itself has been carried out. The project started at the same time in which the lockdown due to Covid-19 health emergency was imposed. The work was performed with no access to the University laboratories, facilities, and instrumentation. For instance, with access to the University facilities, better or additional measurements could have been performed, such as the measurements in transient conditions of the properties of the SMA springs.

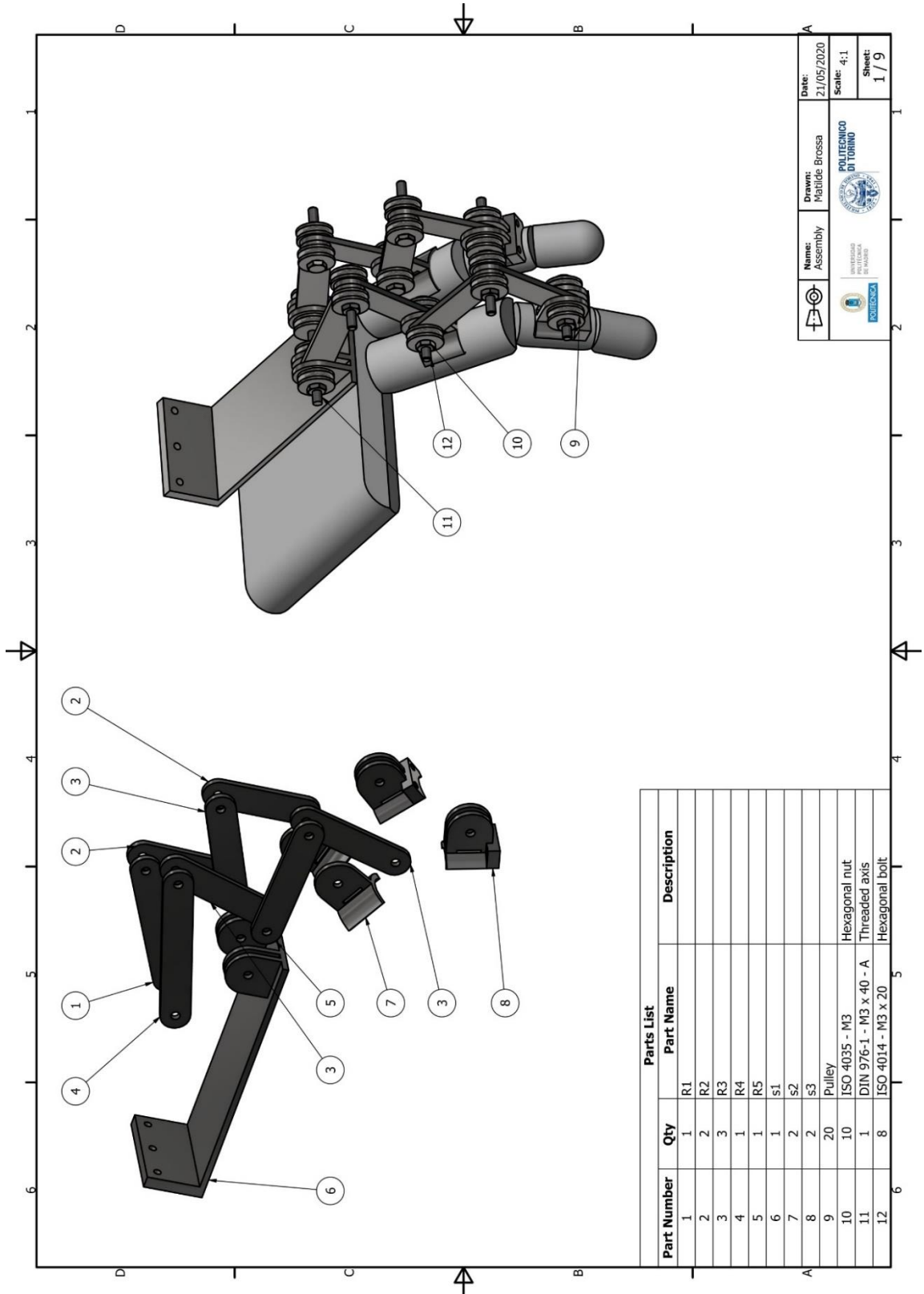


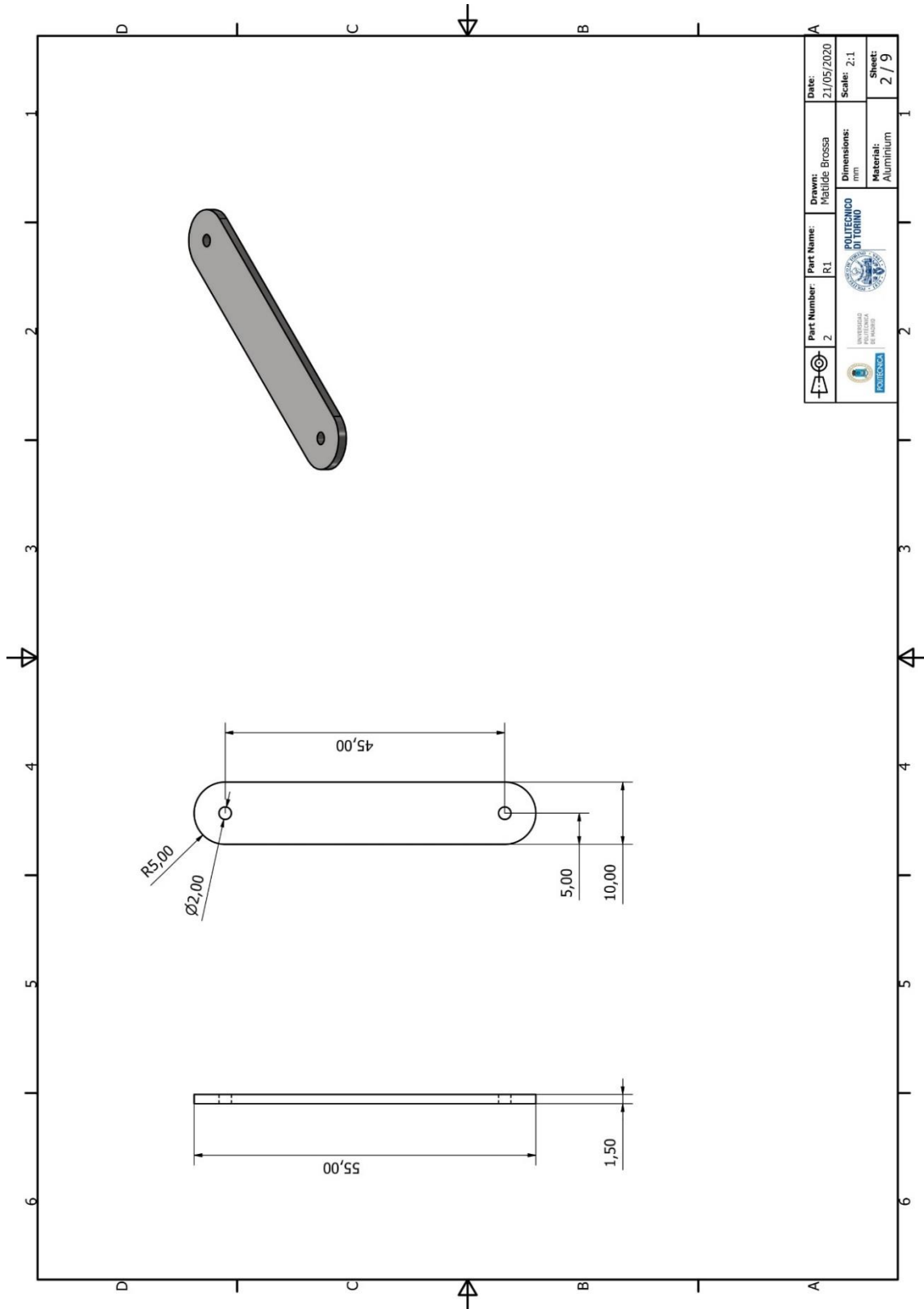
Acronyms

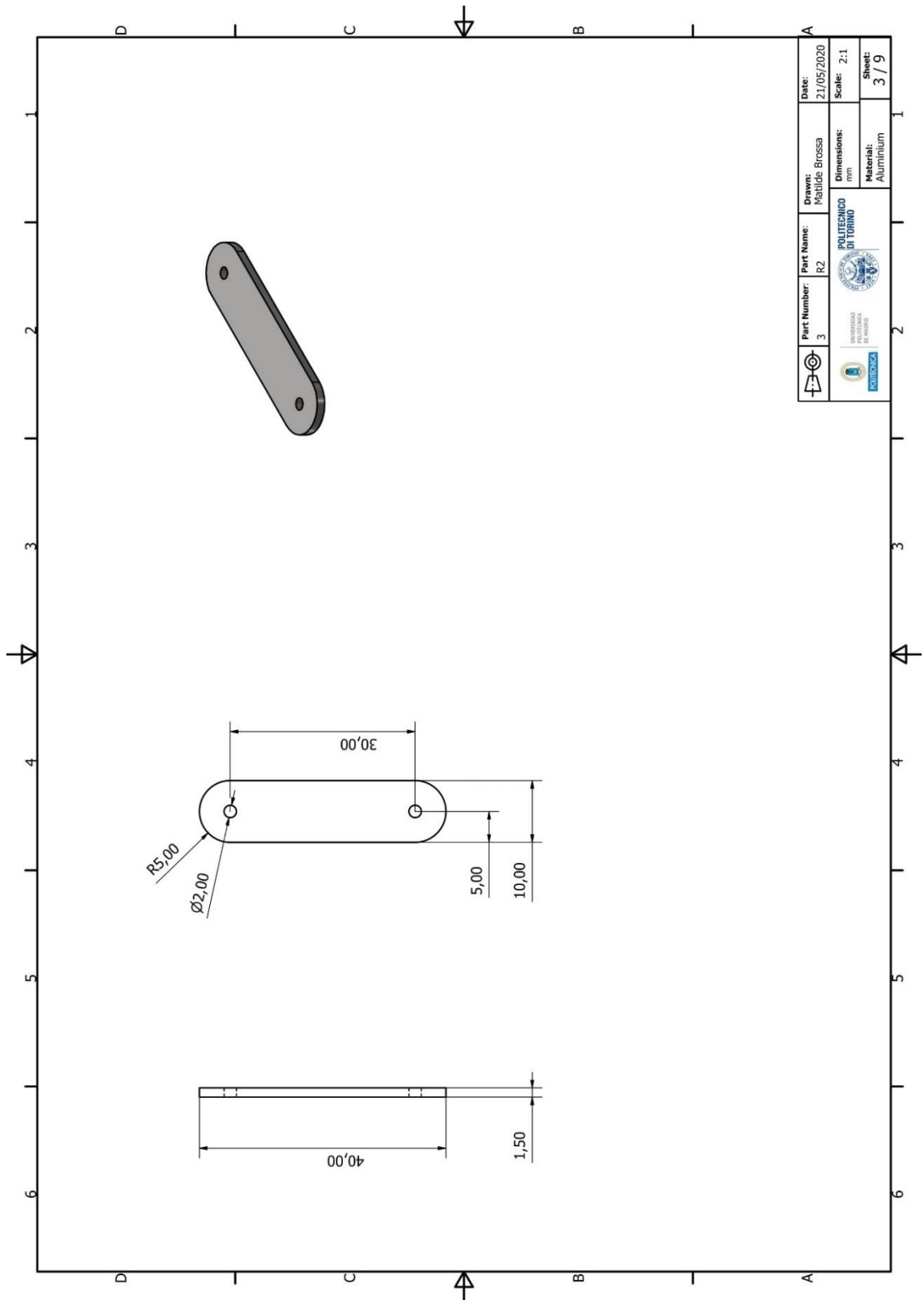
ADL	Activities of daily living
CAD	Computer aided design
CMC	Carpometacarpal
CNS	Central nervous system
DC	Direct current
dc	Duty-cycle
DIP	Distal interphalangeal
DOFs	Degrees of freedom
EEG	Electroencephalogram signal
EMG	Electromyography
FSR	Force-sensing resistor
HM	Humate-metacarpal
IDE	Integrated Development Environment
IP	Interphalangeal
MCP	Metacarpophalangeal
MOSFET	Metal-oxide-silicon field effect transistor
PIP	Proximal interphalangeal
PWM	Pulse width modulation
RCM	Remote center of motion
RCR	Remote center of rotation
ROM	Range of motion
sEMG	Surface electromyography
SMA	Shape memory alloy
SME	Shape memory effect
TMC	Trapeziometacarpal



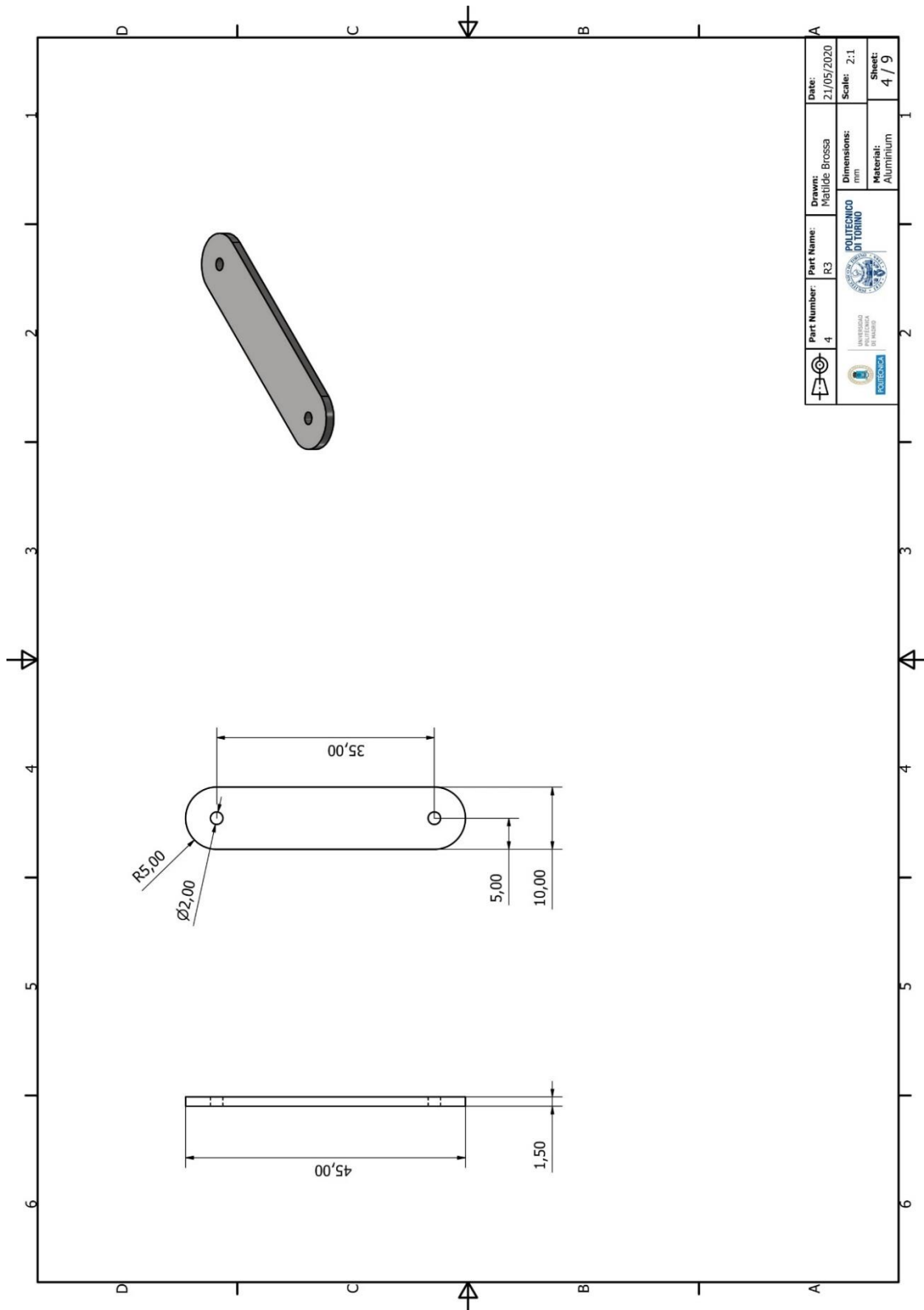
Appendix 1 CAD drawing

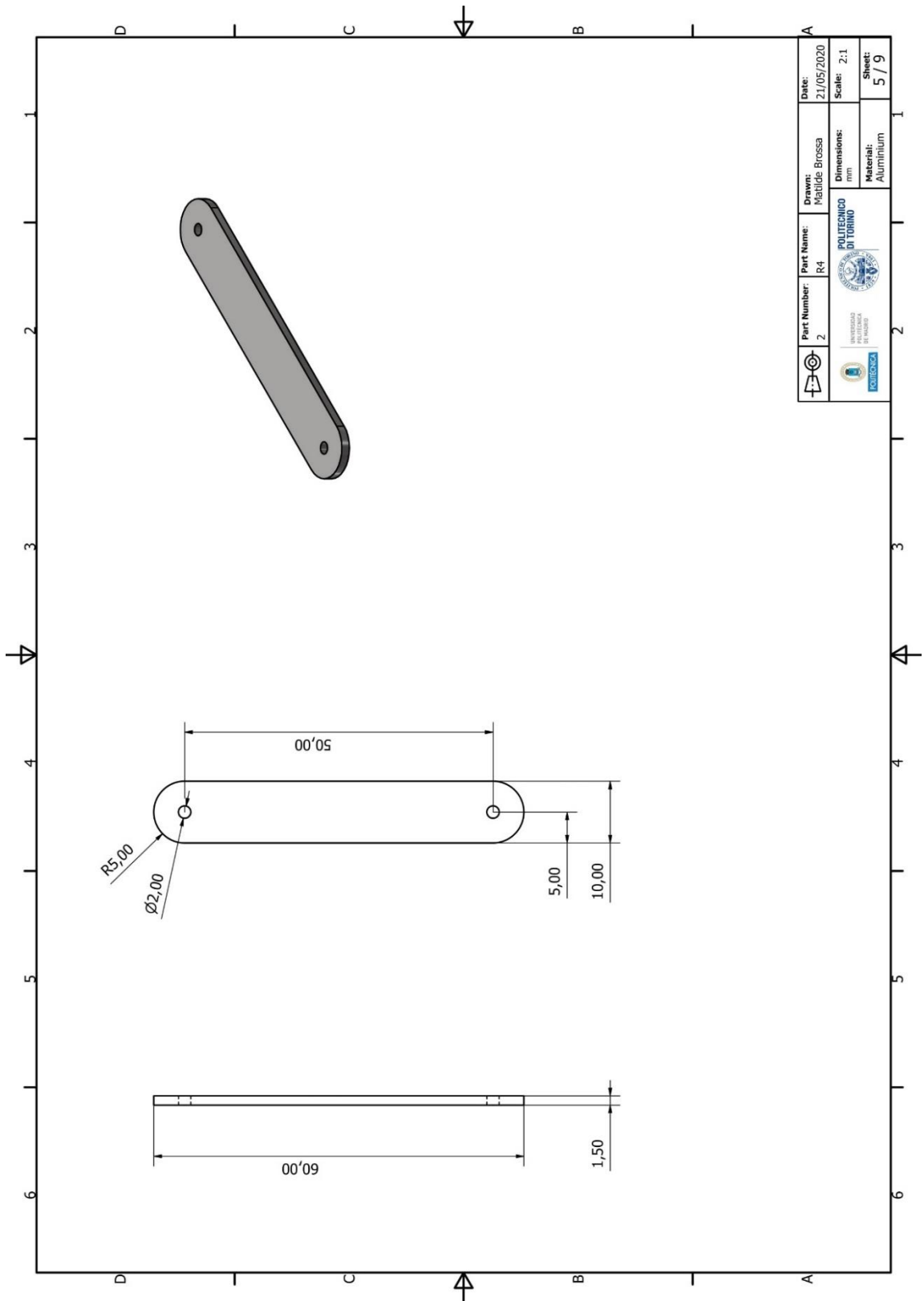


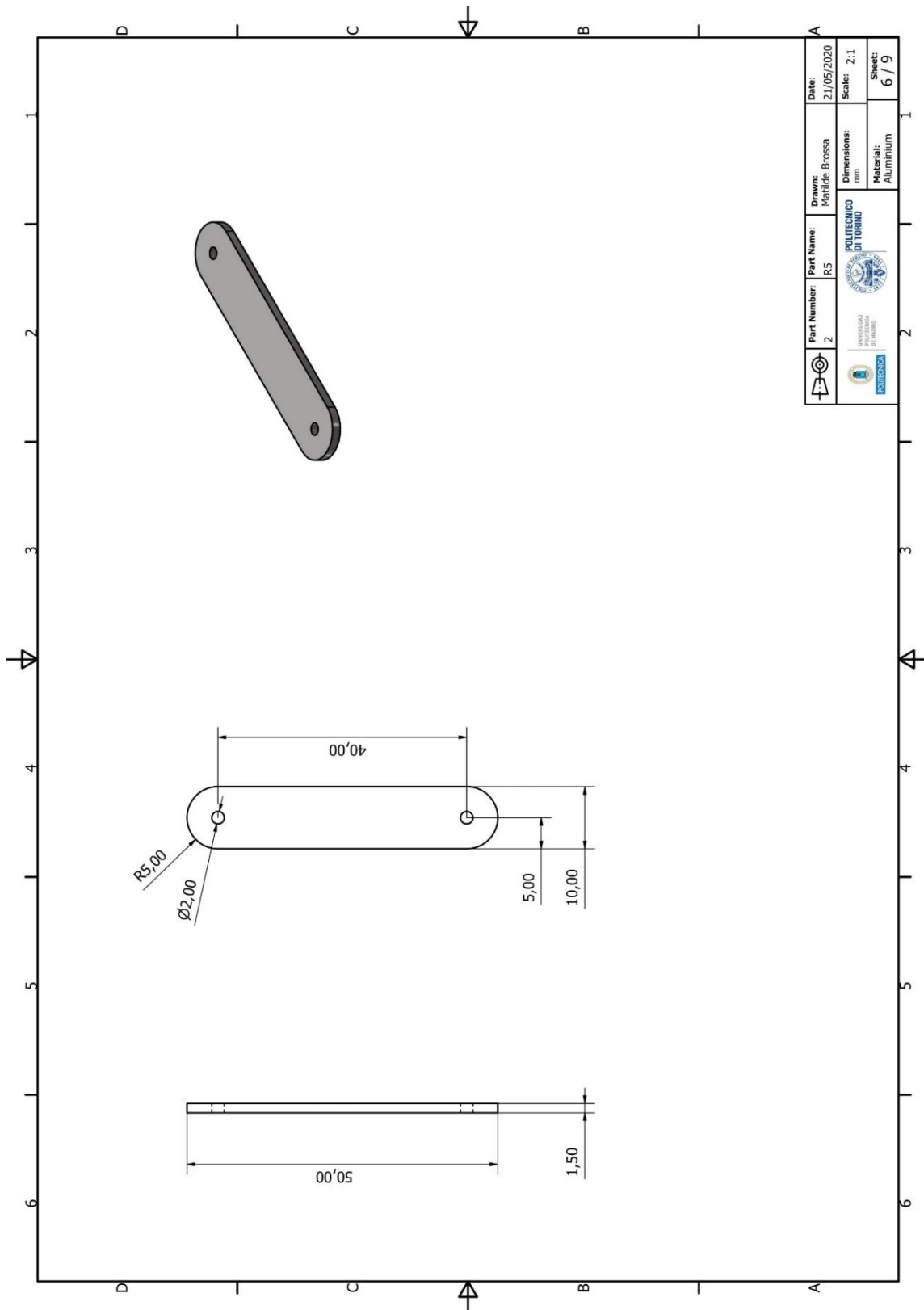




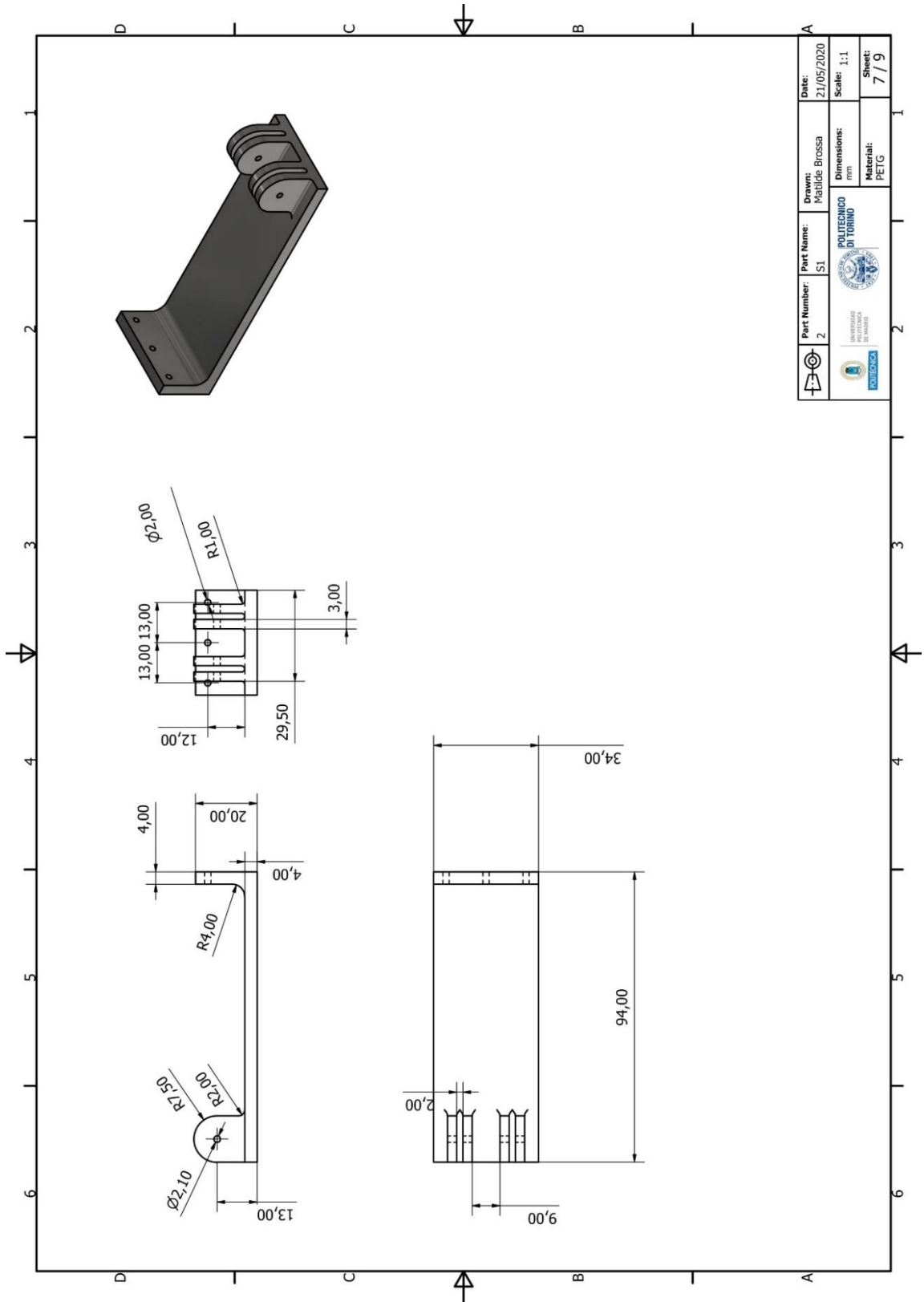
	Part Number:	R2	Part Name:	Mattilde Brossa	Date:	21/05/2020
	3			Dimensions:	Scale:	2:1
				Material:	Sheet:	3 / 9
				Material:	Aluminium	



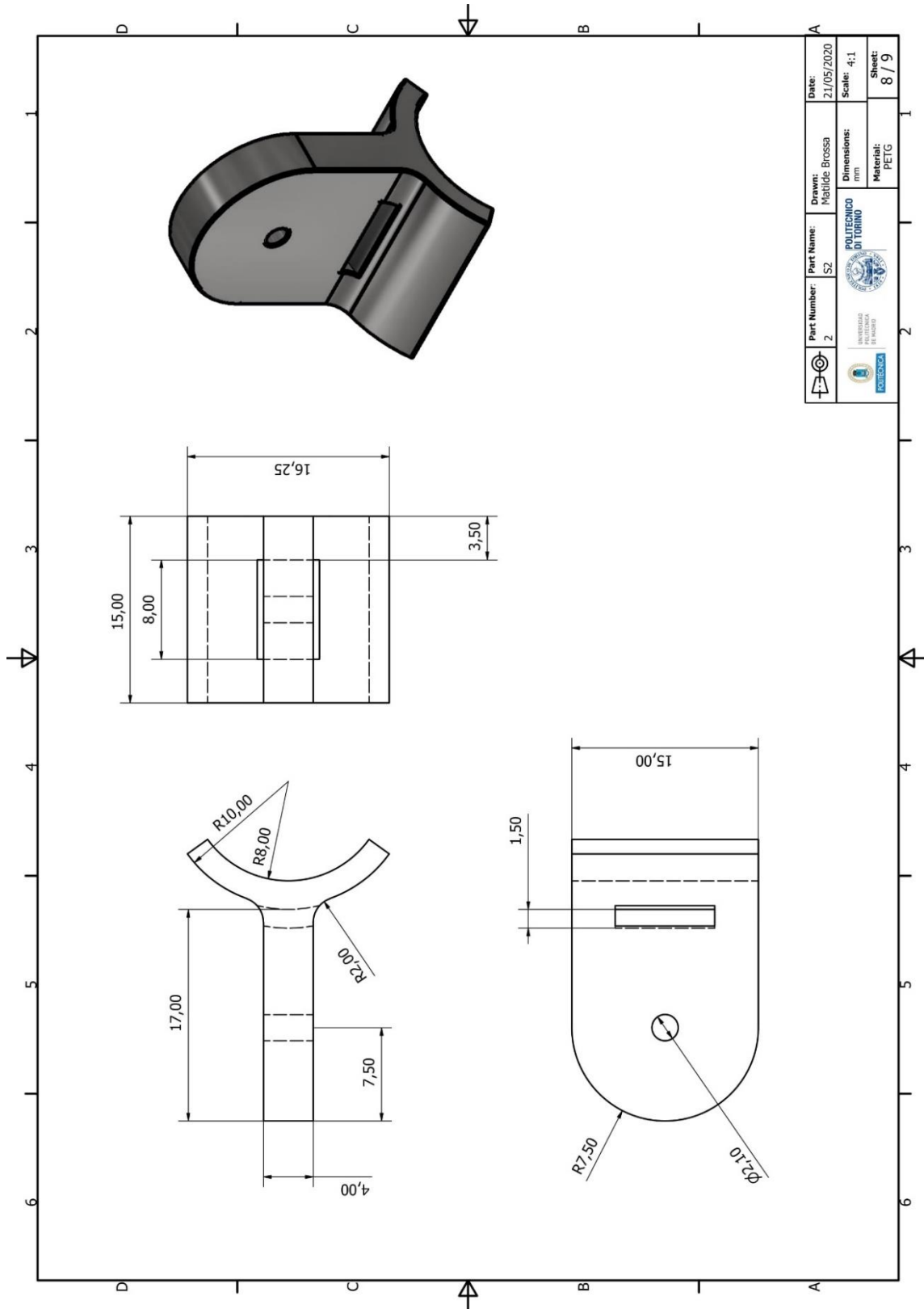


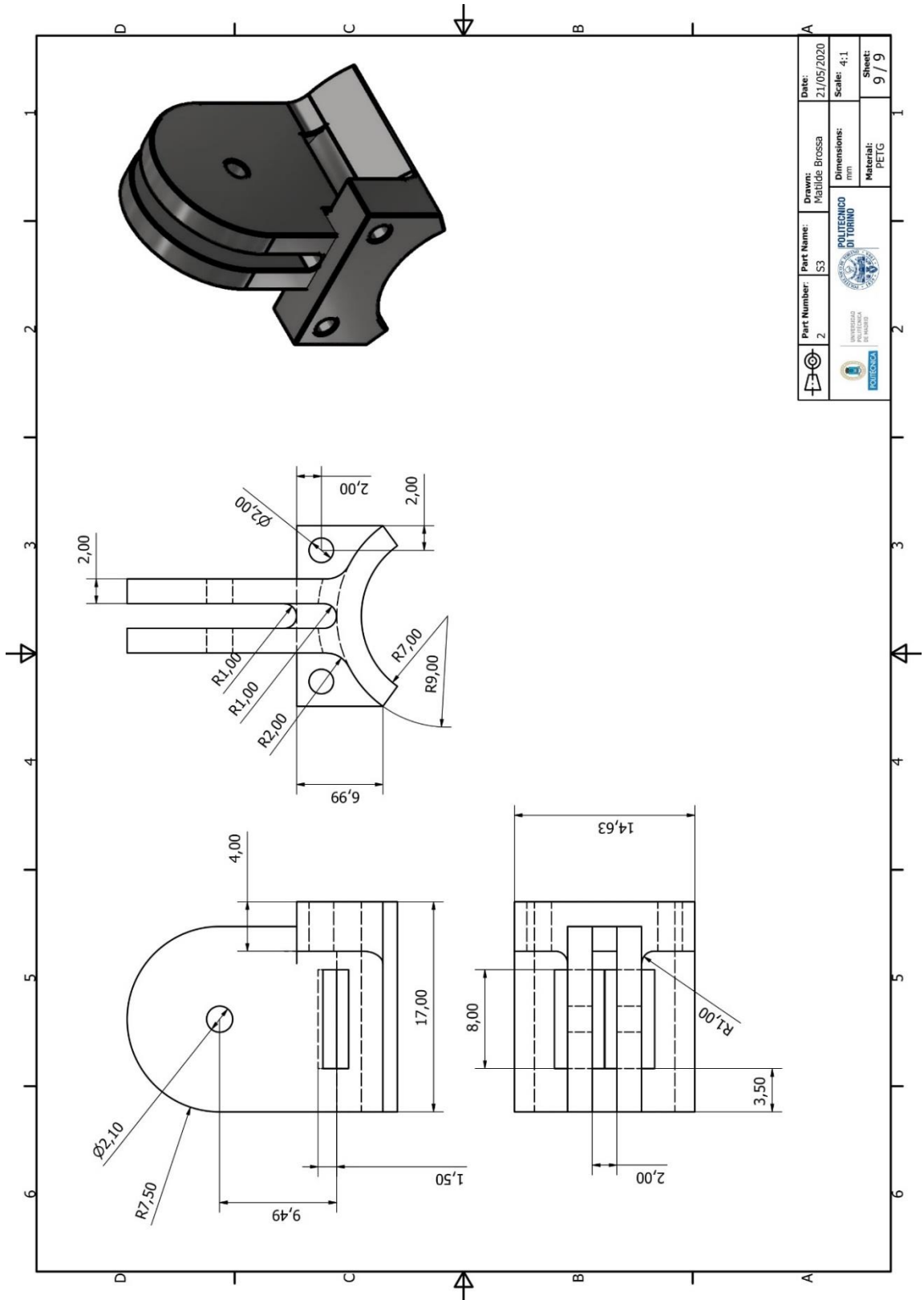


	Part Number:	RS	Drawn:	Mattide Brossa	Date:	21/05/2020
	Part Name:		Dimensions:	mm	Scale:	2:1
			Material:	Aluminium	Sheet:	6 / 9



 POLITECNICO DI TORINO	Part Number:	S1	Drawn:	Martide Brossa	Date:	21/05/2020	
	2	Part Name:		Dimensions:	Scale:	1:1	
 POLITECNICO DI TORINO				Material:	PETG	Sheet:	7 / 9







Appendix 2 Arduino control code

```

bool blink = 0;
int voltage_threshold =0; // to be set accordig to initial measurements
int EMGsensorValue = 0;
int b=0;
int executiontime = 60000; // ms (1 min)
int executiondelay =0;
void setup() {
  Serial.begin(9600); //transmission speed
  pinMode(3,OUTPUT);
  pinMode(0, INPUT);
  threshold_setup();
}
void loop(){
  EMG_read();
  if ((blink==1)&&(executiondelay>millis()-executiontime)){
    while(executiondelay>millis()-(executiontime/2)){
      analogWrite(3,150); // freq=490 Hz dc= 150/255
    }
  }
}
void EMG_read(){
if(analogRead(0) >= voltage_threshold){
  blink = 1;
  executiondelay=millis();
  Serial.println(executiondelay);
}else{
blink = 0;
  analogWrite(3,0);
}
}
void threshold_setup(){
  Serial.print("Extend the fingers (Graphical representation is available using Serial Plotter\n");
  int timedelay = millis();
  // millisecondi: wait 10 sec to get the muscular signal
  while(timedelay +10*1000 > millis()){
    Serial.println(analogRead(0));
  }
  EMGsensorValue = analogRead(0);
  Serial.print("Enter threshold value integer between 0 - 1023:\n");
  while (Serial.available()==0) {
  }
  b = Serial.read()-48; // get the character
  Serial.print("I got ");
  Serial.println(b);
  if((b<0)|| (b>1023))
  {
    b = 1024;
  }
  Serial.print("threshold set to ");
  voltage_threshold = b;
  Serial.println(voltage_threshold);
}

```



Bibliography

- [1] R. L. Sacco, S. E. Kasner, J. P. Broderick and et al, "An updated definition of stroke for the 21st century: a statement for healthcare professionals from the American Heart Association/American Stroke Association," *Stroke*, vol. 44, no. 7, pp. pp. 2064-2089, 2013.
- [2] S. Roy, M. S. Inamdar and S. Bhaumik, "Review of Exoskeleton Hand Exercisers for Paralyzed Patient," *2nd Research Summit on Computer, Electronics and Electrical Engineering*, pp. 35-44, 2016.
- [3] E. B. Brokaw and e. al., "Hand Spring Operated Movement Enhancer (HandSOME): A Portable, Passive Hand Exoskeleton for Stroke Rehabilitation," *IEEE Transactions on Neural Systems and Rehabilitation Engineering*, pp. 391 - 399, 2011.
- [4] D. Reinkensmeyer, C. T. Pang, J. Nessler and C. Painter, "Web-based telerehabilitation for the upper extremity after stroke," *IEEE Transactions on Neural Systems and Rehabilitation Engineering*, p. pp. 102–108, 2002.
- [5] D. Epstein, A. Mason and A. Manca, "The hospital costs of care for stroke in nine European countries," *Health Economics*, pp. vol. 17,pp S21-S31, 2008.
- [6] H. Yamaura, K. Matsushita, R. Kato and H. Yokoi, "Development of hand rehabilitation system for paralysis patient–universal design using wire-driven mechanism.," in *2009 Annual International Conference of the IEEE Engineering in Medicine and Biology Society. IEEE, 2009*.
- [7] P. Heo, G. M. Gu, S.-j. Lee, K. Rhee and J. Kim, "Current hand exoskeleton technologies for rehabilitation and assistive engineering," *International Journal of Precision Engineering and Manufacturing*, pp. 807-824, 2012.
- [8] P. Langhorne, J. Bernhardt and G. Kwakkel, "Stroke rehabilitation," *The Lancet* 377.9778, 2011, pp. 1693-1702.
- [9] G. Prange, M. Jannink, C. Groothuis-Oudshoorn , H. Hermens and M. IJzerman , "Systematic review of the effect of robot-aided therapy on recovery of the hemiparetic arm after stroke.," *Journal of rehabilitation research and development*, pp. 171-184, 2009.
- [10] J. Patton and F. Mussa-Ivaldi, "Robot-assisted adaptive training: custom force fields for teaching movement patterns," *IEEE Transactions on Biomedical Engineering*, pp. pp. 636-646, 2004.
- [11] B. S. Rupal, S. Rafique, A. Singla, E. Singla, M. Isaksson and G. S. Virk, "Lower-limb exoskeletons: Research trends and regulatory guidelines in medical and non-medical

- applications," *International Journal of Advanced Robotic Systems*, November-December 2017.
- [12] Q. Meng, S. Xiang and H. Yu, "Soft Robotic Hand Exoskeleton Systems: Review and Challenges Surrounding the Technology," in *2nd International Conference on Electrical, Automation and Mechanical Engineering (EAME 2017)*. Atlantis Press, 2017.
- [13] L. Randazzo, I. Iturrate, S. Perdakis and J. d. R. Millàn, "mano: A wearable hand exoskeleton for activities of daily living and neurorehabilitation," *IEEE Robotics and Automation Letters* 3.1, pp. 500-507, 2017.
- [14] A. Lince, "ReHand - a portable assistive rehabilitation hand exoskeleton," Politecnico di Torino, 2016.
- [15] Y. Kim, S. S. Cheng, A. Ecins and C. Fermüller, "Towards a robotic hand rehabilitation exoskeleton for stroke therapy," in *ASME 2014 Dynamic Systems and Control Conference.*, 2014.
- [16] M. Fontana, A. Dettori, F. Salsedo and M. Bergamasco, "Mechanical design of a novel hand exoskeleton for accurate force displaying," in *2009 IEEE International Conference on Robotics and Automation.*, 2009.
- [17] T. Tang, D. Zhang, T. Xie and X. Zhu, "An exoskeleton system for hand rehabilitation driven by shape memory alloy," in *IEEE International Conference on Robotics and Biomimetics (ROBIO)*, 2013.
- [18] H. In, B. B. Kang, M. Sin and K.-J. Cho, "Exo-glove: A wearable robot for the hand with a soft tendon routing system," *IEEE Robotics & Automation Magazine* 22.1, pp. 97-105, 2015.
- [19] H. K. Yap, J. H. Lim, F. Nasrallah, J. C. H. Goh and R. C. H. Yeow, "A soft exoskeleton for hand assistive and rehabilitation application using pneumatic actuators with variable stiffness," in *2015 IEEE international conference on robotics and automation (ICRA)*, 2015.
- [20] J. Yang, J. Shi and H. Xie, "Research on SMA actuated tendon driven hand exoskeleton with bidirectional finger joint motion coupling for rehabilitation usage.," *IEEE International Conference on Cyber Technology in Automation, Control, an Intelligent Systems (CYBER)*, 2015.
- [21] A. M. B. Hamid, M. R. Makhdoomi, T. Saleh and M. Bhuiyan, "Development of a Shape Memory Alloy (SMA) based assistive hand.," *Advanced Materials Research. Trans Tech Publications Ltd*, vol. 1115, 2015.
- [22] A. Chiri, F. Giovacchini, N. Vitiello, E. Cattin and et al., "HANDEXOS: Towards an exoskeleton device for the rehabilitation of the hand," *2009 IEEE/RSJ International Conference on Intelligent Robots and Systems*, 2009.

-
- [23] A. Chiri, N. Vitiello, F. Giovacchini, S. Roccella, F. Vecchi and M. C. Carrozza, "Mechatronic design and characterization of the index finger module of a hand exoskeleton for post-stroke rehabilitation," *IEEE/ASME Transactions on mechatronics* 17.5, pp. 884-894, 2011.
- [24] Y. Hasegawa, J. Tokita, K. Kamibayashi and Y. Sankai, "Evaluation of fingertip force accuracy in different support conditions of exoskeleton.," *2011 IEEE International Conference on Robotics and Automation.*, 2011.
- [25] Y. Hasegawa, Y. Mikami, K. Watanabe and Y. Sankai, "Five-fingered assistive hand with mechanical compliance of human finger," in *IEEE international conference on robotics and automation.*, 2008.
- [26] K. Tong, S. Ho, P. M. K. Pang, X. Hu, W. Tam and et al, "An intention driven hand functions task training robotic system," *2010 Annual International Conference of the IEEE Engineering in Medicine and Biology*, IEEE, 2010.
- [27] C. L. Jones, F. Wang, C. Osswald, X. Kang, N. Sarkar and D. G. Kamper, "Control and kinematic performance analysis of an Actuated Finger Exoskeleton for hand rehabilitation following stroke," in *3rd IEEE RAS & EMBS International Conference on Biomedical Robotics and Biomechanics*, 2010.
- [28] C. L. Jones, F. Wang, R. Morrison, N. Sarkar and D. G. Kamper, "Design and development of the cable actuated finger exoskeleton for hand rehabilitation following stroke," *IEEE/ASME Transactions on Mechatronics* 19.1, 2012, pp. 131-140.
- [29] T. Worsnopp, M. Peshkin, J. Colgate and D. Kamper, "An actuated finger exoskeleton for hand rehabilitation following stroke.," *2007 IEEE 10th international conference on rehabilitation robotics*, 2007.
- [30] A. Lince, N. Celadon, A. Battezzato, A. Favetto, S. Appendino, P. Ariano and M. Paleari, "Design and testing of an under-actuated surface emg-driven hand exoskeleton," in *International Conference on Rehabilitation Robotics (ICORR)*. IEEE, 2017.
- [31] A. Wege and A. Zimmermann, "Electromyography Sensor Based Control for a Hand," in *International Conference on Robotics and Biomimetics*, Sanya, China, 2007.
- [32] H. Kawasaki, S. Ito, Y. Ishigure, Y. Nishimoto, T. Aoki, T. Mouri, H. Sakaeda and M. Abe, "Development of a hand motion assist robot for rehabilitation therapy by patient self-motion control.," in *IEEE 10th International Conference on Rehabilitation Robotics.*, 2007.
- [33] J. Arata, K. Ohmoto, R. Gassert, O. Lamercy, H. Fujimoto and I. Wada, "A new hand exoskeleton device for rehabilitation using a three-layered sliding spring mechanism," in *2013 IEEE International Conference on Robotics and Automation.*, Karlsruhe, Germany, 2013.
- [34] A. Wege and G. Hommel, "Development and Control of a Hand Exoskeleton for rehabilitation of hand injuries," *IEEE/RSJ International Conference on Intelligent Robots and Systems.*, 2005.

-
- [35] C.-Y. Chu and R. M. Patterson, "Soft robotic devices for hand rehabilitation and assistance: a narrative review.," *Journal of neuroengineering and rehabilitation* 15.1, p. 9, 2018.
- [36] L. A. Martinez, O. Olaloye, M. Talarico, S. Shah, R. Arends and B. BuSha, "A power-assisted exoskeleton optimized for pinching and grasping motions.," in *Proceedings of the 2010 IEEE 36th Annual Northeast Bioengineering Conference (NEBEC).*, 2010.
- [37] H. Yamaura, K. Matsushita, R. Kato and H. Yokoi, "Development of Hand Rehabilitation System Using Wire-Driven Link Mechanism for Paralysis Patients," *Biologically Inspired Robotics*, vol. 1 3rd ed., 2009.
- [38] A. D. Price, A. Jnifene and N. H. E., "Design and control of a shape memory alloy based dexterous robot hand.," in *Smart Materials and Structures*, 2007, p. 16.4 140.
- [39] K. Ikuta, M. Tsukamoto and S. Hirose, "Shape memory alloy servo actuator system with electric resistance feedback and application for active endoscope," in *Proceedings. IEEE International Conference on Robotics and Automation*, Philadelphia, PA, USA, 198, 1988.
- [40] T. Feix, "Anthropomorphic hand optimization based on latent space analysis," *Thesis, Technical University of*, 2011.
- [41] S. R. Habib and N. N. Kamal, "Stature estimation from hand and phalanges lengths of Egyptians," in *Journal of Forensic and Legal Medicine* 17.3, 2010, pp. 156-160.
- [42] M. Kheirikhah Mahdi, S. Rabiee and M. E. Edalat, "A review of shape memory alloy actuators in robotics.," in *Robot Soccer World Cup.*, Berlin, Heidelberg, Springer, 2010.
- [43] D. Reynaerts, J. Peirs and H. Van Brussel, "Shape memory micro-actuation for a gastrointestinal System," *Sensors and Actuators*, 1999.
- [44] S. Barbarino, E. I. Saavedra Flores, A. R. M., I. Dayyani and F. M. I., "A review on shape memory alloys with applications to morphing aircraft," *Smart materials and structures*, p. 23.6 (2014): 063001., 10 April 2014.
- [45] R. MacGregor, "Shape memory alloy actuators and control methods," *U.S. Patent* , Vols. No. 6,574,958, 10 Jun. 2003.
- [46] E. Kaplanoglu, "Design of shape memory alloy-based and tendon-driven actuated fingers towards a hybrid anthropomorphic prosthetic hand.," *International Journal of Advanced Robotic Systems* 9.3, p. 77, 2012.
- [47] [Online]. Available: <https://simplemed.co.uk/subjects/msk/musculoskeletal-anatomy/muscles-of-the-forearm>.
- [48] [Online]. Available: <https://www.mikroe.com/emg-click>.
- [49] M. Di Girolamo, C. F. Pirri, M. G. Ajmone and P. Ariano, "Post-stroke rehabilitation of hand function based on Electromyography biofeedback," Politecnico di Torino, 2018.

- [50] C. Pacchierotti, S. Sinclair, M. Solazzi, A. Frisoli and e. al, "Wearable haptic systems for the fingertip and the hand: taxonomy, review, and perspectives.," pp. 580-600., *IEEE transactions on haptics* 10.4 (2017).
- [51] F. Kobayashi, G. Ikai, W. Futui and F. Kojima, "Two-fingered haptic device for robot hand teleoperation," *Journal of Robotics* 2011, 2011.
- [52] A. Saudabayev and H. A. Varol, "Sensors for robotic hands: A survey of state of the art," *IEEE Access* 3, pp. 1765-1782, 2015.

